In Vitro Evaluation of Blood-Brain Barrier Transport

Inauguraldissertation

zur

Erlangung der Würde eines Doktors der Philosophie

vorgelegt der

Philosophisch-Naturwissenschaftlichen Fakultät

der Universität Basel

von

Le-Ha Dieu

aus Grenchen, SO

Basel, 2014

Genehmigt von der Philosophisch-Naturwissenschaftlichen Fakultät

auf Antrag von

Prof. Dr. Jörg Huwyler

Prof. Dr. Henriette E. Meyer zu Schwabedissen

Basel, den 18.02.2014

Prof. Dr. Jörg Schibler

Dekan

Originaldokument gespeichert auf dem Dokumentenserver der Universität Basel
edoc.unibas.ch

Dieses Werk ist unter dem Vertrag „Creative Commons Namensnennung-Keine kommerzielle Nutzung-Keine Bearbeitung 3.0 Schweiz“ (CC BY-NC-ND 3.0 CH) lizenziert.
Die vollständige Lizenz kann unter
creativecommons.org/licenses/by-nc-nd/3.0/ch/
eingesehen werden.

Namensnennung-Keine kommerzielle Nutzung-Keine Bearbeitung 3.0 Schweiz
(CC BY-NC-ND 3.0 CH)

Sie dürfen: **Teilen** — den Inhalt kopieren, verbreiten und zugänglich machen

Unter den folgenden Bedingungen:

Namensnennung — Sie müssen den Namen des Autors/Rechteinhabers in der von ihm festgelegten Weise nennen.

Keine kommerzielle Nutzung — Sie dürfen diesen Inhalt nicht für kommerzielle Zwecke nutzen.

Keine Bearbeitung erlaubt — Sie dürfen diesen Inhalt nicht bearbeiten, abwandeln oder in anderer Weise verändern.

Wobei gilt:

- **Verzichtserklärung —** Jede der vorgenannten Bedingungen kann **aufgehoben** werden, sofern Sie die ausdrückliche Einwilligung des Rechteinhabers dazu erhalten.
- **Public Domain (gemeinfreie oder nicht-schützbare Inhalte) —** Soweit das Werk, der Inhalt oder irgendein Teil davon zur Public Domain der jeweiligen Rechtsordnung gehört, wird dieser Status von der Lizenz in keiner Weise berührt.
- **Sonstige Rechte —** Die Lizenz hat keinerlei Einfluss auf die folgenden Rechte:
    - Die Rechte, die jedermann wegen der Schranken des Urheberrechts oder aufgrund gesetzlicher Erlaubnisse zustehen (in einigen Ländern als grundsätzliche Doktrin des **fair use** bekannt);
    - Die **Persönlichkeitsrechte** des Urhebers;
    - Rechte anderer Personen, entweder am Lizenzgegenstand selber oder bezüglich seiner Verwendung, zum Beispiel für **Werbung** oder Privatsphärenschutz.
- **Hinweis —** Bei jeder Nutzung oder Verbreitung müssen Sie anderen alle Lizenzbedingungen mitteilen, die für diesen Inhalt gelten. Am einfachsten ist es, an entsprechender Stelle einen Link auf diese Seite einzubinden.

Quelle: http://creativecommons.org/licenses/by-nc-nd/3.0/ch/ Datum: 12.11.2013

To my family and Stephan

Acknowledgements

First, I would like to thank Prof. Dr. Jörg Huwyler for giving me the opportunity to work on this fascinating and challenging project in his research group. He has always found time for discussions and has given me helpful advice. I appreciate very much that he gave me the possibility to work on an international project as well as several interesting projects involving partners in the industry as well as the university.

Special thanks go to my committee members, Prof. Dr. Henriette E. Meyer zu Schwabedissen for being my co-referee and Prof. Dr. Markus Affolter for chairing my defense.

I also would like to thank Dr. Linda Simmler, Prof. Dr. med. Matthias Liechti from the Institute of Clinical Pharmacology and Toxicology at the University Hospital and University of Basel for the collaboration in the field of designer drugs.

Special thanks go to Dr. Yasuteru Sano and his group from the University of Yamaguchi in Japan for the collaboration with the TY09 cell line.

Furthermore, I would like to thank Prof. Dr. Cornelia Palivan, Prof. Dr. Wolfgang Meier and Dalin Wu from the Department of Chemistry at the University of Basel for introducing me to the field of polymer science. I thank Andrea Allmendinger from Roche and the University of Basel for the insights to protein viscosity and the collaboration with regards to capillary electrophoresis.

The collaborations have been especially beneficial to my work.

Many thanks to the current and former members of Prof. Dr. Jörg Huwyler's group, especially Dr. Vimalkumar Balasubramanian, Dr. Susanne Schenk, Dr. Urs Duthaler, Dr. Fabiola Porta, Tanja Stirnimann, Veronika Eberle, Daniel Preisig, Rainer Alles, Dr. Maxim Puchkov, Dr. André Ziegler, Stefan Jenzer, Isabel Meister, Marine Camblin, Anacelia Rios, Emilien Folzer, Tobias Werk, Laura Schiesser, Cécile Minder, Marina Wieland, Sandro Sieber, Stefan Winzap, and Christina Erb for the pleasant working environment and helpful discussions.

Special thanks go to my current and former lab mates Dr. Pascal Detampel, Helene Kettiger, Dr. Gabi Québatte, Dr. Carla Kirchhofer, Dominik Witzigmann, and Philip Grossen for the scientific and personal discussions, many nice and funny moments, the motivating words and support whenever I needed it. It was a great pleasure for me to have shared the lab with you!

親愛的爸爸媽媽，你們一直在耐心教導我們教育非常重要，對於二老的諄諄教誨，小女沒齒難忘。尤其是爸爸對於醫學和生物化學的熱情更是我一生中的靈感之源。二老多年的辛苦操勞都是為了女兒們能接受最好的教育，成為對社會有用之人。我們今日能順利從大學畢業，成功踏上人生的下一段都是二老的功勞。希望我們永遠是二老的驕傲。謝謝二老的養育之恩和不懈支持。

姚麗瓊、麗譽、麗俐、麗文在此衷心感謝二老的支持、鼓勵和教誨。麗霞特別感謝二老的厚愛，雖然我因忙於學業鮮有時間回家探望二老，但求來日加倍報答。

Special thanks to Stephan for his endless support and encouragement during the last 3 years!

Abbreviations

AJ	adherens junction
AMT	adsorptive-mediated transport
ATP	adenosine-5’-triphosphate
BBB	blood-brain barrier
bFGF	basic fibroblast growth factor
BSA	bovine serum albumin
CE	capillary electrophoresis
CMT	carrier-mediated transport
CNS	central nervous system
CPT	commercial protein therapeutics
CSF	cerebrospinal fluid
DLS	dynamic light scattering
HIR	human insulin receptor
hTERT	human telomerase reverse transcriptase
LDL	low-densitiy lipoprotein
L-DOPA	L-3,4-dihydroxyphenylalanine
LIF	laser-induced fluorescence
LLOQ	low limit of quantification
LRP	low density lipoprotein receptor-related protein
mAb	monoclonal antibody
MDPV	methylenedioxypyrovalerone
MDR	multidrug resistance
MRP	multidrug resistance-associated protein

PBS	phosphate buffered saline
PDMS-*b*-PMOXA	poly(dimethylsiloxane)-*block*-poly(2-methyl-2-oxazoline)
P_e	permeability coefficient
Pgp	P-glycoprotein
pI	isoelectric point
PSA	polar surface area
RMT	receptor-mediated transport
RT-PCR	reverse transcription PCR
SEM	standard error of the mean
SLS	static light scattering
SV40 T-antigen	simian virus 40 T-antigen
TEER	transendothelial electrical resistance
Tf	transferrin
TfR	transferrin receptor
TJ	tight junction
TEM	transmission electron microscopy
ZO	zonula occludens

Table of Contents

Summary

The blood-brain barrier (BBB), which is formed by brain capillary endothelial cells, effectively protects the central nervous system (CNS) from potential neurotoxic agents and maintains the brain homeostasis for synaptic signaling (Abbott, 2004). Unfortunately, the restrictive permeability properties of the BBB also exclude the majority of potential therapeutics from entering the brain and present a major challenge in the treatment of many CNS disorders such as Alzheimer's disease and brain tumors (Pardridge, 2003). Therefore, strategies to deliver drugs across the BBB to the brain are of increasing interest. Moreover, a predictive *in vitro* BBB model retaining barrier-specific properties for the screening of drug candidates and for the evaluation of drug delivery strategies to the brain would be of great benefit in the development of CNS therapeutics.

Primary brain capillary endothelial cells mimic the *in vivo* BBB characteristics the best with respect to paracellular tightness and functional expression of transporters and receptors (Gumbleton and Audus, 2001). However, primary cells can be maintained in culture only for a limited life span before they undergo senescence. Moreover, since primary brain endothelial cells are often isolated from animals, species differences may exist (Reichel et al., 2003). Immortalized cells can be used to overcome these drawbacks of short life span and species differences. However, immortalized cell lines suffer from reduced paracellular resistance and downregulation of gene expression of most transporters (Pardridge, 2004a). A potential approach to overcome these limitations is to generate a conditionally immortalized cell line using a temperature-sensitive immortalization gene. This immortalization gene is only active at a temperature of 33°C that leads to cell proliferation. At physiological temperature of 37°C, this immortalization gene is inactivated and cell differentiation is favored (Terasaki et al., 2003).

Therefore, a focus of the present thesis was to characterize the conditionally immortalized human BBB *in vitro* model, termed TY09, with respect to its BBB-specific characteristics and its potential application in transendothelial drug transport screening (**section 3.1**). This *in vitro* model was obtained by immortalization of primary microvascular endothelial cells isolated from a human brain tissue with a temperature-

sensitive immortalization gene. The cells exhibited spindle-shaped morphology similar to primary cells, expressed von Willebrand factor and γ-glutamyl transpeptidase, and showed acetylated LDL uptake. Western blot and mRNA analysis revealed the expression of important tight junction proteins, solute carriers, and ATP efflux transporters up to a passage of 50. Transendothelial transport experiments of reference compounds with different physicochemical properties in TY09 cells showed similar transport characteristics as compared to the well-characterized human hCMEC/D3 model. However, the slightly higher paracellular tightness of TY09 model led to a lower background signal and allowed a better differentiation of compounds with low, medium and high permeability. This enhanced tightness enables mechanistic bidirectional transport studies of compounds with similar lipophilicity. Transport studies of psychoactive compounds (i.e. cathinones) in TY09 cells revealed good brain penetration for all tested cathinones. An asymmetric transport characteristic was detected for methylenedioxypyrovalerone (MDPV), indicating the potential participation of an active uptake process, which may contribute to the high potency of this compound. **Section 3.2** discusses the *in vitro* evaluation of the BBB permeability of the psychoactive compounds.

As stated above, the poor penetration of neurotherapeutics remains a challenge for the treatment of brain diseases. Therefore, much research has been put on the development of drug delivery strategies. Utilization of endogenous receptor-mediated transport systems that are highly expressed at the brain endothelium offers an effective strategy to overcome the BBB (Pardridge, 2003). Antibodies directed against these receptors have been shown to undergo transcytosis in animals and can be used as transport vectors for brain drug delivery (Pardridge, 1997; Pardridge et al., 1995). Conjugation of nanoparticles to targeting antibodies directed against an endogenous receptor system offers the possibility to carry drugs to the brain in pharmacologically significant quantities. Hence, much research has been focused on the development of different nanoparticles for brain drug delivery. In the past years, drug delivery systems based on artificial vesicles, such as polymersomes, have attracted much attention due to their tunable carrier properties and their ability to carry hydrophilic compounds in their aqueous core and lipophilic substances in their membrane (Ahmed and Discher, 2004; Christian et al., 2009; Discher and Eisenberg, 2002).

Hence, another aim of this thesis was to evaluate the potential of antibody-targeted polymersomes for the implementation of drug targeting strategies to the brain (**section 3.3**). For this purpose, the anti-human insulin receptor antibody 83-14 (83-14 mAb) was used as targeting vector because this antibody has been shown to undergo transcytosis *in vivo* upon binding to the insulin receptor with high affinity (Pardridge et al., 1995). Polymersomes based on poly(dimethylsiloxane)-*block*-poly(2-methyl-2-oxazoline) [PDMS-*b*-PMOXA] block copolymers were used in this study. Characterization of polymersomes confirmed their hollow sphere and vesicle-shaped morphology. Fluorescence correlation spectroscopy experiments showed the successful conjugation of the 83-14 mAb to the polymersomes. Flow cytometry analysis revealed binding and uptake of the 83-14 mAb conjugated polymersomes by brain capillary endothelial cells expressing the insulin receptor. Competitive uptake inhibition studies confirmed the specificity of this process. Intracellular trafficking analysis showed the colocalization of the 83-14 mAb with a subpopulation of early endosomes and lysosomes after incubation for 20 min. An altered intracellular localization of the 83-14 mAb conjugated polymersomes was observed. The transcytosis process of the 83-14 mAb across the BBB remains unresolved and the factors involved in the altered trafficking of 83-14 mAb conjugated polymersomes need to be elucidated. Nevertheless, these observations contribute to the further understanding of the transcytosis process of the 83-14 mAb and the intracellular pathway of 83-14 mAb conjugated nanoparticles.

With respect to screening of BBB permeability of compounds, sensitive analytical methods are required. This is particularly important for substances where only small quantities cross the BBB such as macromolecules. Capillary electrophoresis represents with its advantages (high sensitivity, low sample requirement, fast and automated measurements) a promising analytical technique for the quantification of molecules in the context of transport studies.

Therefore, another objective of this thesis was to develop a sensitive analytical method based on capillary electrophoresis equipped with laser-induced fluorescence detector (CE-LIF) for the quantification of the transport of macromolecules across the BBB *in vitro* (**section 3.4**). In this study, we aimed to quantify the BBB permeation of fluorescently labeled 83-14 mAb across monolayers of hCMEC/D3 and TY09 cells

expressing the insulin receptor. The analytical method using CE-LIF obtained a low limit of quantification (LLOQ) for the antibody in the picomolar range. However, in contrast to the *in vivo* observation of the 83-14 mAb transcytosis to the brain (Pardridge et al., 1995), *in vitro* analysis of the transported amount of fluorescently labeled 83-14 mAb across human brain endothelial cell monolayers did not reveal the active process of transcytosis. Possible reasons for this observation are discussed in this section.

With regard to future applications of therapeutic antibodies, one of the topics of the present thesis was to extend the analytical method based on capillary electrophoresis for the viscosity determination of therapeutic antibody solutions (**section 3.5**). Therapeutic antibodies are often administered as highly concentrated solutions in order to achieve a therapeutic effect. These highly concentrated solutions show an increase in viscosity which limits their application. Therefore, in drug development, the viscosity of the protein solutions needs to be determined in order to optimize the formulation and adjust the viscosity appropriate for parenteral application. Different methods are applied for viscosity measurements. Most methods need a relatively high amount of the expensive samples and are time consuming. Therefore, in the present thesis, the possibility to employ capillary electrophoresis for viscosity measurements of protein samples was evaluated. Using CE, it was possible to estimate the viscosities (in the range of 2 to 40 mPas) of typical protein formulations with Newtonian flow behavior. The advantages of this analytical method over other methods for viscosity measurements are the low sample consumption and the fully automated viscosity determination.

1 Introduction

This chapter introduces the structure, functions and key features of the blood-brain barrier (BBB) and gives an overview of strategies to bypass this restrictive barrier including their advantages and disadvantages. Furthermore, BBB models are outlined and their possibilities and limitations are discussed.

1.1 History of the blood-brain barrier

Paul Ehrlich (1854-1915) observed that water-soluble dyes injected into the peripheral circulation practically stained all organs, except the brain and the spinal cord. He first explained this observation with the low binding affinity of the dye to the central nervous system. Additional experiments by his student Edwin Goldmann showed that a direct injection of the dye trypan blue into the cerebrospinal fluid (CSF) stained all brain cells including the spinal cord, but not the tissue in the periphery. In 1900, Max Lewandowsky (1876-1918) was the first who introduced the term "Bluthirnschranke" (Eng. blood-brain barrier) based on his studies with the dye potassium ferrocyanate. After intravenous injection, this dye showed only limited permeation into the brain (Hawkins and Davis, 2005; Ribatti et al., 2006).

1.2 Structure and functions of the blood-brain barrier

The BBB, created at the level of cerebral endothelial cells, forms the key interface between the blood circulation and the brain (Abbott et al., 2006). Although the BBB capillaries only occupy 1% of the total brain volume, it has a combined length of approximately 600 km, and a total surface area of 20 m^2 for exchange in an average

human adult (Pardridge, 2001). The cerebral endothelium of the BBB differs from the periphery endothelial cells in an increased mitochondrial content, absence of fenestrations, minimal pinocytotic vesicles, and the presence of tight interendothelial junctions (Hawkins and Davis, 2005; Joó, 1996). The permeability is about two orders of magnitude lower than that of the endothelia in peripheral organs (Tuma and Hubbard, 2003). Other brain cells, such as pericytes, astrocytes, microglia, and nerve cells, are in close association with the cerebral endothelium and together they constitute the neurovascular unit (Figure 1). This close interaction of the brain capillaries with other brain cells plays a crucial role in the induction and maintenance of the physiological function of the BBB (Abbott et al., 2010).

The BBB maintains an optimal ionic composition for synaptic signaling (Abbott et al., 2010). This is accomplished by a protective barrier and a selective transport function. Potential neurotoxic agents are effectively excluded from the brain by interendothelial tight junction formation and expression of active efflux transporters. The presence of enzymes further prevents a variety of compounds from entering the brain. Circulating lipophilic compounds reach the brain via diffusion, except they are substrate of efflux transporters. Polar solutes and macromolecules selectively gain access to the brain via carrier- and receptor-mediated transporters.

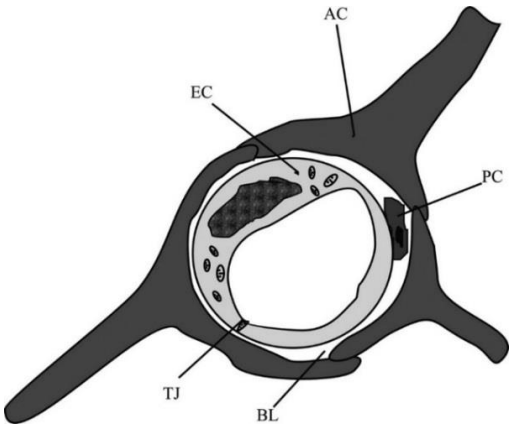

Figure 1: Schematic cross-sectional representation of a cerebral capillary. The capillary lumen is formed by a single endothelial cell (EC) with its both ends connected by tight junction. Astrocyte (AC) end-feet, pericytes (PC) are in close association with the EC. The basal lamina (BL) surrounds the EC and the PC, and is contiguous with the plasma membrane of the AC. This cell association forms the neurovascular unit (Hawkins and Davis, 2005).

Protective function of the blood-brain barrier

Tight interendothelial junctions

The brain capillary endothelial cells are characterized by the presence of extremely restrictive tight junctions (TJ) between the cells limiting the paracellular diffusion pathway for ions, polar solutes and macromolecules (Abbott et al., 2006). The transendothelial electrical resistance (TEER) *in vivo* reaches a value of approximately 1800 Ωm^2 (Abbott et al., 2010). The complexes between the endothelial cells, including adherens junctions (AJ) and TJ proteins, contribute to the characteristic of tight interendothelial junctions. AJs are responsible for keeping the cells together and giving the tissue structural support. AJ proteins, including VE-cadherin and PECAM (Abbott et al., 2010), play an essential role for tight junction formation (Abbott et al., 2010; Wolburg and Lippoldt, 2002). The TJ proteins include occludin (Furuse et al., 1993; Hirase et al., 1997), claudin (Nitta et al., 2003; Ohtsuki et al., 2007; Wolburg et al., 2003) and junctional adhesion molecules (JAMs). Occludin and claudins interact with zonula occludens 1, 2, 3 (ZO-1, ZO-2, ZO-3) which are responsible for cytoplasmic scaffolding and regulatory processes (Abbott et al., 2010). These proteins have been shown to play an important role in the restrictive BBB property. Figure 2 illustrates schematically the junctional protein complexes.

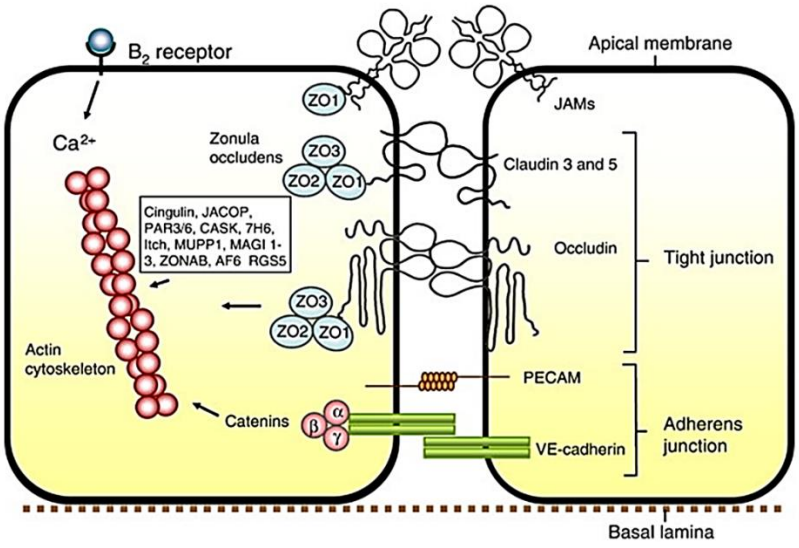

Figure 2: Junctional protein complexes of the BBB (Abbott et al., 2010).

The interaction of the junctional protein complexes is modulated by locally produced circulating factors released in the CNS and regulate the paracellular diffusion across the BBB (Abbott et al., 2010; Wolburg et al., 2003). Many cell types of the neurovascular unit release vasoactive substances and cytokines (Abbott et al., 2006, 2010). Culturing primary porcine brain endothelial cells reveal the relevance of the circulating factors on junction modulation. Cells cultured with astrocytes conditioned medium show a strong staining pattern of ZO-1 and reorganized structure of actin cytoskeleton (Török et al., 2003).

Active efflux transport

Potential harmful endogenous substances or xenobiotics are prevented from entering the brain by means of active efflux transporters. These transporters belong to the ATP-binding cassette (ABC) gene family (Begley, 2004). The ATP-binding cassette (ABC) genes represent one of the largest families of transmembrane proteins. ABC transporters are integral membrane proteins that use the energy derived from ATP hydrolysis to transport various molecules across cell membranes (Dean, 2002; Loscher and Potschka, 2005). Their main function at the BBB is the transport of a broad variety of lipid-soluble substances out of the cerebral endothelium and the brain. The multidrug resistance protein, P-glycoprotein (Pgp; MDR1, ABCB1), multidrug resistance-associated proteins (MRP; ABCC) family members, and the breast cancer resistance protein (BCRP; ABCG2) are found at the BBB. Pgp and BCRP are only located at the apical side of the BBB and transport compounds from the endothelial cells back to the blood. MRP family members are found either at the apical, basolateral or even at both sides of the endothelium (Loscher and Potschka, 2005) [Figure 3].

These ABC transporters play an important role in the maintenance of vital functions of the brain (Dallas et al., 2006) by means of active efflux of potential neurotoxic compounds (Abbott et al., 2010; Dallas et al., 2006). Their broad substrate specificity effectively hinders potential toxic agents from reaching the CNS (Loscher and Potschka, 2005). However, this characteristic also presents a major challenge in the development of CNS drugs, since a variety of potential drug molecules are substrate of the efflux transporters.

Transport across the blood-brain barrier

Lipid-mediated transport of small lipophilic compounds

A broad range of small molecular weight lipophilic molecules is able to cross the BBB via lipid-mediated diffusion. Lipophilicity, determined as the logP (logarithmic octanol/buffer partition coefficient of the neutral species), correlates positively with brain permeation. LogP values between 2-4 have been correlated with good brain penetration (Waterhouse, 2003). Factors which restrict passive permeability include polar surface area greater than 60-80 $Å^2$ (Kelder et al., 1999; Pardridge, 2003), number of hydrogen bonding capacity exceeding 10 (Pardridge, 2005a), and a molecular weight higher than 450 Da (Clark, 2003; van de Waterbeemd et al., 1998; Waterhouse, 2003). However, the prediction of BBB permeability based on physicochemical characteristics is limited to compounds which are not subjected to active transport mechanisms (Clark, 2003). For example, lipophilic drugs which are substrates of active efflux transporters do not comply these general rules (Loscher and Potschka, 2005).

Carrier-mediated transport

Tight junctions effectively block the paracellular diffusion of polar solutes. Thus, to supply the CNS with essential polar nutrients (e.g. glucose and amino acids) a number of specific solute carriers are expressed at the cerebral endothelium including the GLUT1 glucose transporter, the MCT1 monocarboxylic acid carrier, the LAT1, CAT1 amino acid carriers, and the CNT2 purine nucleoside carrier (Pardridge, 2005b). Some transporters are either expressed on the apical or basolateral side of the membrane only, whereas other transporters are found at both sides of the membrane. With the distinct orientation of the transporters, substrates can be preferably transported either from the blood circulation into the brain or vice versa, from the brain out to the blood (Abbott et al., 2010).

Receptor- and adsorptive-mediated transport

Large molecular weight compounds are transported to the brain via the transcytotic pathway. This transport process involves either specific receptor-mediated transcytosis (RMT) or adsorptive-mediated transcytosis (AMT). In RMT, the specific ligand-receptor

interaction mediates the internalization of the complex. The complex is then transported across the cytoplasm and finally, exocytosis at the opposite side of the membrane takes place. The ligand-receptor dissociation occurs either during the cellular transit or during the exocytosis (Abbott et al., 2010; Pardridge, 2002). Examples for essential macromolecules which are transported to the brain via receptor-mediated transcytosis include insulin and transferrin (Pardridge, 1997). Some cationic molecules are able to cross the BBB non-specifically via the adsorptive-mediated transcytosis (AMT) after interaction with the negative charged surface of the cerebral endothelium (Abbott et al., 2006). Figure 3 illustrates schematically different transport mechanisms across the BBB.

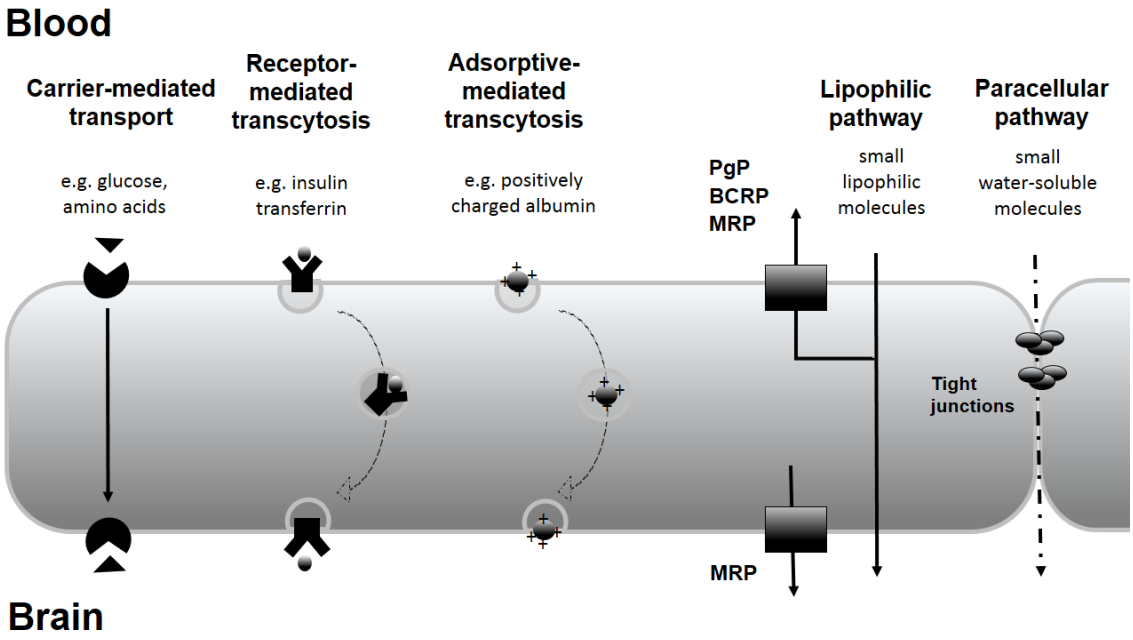

Figure 3: Schematic representation of different transport mechanisms and selected ABC efflux transporters located at the BBB. Pgp and BCRP are expressed at the apical membrane and MRPs are expressed on the apical, basolateral or both membrane sides (adapted from Abbott et al., 2006).

The restrictive permeability properties of the BBB effectively protect the brain from potential neurotoxic agents. However, these restrictive characteristics also prevent the majority of drug candidates from reaching the CNS (Pardridge, 2003) and represent a major limiting factor in the development of drugs for treatment of neurological diseases

(Jeffrey and Summerfield, 2010). Therefore, different invasive and non-invasive strategies are currently being used or investigated for the delivery of drugs to the brain.

1.3 Strategies for brain drug delivery

1.3.1 Invasive methods

Drug delivery to the brain can be achieved using invasive methods, such as direct intracerebroventricular injection or intracerebral implantation. The low drug diffusion from the injection site into the brain parenchyma limits the effectiveness of these methods. Some areas may not be reached by the drug due to low diffusion (Gabathuler, 2010; Pardridge, 2003). Therefore, these methods are only effective if a drug has only to be delivered to a local defined part of the brain (Gabathuler, 2010). Thus, the most effective way to achieve a widespread distribution of drugs into the whole brain is via crossing the cerebral microvascular capillaries, since every single neuron is perfused by its own capillary. However, since the majority of CNS drugs cannot penetrate the BBB (Pardridge, 2003), strategies are needed to overcome this barrier.

One approach to deliver drugs across the BBB is by intracarotid injection of a hyperosmolar solution, which causes a transient disruption of the tight junctions resulting in the opening of the BBB for drugs. This method has been used to reach therapeutic concentration of chemotherapeutic agents in human (Neuwelt et al., 1986). However, the disadvantage of this strategy is the general increase in passage of blood components to the CNS which may damage the brain cells (Gabathuler, 2010). Therefore, much research is focused on physiological approaches to overcome the BBB.

1.3.2 Physiological methods

A physiological strategy to overcome the BBB is based on using endogenous transporters and receptors expressed at the cerebral endothelium (Figure 3). Reformulation of the drugs is often required to be delivered to the brain via endogenous BBB transport mechanisms (Pardridge and Boado, 2012). Table 1 summarizes the physiological strategies available for drug delivery to the CNS and the limitations of the different approaches. Selected examples of the different strategies are listed.

Carrier-mediated transport

There are several nutrient transport systems expressed at the BBB, which transport small water-soluble nutrients into the brain. Drugs with structural similarity to an endogenous nutrient of a transporter system may enter the brain via a carrier-mediated transport (CMT) pathway. CMT mechanism has been successfully used for the delivery of L-DOPA (L-3,4-dihydroxyphenylalanine) to the brain via LAT1. L-DOPA is a prodrug of dopamine that itself does not penetrate the BBB. Once L-DOPA is transported to the brain via LAT1, it is subsequently metabolized to the water-soluble dopamine by the aromatic amino acid decarboxylase. This molecule is used for the therapy of Parkinson's disease (Pardridge, 2003).

Adsorptive- and receptor-mediated transcytosis

Macromolecules can be transported to the brain via adsorptive-mediated transport (AMT) and receptor-mediated transport (RMT). In AMT, positively charged molecules or particles are internalized to the cells upon binding to the negatively charged plasma membrane. This process is highly non-specific, therefore, the application of this strategy in the clinics is limited (Gabathuler, 2010).

RMT offers the possibility to selectively transport macromolecules or nanoparticles to tissues expressing a specific receptor. The BBB is enriched with different receptor systems, including the insulin receptor (IR), transferrin receptor (TfR), and low density lipoprotein (LDL) receptor and its related proteins (Dehouck et al., 1997; Gabathuler, 2010; Pardridge, 2003). Drugs can be conjugated to a peptide or protein (e.g. monoclonal antibody) that mediates cellular transcytosis of the conjugates upon interaction with an endogenous receptor system (Pardridge, 2003).

A receptor system exploited for brain drug delivery is the low-density lipoprotein (LDL) receptor and its related proteins 1 and 2 (LRP1 and LRP2). LRP is a type I transmembrane protein and is expressed in many tissues including the CNS. These receptors have been described to be involved in the internalization and degradation of multiple ligands of diverse metabolic pathways (Gabathuler, 2010). Compared to antibodies targeting the TfR in mouse, the brain uptake value is 10-fold lower (Pardridge, 2012)

The transferrin receptor system is most widely characterized for brain drug targeting (Gaillard et al., 2005). While the high endogenous plasma concentration of transferrin limits its application as a vector for drug targeting *in vivo* (Gaillard et al., 2005), antibodies directed against the transferrin receptor (TfR) can be used for delivery of drugs to the brain. Pardridge and colleagues have extensively exploited this receptor system for brain drug delivery with the murine anti-rat TfR OX-26 mAb (Pardridge, 2003). This antibody interacts with the receptor on a distinct epitope that is not involved in transferrin binding and thus avoid a competitive binding inhibition between the endogenous Tf and OX-26 mAb (Pardridge, 2012). Several macromolecules and nanoparticles have been successfully delivered to the brain via receptor-mediated transport by TfR system (Huwyler et al., 1996; Zhang and Pardridge, 2005, 2006).

Similar to the TfR, the insulin receptor (IR) has been widely used for the implementation of drug delivery strategies to the brain (Pardridge and Boado, 2012; Zhang et al., 2003a, 2003b). For instance, Pardridge and coworkers used the high-affinity murine anti-human insulin receptor monoclonal antibody 83-14 (83-14 mAb) as a vector for drug and gene delivery (Pardridge and Boado, 2012; Zhang et al., 2003a, 2003b). The antibody binding site on the receptor is different from that of the endogenous insulin. An interference with the function of the endogenous ligand is thus avoided (Pardridge and Boado, 2012). Moreover, since overdosing of insulin causes hypoglycemia, the use of insulin as a targeting vector is limited (Partridge, 2012). The 83-14 mAb interacts with an exofacial epitope on the insulin receptor and is rapidly transported across the BBB to the brain after intravenous administration. The brain uptake 83-14 mAb accounts 3.8% per initial dose per 100g brain in primates (Pardridge et al., 1995). The BBB permeability surface area (PSA) product of the 83-14 mAb is nine-fold higher than that of the OX-26 mAb. The most active BBB molecular Trojan horse is an antibody directed against the human IR (Pardridge and Boado, 2012). Moreover, in contrast to OX26 mAb, chimeric and humanized forms of the 83-14 mAb are available. Therefore, this antibody may be used in humans with less immunogenic response (Boado et al., 2007; Coloma et al., 2000).

In addition, RMT offers the possibility to specifically transport nanocarriers containing drugs to the brain (Huwyler et al., 1996). Drugs that are normally not able to penetrate

the BBB due to their unfavorable physicochemical properties or not in sufficient quantities can be loaded into ligand-targeted nanocarriers and specifically delivered to the brain.

Table 1: Summary of physiological strategies for delivery of drugs to the CNS (with selected examples).

Strategy	Principal	Examples	Limitations	References
Lipid-mediated transport	Low molecular weight lipophilic compounds with specific physicochemical properties passively diffuse to the brain.	Sedatives (e.g. diazepam), antipsychotic drugs (e.g. haloperidol)	Only access for lipophilic compounds, which are not substrate of active efflux transporters. Many CNS disorders (e.g. AD, MS) do not respond to small lipophilic molecules. Modification of compounds to render them more lipophilic may result in activity loss and/or reduction in brain uptake due to active efflux transport.	(Fischer et al., 1998; Loscher and Potschka, 2005; Pardridge, 2003)
Carrier-mediated transport	Water-soluble compounds that mimic CMT substrates are actively transported to the brain.	L-DOPA (LAT1 transporter)	Cannot transport macromolecules to the brain; chemical modification of a molecule may impair its activity *in vivo*.	(Gabathuler, 2010; Pardridge, 2003)
Receptor-mediated transport	Transport mediated by ligands directed against a specific BBB receptor (e.g. IR, TfR, LDL receptor).	Small or large molecules conjugated to an antibody, fusion proteins Nanoparticles conjugated to antibodies (e.g. 83-14 mAb, OX26) or ApoE	Expression of the receptors on peripheral organs; drugs need reformulation.	(Pardridge, 2002a, 2002b; Pardridge and Boado, 2012; Zhang et al., 2003a, 2003b)
Adsorptive-mediated transport	Positively charged molecules interact with negatively charged membrane.	TAT peptide	highly non-specific, limited clinical use	(Liu et al., 2008)

MS: multiple sclerosis; AD: Alzheimer's disease; CMT: carrier-mediated transport; L-DOPA: L-3,4-dihydroxyphenylalanine; IR: insulin receptor; TfR: transferrin receptor; LDL: low-density lipoprotein; ApoE: apolipoprotein E; fusion proteins: recombinant proteins linked to transport vector; TAT: transactivator of transcription, cell-penetrating peptide of HIV.

1.3.2.1 Brain drug delivery using nanoparticles

The advantages of the application of nanoparticles in drug delivery include the possibility to determine the biodistribution and pharmacokinetic of the encapsulated compounds by tuning the physicochemical properties of the nanocarriers. The circulation half-life and drug accumulation at the target site can be modulated. Conjugation to a targeting ligand enhances the cellular uptake at the target sites (Kamaly et al., 2012). Different nanoparticles with active targeting properties have been created to deliver drugs to the brain in animals. These nanoparticles include targeted liposomes and polymersomes (Boado and Pardridge, 2011; Pang et al., 2008).

Liposomes

Liposomes are phospholipid vesicles that have been widely employed as drug carriers in pharmaceutical fields (Torchilin, 2005). Liposomes possess the ability to carry and deliver large amounts of drugs to the site of action. Biocompatibility and the lack of toxicity of the phospholipids make liposomes good and safe candidates for the implementation of drug delivery systems to the brain. Much research has been put on ligand-targeted liposomes for brain drug delivery (Huwyler et al., 1996; Schnyder and Huwyler, 2005).

Polymersomes

In the past years, artificial vesicles, such as polymersomes, have attracted much attention. Polymersomes are vesicles that are formed upon hydration of synthetic amphiphilic block copolymers, which constitute of at least two distinct fully synthetic hydrophilic and hydrophobic polymers that are covalently linked (Discher and Eisenberg, 2002) [Figure 4]. Polymersomes can entrap hydrophilic compounds in its aqueous core and lipophilic molecules in its membrane (Lee and Feijen, 2012). Depending on the molecular weight of the block copolymers, their membrane thickness ranges between 10 to 50 nm. In comparison, liposomes possess a membrane thickness of approximately 3-5 nm (Le Meins et al., 2011). This explains the increased mechanical stability and enhanced diffusional barrier property to encapsulated compounds of polymersomes compared to liposomes (Le Meins et al., 2011).

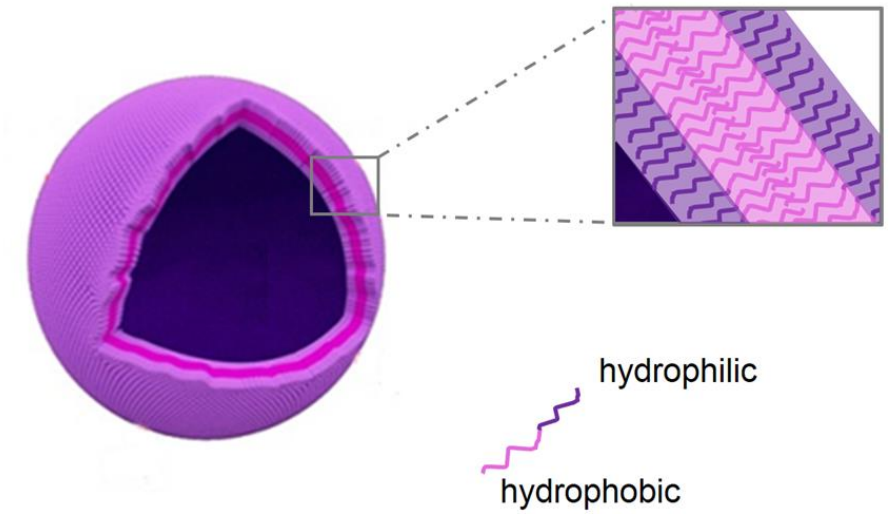

Figure 4: Schematic illustration of a polymersome formed by spontaneous self-assembly of amphiphilic diblock copolymers in dilute aqueous solution.

The large variety of amphiphilic block copolymers offers the possibility to form polymersomes with a broad range of carrier properties. Polymersomes with desirable characteristics, such as stimuli-responsiveness, multifunctionality, loading capacity, and membrane permeability, can be designed by applying block copolymers with specific chemical composition, hydrophilic to lipophilic ratio, molecular weight, and functionality (Cabane et al., 2012; Discher and Ahmed, 2006; Gaitzsch et al., 2012; Najer et al., 2013; De Oliveira et al., 2012). These tunable properties of polymersomes render them attractive for biomedical applications. Moreover, bioconjugation of polymersomes to targeting moieties offers the possibility for selective drug delivery to the site of interest (Egli et al., 2011; Ben-Haim et al., 2008; Lin et al., 2006; Meng et al., 2005). Hence, there is an increasing interest in the implementation of drug delivery systems using polymersomes. A variety of block copolymers, including poly(2-methyloxazoline)-block-poly(dimethylsiloxane)-block-poly(2-methyloxazoline) [PMOXA-*b*-PDMS-*b*-PMOXA] triblock copolymer, have been employed for drug delivery applications (Egli et al., 2011; Lee and Feijen, 2012).

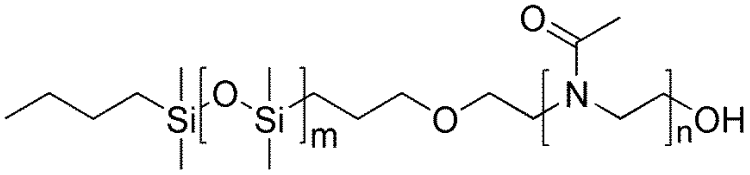

Figure 5: Chemical structure of PDMS-*b*-PMOXA diblock copolymer.

Polymersomes based on PDMS-*b*-PMOXA or PMOXA-*b*-PDMS-*b*-PMOXA block copolymers (Figure 5) are biocompatible and have a low toxicity *in vitro*. They have been designed for the application as nanoscale bioreactor (Nardin et al., 2000), artificial peroxisomes (Tanner et al., 2013), and for specific targeting of cancer cells (Egli et al., 2011) and macrophages (Brož et al., 2005). Interestingly, non-specific uptake by macrophages was not observed for non-targeted polymersomes, indicating a reduced nonspecific elimination of these polymersomes by macrophages (Brož et al., 2005).

The stealth property of these polymersomes is due to the protein-repellent effect of the hydrophilic PMOXA polymer. This polymer has been described to show similar stealth property as PEG polymer but is less prone to degradation in physiological and oxidative environment (Konradi et al., 2008; Pidhatika et al., 2012). Therefore, previous work suggested PMOXA polymer as a good alternative to PEG polymer (Pidhatika et al., 2012). These findings highlight the potential of polymersomes based on PDMS-*b*-PMOXA diblock or PMOXA-*b*-PDMS-*b*-PMOXA triblock copolymers for biomedical applications, including specific drug delivery.

1.4 BBB models

To predict the BBB permeability of drug candidates different BBB models have been exploited. BBB models based on *in silico* and *in vitro* techniques allow for high throughput screening and optimization of drug candidates prior to *in vivo* studies in animals (Booth and Kim, 2012). Each of these models has its own advantages and limitations.

1.4.1 *In silico* models

In silico models can be used for screening a large number of compounds with respect to the BBB permeability. These computational methods attempt to predict the passive BBB permeability based on the molecular structures and physicochemical properties (Feng, 2002). Parameters such as lipophilicity (logP), hydrogen bonding, polar surface area, and molecular weight are used to estimate the BBB permeability (Clark, 2003; Kelder et al., 1999). *In vivo* log BB (drug concentration in brain to that in blood) values at steady states or BBB PS (permeability surface area) products have been employed to correlate with physicochemical properties of the drug candidates in order to define rules or equations to predict CNS penetration (Abbott, 2004; Nicolazzo et al., 2006). Log BB values correspond to the ratio of the whole drug concentration in the brain to that in the blood. This parameter does not only consider the free drug, which is responsible for the pharmacological action but also cytoplasmic bound drug. Therefore, discussions about the validity of *in silico* models based on log BB values has been arisen (Martin, 2004). Another approach to generate an *in silico* model for prediction of BBB permeation is to use *in vivo* BBB PS product values, which give a measure of unidirectional clearance from blood to brain across the BBB. BBB PS product predicts the level of free drug in the brain and is more reliable than log BB. Therefore, it has been suggested to replace log BB by BBB PS product for *in silico* predictions (Pardridge, 2004a). The quality and quantity of the training set applied for the generation of the computational models determines the validity of the *in silico* prediction (Abbott, 2004). To date, it is still difficult to generate *in silico* models that are able to predict active transport and metabolic processes since detailed knowledge on the structure-activity relationship of transporters

and enzymes is still missing. Therefore, *in vitro* and *in vivo* models are needed to account for active transport mechanisms (Abbott, 2004, 2013).

1.4.2 *In vitro* models

In order to predict the *in vivo* situation, *in vitro* models need to reproduce BBB characteristics as much as possible. Such an *in vitro* model offers the possibility to examine several processes at the BBB, including the mechanistic aspects of BBB transport, cell-to-cell interaction, and fundamental biological and pathological processes (Abbott, 2004; Gumbleton and Audus, 2001). Functional expression of important tight junctional proteins providing restrictive paracellular barrier properties to polar molecules as well as polarized expression of influx and efflux transporters are prerequisites for an *in vitro* model to reliably screen transendothelial transport of potential CNS drug candidates (Cecchelli et al., 2007).

One of the first *in vitro* BBB models was reported in the 1970s after successful isolation of brain capillaries from rat brain (Joó and Karnushina, 1973). This model was then followed by the isolation of brain capillaries of different species. Isolated brain capillaries can be used for the investigations of transport systems, for mechanistic studies, such as receptor- and adsorptive-mediated endocytosis, and for the investigations of BBB alterations in CNS pathology (Pardridge, 1999). Isolated brain capillaries resemble *in vivo* BBB to the highest extend. However, since the apical side of the capillaries is not easily accessible *in vitro*, permeability studies are difficult. This limitation led to the development of *in vitro* models based on culturing isolated primary brain endothelial cells on semipermeable supports (Bowman et al., 1983).

Apart from isolated capillaries, primary or low passage brain capillary endothelial cells retain many BBB key properties and resemble the *in vivo* BBB the best, although many BBB-specific features are downregulated (Gumbleton and Audus, 2001; Reichel et al., 2003). These cells are mostly obtained from bovine and pig because they provide a larger amount of brain capillaries compared to rodents (Gumbleton and Audus, 2001; Wilhelm et al., 2011). Primary brain endothelial cells have been successfully employed as BBB *in vitro* models for several studies, including permeability screening, BBB efflux transport experiments, and mechanistic investigations on brain permeation (Reichel et al.,

2003). However, the short lifespan of primary cells combined with the time-consuming and technical demands required for the isolation, limit their routine use as BBB *in vitro* models. Moreover, potential species differences to human and variability in the phenotypic properties between the isolated batches further limit their widespread use (Gumbleton and Audus, 2001).

Therefore, immortalized cell lines have been created in order to allow prolonged passage of the cells and thus reducing the need for isolation (Wilhelm et al., 2011). Immortalization can be achieved by transfection of primary endothelial cells using a viral tumor gene, such as simian virus 40 (SV40) large T-antigen gene. Immortalization genes inactivate tumor suppressor genes that are responsible for replicative senescent (Sano et al., 2010). Different immortalized cell lines have been generated and characterized to different extends. The most widely used cell lines include the RBE4 (Roux et al., 1994) and GPNT (Régina et al., 1999), both derived from rat, and the mouse b.End3 (Omidi et al., 2003). Immortalized brain endothelial cell lines of human origin have been developed in order to avoid potential species differences, e.g. BB19 (Prudhomme et al., 1996). In contrast to primary cells, monolayers of immortalized cells generally suffer from the drawback of insufficient tightness (Reichel et al., 2003).

Recently, a human BBB immortalized cell line, hCMEC/D3, has been developed by SV40 T antigen transfection (Weksler et al., 2005). Since then, much research has been put on the characterization of this cell line. It has been shown to retain many BBB characteristics, including the expression of tight junction proteins and efflux transporters (Poller et al., 2008; Weksler et al., 2005). For the hCMEC/D3 model, a better paracellular tightness compared to other cell lines was reported. This property allows its use for transendothelial transport studies discriminating between low and high permeabilities of compounds (Poller et al., 2008).

To date there is no *in vitro* cell culture model reaching the paracellular tightness comparable to primary cells. Immortalization enables the brain endothelial cells to stably grow and maintain a prolonged passage in culture. However, it is a general challenge to make the immortalized cells arrest their proliferation and differentiate after they have reached confluency. Therefore, many immortalized cell lines failed to reach an appropriate paracellular tightness (Reichel et al., 2003).

An attempt to overcome this limitation is to generate a conditionally immortalized cell line. Conditionally immortalized BBB cell lines derived from transgenic mice and rats harboring a temperature-sensitive immortalization gene have been generated. This immortalization gene is only active at a temperature of 33°C. At physiological temperature of 37°C, the immortalization gene is inactive and the cells resemble primary cells lacking tumor gene again. These cell lines have been shown to highly express transporters specific to BBB (Hosoya et al., 2000a, 2000b; Pardridge, 2004b; Terasaki et al., 2003). Recently, Sano and his coworkers have developed a human conditionally immortalized BBB *in vitro* model using a temperature-sensitive SV40-T antigen. These cells express several important tight junction proteins and efflux and influx transporters (Sano et al., 2010). Therefore, conditionally immortalization might be an interesting approach to generate *in vitro* BBB cell models retaining barrier-specific properties.

1.4.2.1 Analytical methods to measure blood-brain barrier transport *in vitro*

To monitor the transport of compounds across the BBB, sensitive analytical techniques are required. Scintillation counting is a sensitive method and it has been employed to quantify the amounts of compounds transported across the BBB *in vitro* (Audus and Borchardt, 1986; Poller et al., 2008; Shah et al., 1989). Compounds of interest are radioactive labeled and applied to the cell culture system. Sample preparation for analysis is very simple, as it only requires the addition of scintillation liquid. However, this analytical method does not provide any information about the metabolism of the molecule since metabolites, if bearing the radioactive label, would show the same radioactive signal as the intact molecule. Moreover, this technique can be expensive due to the cost resulting from the radiolabeling and the infrastructure required (Sloan et al., 2012).

Another analytical method for transport studies is capillary electrophoresis (CE). This technique offers several advantages, including low sample consumption and the possibility to couple CE to a laser-induced fluorescence (LIF) detector that enables a higher sensitivity compared to an UV detector. The low sample volume injected for a measurement, which is in the range of a few nanoliters, render CE very attractive for the analysis of samples derived from *in vitro* transport experiments (Freed et al., 2002). The most commonly used experimental setup for *in vitro* transport studies is based on

Transwell systems (Bickel, 2005). The transport experiments often require repeated sampling over a defined period of time. To keep the hydrostatic pressure on the cell monolayer from both sides of the Transwell system constant, the removed sample volume is usually replaced by the same amount of fresh transport buffer or medium leading to a dilution of the compound of interest in the acceptor chamber. This is particularly critical for substances where only small quantities cross the BBB, such as peptides or macromolecules. However, the low sample volume needed for CE measurements minimizes this dilution effect and presents a considerable benefit. Furthermore, CE technique allows to detect potential metabolic fragments of parent molecules resulting from the interaction with endothelial cells (Freed et al., 2001).

Liquid chromatography - mass spectrometry (LC-MS) provides another analytical approach to detect compounds in BBB transport experiments. LC-MS/MS has been employed for the quantification of transport of peptide across an *in vitro* BBB model. This technique has been shown to be more sensitive as compared to CE-LIF (Chappa et al., 2007; Freed et al., 2002) and be able to detect peptide metabolites (Chappa et al., 2007; Sloan et al., 2012). Advantages of this analytical method over other techniques include the possibility to detect compounds based on mass-to-charge (*m/z*) ratio without prior derivatization (e.g. fluorescence or radiolabeling), good sensitivity and selectivity, and the absence of e.g. radioactive waste (Chappa et al., 2007). However, using this method, buffer or cell culture medium present a challenge since the high salt concentration required for the proper cellular function during the experiment may damage the MS. Therefore, careful sample preparation and optimization of the analytical method is required prior to analysis.

Taken together, all analytical techniques mentioned above have their own advantages and limitations. When choosing an analytical method for measurements of BBB transport studies, several factors need to be considered. These include the expected amount of compound transported to the acceptor side, the sample volume needed for the measurements, the ability to modify the test compound with fluorescence or radioactive marker, and the compatibility of the cell culture medium or buffer with the chosen technique (Sloan et al., 2012).

1.4.3 *In vivo* models

To determine brain uptake *in vivo*, several techniques are used. These include the carotid artery single injection or perfusion technique, intravenous injection technique, cerebrospinal fluid (CSF) sampling, and intracerebral microdialysis. Animal models have the advantage to detect the complex *in vivo* situation. However, they are rather costly compared to computational and cell culture models and they cannot be used for high-throughput screening of potential CNS compounds.

2 Aim of the Thesis

The blood-brain barrier (BBB) excludes the majority of drug candidates from entering the brain. Therefore, it is of substantial importance to evaluate the BBB permeability of potential drugs in an early phase of drug development. For this purpose, predictive *in vitro* BBB models that exhibit important key characteristics of the human BBB are needed. Downregulation of BBB specific proteins in culture presents a major challenge in the development of *in vitro* models. Conditionally immortalized cell lines have been proposed to have a great potential to be employed as an ideal *in vitro* BBB model since the gene expression of specific brain endothelial proteins remains high in culture (Bickel, 2005; Pardridge, 2004b; Terasaki et al., 2003). Therefore, an aim of the present thesis was to characterize the newly generated human conditionally immortalized cell line TY09 derived from primary isolated brain capillary endothelial cells with respect to the expression of BBB key proteins and the potential to screen compounds with different physicochemical properties.

Synthetic cathinones have become increasingly popular as recreational drugs (Simmler et al., 2013). Although it is known that the cathinones exert a pharmacological effect in the CNS, to which extent these psychoactive compounds cross the BBB remains unclear. Another topic of this thesis was to analyze the BBB permeation of the psychoactive compounds and to elucidate potential involvement of active transport processes using the TY09 cell line.

Specific drug delivery systems to overcome the BBB are of great benefit to deliver drugs with unfavorable physicochemical properties to the brain. Therefore, a further goal of this thesis was to develop a specific drug delivery system using novel polymeric

nanoparticles and to evaluate the cellular binding, uptake, and intracellular trafficking of this drug delivery system in human brain capillary endothelial cells.

To quantify the permeability of compounds across the BBB, a sensitive analytical method is required. This is particularly relevant for substances where only small amounts penetrate the brain such as macromolecules. Capillary electrophoresis (CE) with its advantages (high sensitivity, low sample requirement, fast and automated measurements) presents a promising technique to quantify the permeability of compounds across the BBB. Antibodies have been widely used as targeting vectors for drug delivery systems. Thus, it is of increasing interest to measure the transcytotic capacity of the targeting antibodies across the BBB *in vitro*. Hence, another focus of this thesis was to develop a sensitive analytical method based on CE for the quantification of macromolecules, i.e. antibodies, in the context of transendothelial transport and transcytosis *in vitro*.

Monoclonal antibodies gain increasing relevance not only as targeting vectors but also in the treatment of diseases such as cancer, autoimmune diseases, and others. Therapeutic antibodies are often administered as highly concentrated solutions in order to achieve the therapeutic effect. These highly concentrated protein solutions also show an increase in viscosity that limit their parenteral application. Thus, the viscosity of antibody solutions needs to be determined in drug development process in order to optimize the formulations. A high-throughput method with minimal sample consumption would be of great benefit for the viscosity measurement of expensive antibody solutions. Therefore, the suitability of CE for high-throughput viscosity determination of antibody formulations was further evaluated.

3 Results

3.1 Stable Human Brain Microvascular Endothelial Cell line Retaining its Barrier-Specific Nature Independent of the Passage Number

Yasuteru Sano,[1] Yoko Kashiwamura,[1] Masaaki Abe,[1] Le-Ha Dieu,[2] Jörg Huwyler,[2] Fumitaka Shimizu,[1] Hiroyo Haruki,[1] Toshihiko Maeda,[1] Kazuyuki Saito,[1] Ayako Tasaki[1] and Takashi Kanda[1]

[1]Department of Neurology and Clinical Neuroscience, Yamaguchi University Graduate School of Medicine, Yamaguchi, Japan

[2]Department of Pharmaceutical Sciences, University of Basel, Basel, Switzerland

Clinical and Experimental Neuroimmunology 3 (2012) 1-12

Clinical & Experimental Neuroimmunology

Clinical and Experimental Neuroimmunology **4** (2013) 92–103

ORIGINAL ARTICLE

Stable human brain microvascular endothelial cell line retaining its barrier-specific nature independent of the passage number

Yasuteru Sano,[1] Yoko Kashiwamura,[1] Masaaki Abe,[1] Le-Ha Dieu,[2] Jörg Huwyler,[2] Fumitaka Shimizu,[1] Hiroyo Haruki,[1] Toshihiko Maeda,[1] Kazuyuki Saito,[1] Ayako Tasaki[1] and Takashi Kanda[1]

[1]Department of Neurology and Clinical Neuroscience, Yamaguchi University Graduate School of Medicine, Yamaguchi, Japan, [2]Department of Pharmaceutical Sciences, University of Basel, Basel, Switzerland

Keywords
blood–brain barrier; telomerase; temperature-sensitive SV40 large T-antigen; tight junction; transporter

Correspondence
Takashi Kanda, MD, PhD, Department of Neurology and Clinical Neuroscience, Yamaguchi University Graduate School of Medicine, 1-1-1 Minamikogushi, Ube, Yamaguchi 7558505, Japan.
Tel: 81-83-622-2719
Fax: 81-83-622-2364
Email: tkanda@yamaguchi-u.ac.jp

Received: 17 April 2012; revised: 12 September 2012; accepted: 18 September 2012.

Abstract

Objectives: The breakdown of the blood–brain barrier (BBB) has been considered to be a key step in the disease process of a number of neuroimmunological disorders. Although several *in vitro* BBB models derived from human tissues have been established, no human conditionally immortalized *in vitro* BBB models using a temperature-sensitive SV40-T antigen (*tsA58*) and human telomerase reverse transcriptase (*hTERT*) have ever been reported. In the present study, we established a new human brain microvascular endothelial cell line harboring *tsA58* and *hTERT* genes, and extensively characterized this new model.
Methods: TY08 cells, derived from the human BBB and harboring *tsA58*, were infected with retroviruses possessing *hTERT* genes. We examined whether this new model retains its barrier-specific nature, independent of the passage number.
Results: The obtained endothelial cell line, termed TY09, proliferated well under the permissive temperature and stopped growing under the non-permissive temperature, despite the acquisition of *hTERT* as an additional immortalizing gene. Even with a high-passage number, the cells maintained a spindle-shaped morphology, the expression of the von Willebrand factor, tight junction proteins and transporters. Furthermore, we carried out a transendothelial transport study for TY09 cells and hCMEC/D3 cells, thereby proving that both cell lines have almost the same nature with respect to transcellular permeability of various hydrophilic and hydrophobic substances.
Conclusions: The new stable conditionally immortalized TY09 cells, retaining the *in vivo* BBB functions, should facilitate the performance of future studies for determining the pathophysiology of various neuroimmunological diseases. (Clin Exp Neuroimmunol doi: 10.1111/cen3.12001, October 2012)

Introduction

The blood–brain barrier (BBB) is formed by highly specialized endothelial cells. The features that distinguish brain microvascular endothelial cells (BMEC) from those of peripheral organs include their lack of fenestration, the formation of complex intercellular tight junctions preventing passive diffusion between cells, minimal endocytosis, the expression of specific transporters and increased activity of enzymes that metabolize xenobiotics.[1–4] Cultured BMEC are an important *in vitro* BBB model that can be used to analyze the physiological and biological functions of the BBB, as well as to estimate BBB permeability of compounds.[5] The significant scientific and industrial interest in the physiology and pathology of the BBB has led to the development of many *in vitro* BBB models.[6,7] Weksler et al. have extensively characterized a human brain microvascular endothelial cell line, hCMEC/D3.[8] Recently, we described a new conditionally immortalized human brain microvascular cell line, TY08, which were transduced with a temperature sensitive SV40-T antigen (*tsA58*).[9] TY08 cells have been characterized as well as hCMEC/D3 cells, and have been shown to have many barrier-specific properties, such as the expression of tight junction proteins, and influx and efflux transport-

© 2012 Japanese Society for Neuroimmunology

ers. Although human telomerase, as well as the SV40-T antigen, was used to immortalize HBMEC to generate the hCMEC/D3 cells, only *tsA58* was used to immortalize the TY08 cells. TY08 cells grew stably at the permissive temperature until around 15 passages. However, these cells did not grow beyond the 16th to 18th passages, even under the permissive temperature, thus showing that the tsA58 protein was not sufficient to allow HBMEC to bypass senescence and acquire immortality. To overcome this disadvantage of TY08 cells, we constructed a new cell line using the catalytic subunit of human telomerase (*hTERT*) to generate a more useful cell line that is able to grow for more than 50 passages while retaining barrier-specific characteristics. The new cell line, termed TY09, has a longer lifespan *in vitro* and retains its barrier-specific nature like TY08. In addition, we compared TY09 with the hCMEC/D3 cell line with respect to transendothelial permeability of various substances. Our results suggest that TY09 is a useful *in vitro* BBB model for estimating drug permeability across the human BBB and to understand the mechanisms underlying the BBB insufficiency in a number of neurological diseases.

Methods

Materials

The polyclonal rabbit anti-occludin, rabbit anti-zonula occludens-1 (ZO-1) and rabbit anti-claudin-5 antibodies were obtained from Zymed (San Francisco, CA, USA). Fluorescein isothiocyanate (FITC)-conjugated secondary antibodies were also purchased from Zymed. Polyclonal goat anti-hTERT, anti-von Willebrand factor (vWF) antigen, polyclonal rabbit anti-multidrug resistance-associated protein 4 (MRP4), mouse monoclonal anti-γ-tubulin and anti-actin were obtained from Santa Cruz Biotechnologies (Santa Cruz, CA, USA). The polyclonal anti-SV40 T antigen antibody was purchased from Calbiochem (Darmstadt, Germany). The monoclonal mouse anti-P-glycoprotein (P-gp) antibody was obtained from Covance (Dedham, MA, USA). Verapamil was purchased from WAKO (Osaka, Japan). Rhodamine 123 was obtained from Sigma (St. Louis, MO, USA). The retrovirus vector, pDON-AI, was purchased from TAKARA Bio (Otsu, Japan). [^{14}C]-Epigallocatechin gallate ([^{14}C]-EGCG), [^{14}C]-resveratrol, [^{14}C]-carvacrol and [^{14}C]-thymoquinone were kindly provided by DSM (Kaiseraugst, Switzerland). [^{3}H]-Sucrose was purchased from American Radiolabeled Chemicals (St. Louis, MO, USA). Lucifer yellow CH dilithium salt and sodium pyruvate were obtained from Sigma (Buchs, Switzerland). 1,1′-dioctacecyl-3,3,3′,3′-tetramethyl indocarbocyanine perchlorate acetylated low-density lipoprotein (DiI-Ac-LDL) was purchased from Biogenesis (Poole, England). The rat tail collagen type I solution was purchased from Becton Dickinson (Allschwil, Switzerland). Transwell polycarbonate membrane inserts (0.4 μm pore size, 12 mm insert diameter) were obtained from Corning (Baar, Switzerland) and culture flasks were purchased from Techno Plastic Products (TPP) AG (Trasadingen, Switzerland). Basic fibroblast growth factor (FGF) was obtained from R&D Systems (Abingdon, UK). HEK293 cells were purchased from Japan Health Sciences Foundation (Osaka, Japan). Immortalized human brain capillary endothelial cells (hCMEC/D3)[8] were obtained under license from the Institut National de la Santé et de la Recherche Médicale (Paris, France).

Culture media

Cells were cultured in endothelial cell (EC) growth medium (EBM-2 medium supplemented with EGM-2 MV [Cambrex, Walkersville, MD, USA], 20% fetal bovine serum (FBS), 100 U/mL penicillin [Sigma], 100 μL/mL streptomycin [Sigma] and 25 ng/mL amphotericin B [Invitrogen (Grand Island, NY, USA)]).

Production of TY09 cells harboring *tsA58* and *hTERT*

The study protocol for human brain tissue was approved by the ethics committee of the Medical Faculty of Yamaguchi University, and the study was carried out in accordance with the Declaration of Helsinki, as amended in Somerset West in 1996. Written informed consent was obtained from the participant before entering the study. Isolation of HBMEC and establishment of TY08 cells were described in our previous report.[9] In the present study, we first added the cDNA of hTERT from pcDNA3/*hTERT* into pcDON-AI. The pcDNA3/*hTERT* was a kind gift from Dr Tetsuya Terasaki, Tohoku University, Japan. TY08 (passage 8) cells were incubated overnight with a retrovirus containing pDON-AI/*hTERT*. After 24 h, the cells were washed with 1 × Hanks' balanced salt solution (HBSS; Invitrogen) several times and were subsequently grown on type I collagen-coated dishes (Iwaki, Tokyo, Japan) at 33°C in a humidified atmosphere of 5% CO_2 and 95% air. We fully characterized this newly constructed cell line (TY09).

© 2012 Japanese Society for Neuroimmunology

Immunocytochemistry

The cells were fixed in 4% paraformaldehyde (Wako, Osaka, Japan) for 15 min at room temperature in preparation for von Willebrand factor immunocytochemistry. Next, the cells were permeabilized with 0.1% Triton X-100 (Sigma) for 10 min and then blocked with 1% bovine serum albumin in phosphate-buffered saline (PBS) for 1 h. The cells were fixed with 100% ethanol for 30 min at 4°C for the staining of claudin-5, occludin, and ZO-1, then, were washed three times in PBS, permeabilized with 1% Triton X-100 for 20 min at room temperature, washed again in PBS and blocked with 0.1% FBS before staining. After several washes with PBS, the cells were incubated with the relevant antibodies (1:50 dilution) at 4°C overnight. The cells were subsequently washed with PBS and incubated with FITC-conjugated secondary antibodies (1:200 dilution) for 1 h at room temperature.

Transendothelial electrical resistance studies

The Transwell inserts (pore size 0.4 μm; effective growth area 0.3 cm^2; BD Bioscience, Franklin Lakes, NJ, USA) were coated with rat tail collagen type I (BD Bioscience) in accordance with the manufacturer's instructions. The cells were seeded at a density of 1.0×10^4 cells per insert. The cells were grown at 33°C. After allowing the cells to attach to the bottom of the insert (24–48 h) and become confluent, the transendothelial electrical resistance (TEER) of cell layers was measured with a Millicell electrical resistance apparatus (Endohm-6 and EVOM; World Precision Instruments, Sarasota, FL, USA).

Reverse transcription polymerase chain reaction analysis

Total RNA was prepared from PBS-washed TY09 cells using an RNeasy Plus Mini kit (Qiagen, Hilden, Germany). Reverse transcription (RT) and polymerase chain reaction (PCR) amplifications were carried out with TAKARA PCR Thermal Cycler Dice (TaKaRa, Otsu, Japan). Single-stranded cDNA was synthesized from 500 ng of total RNA using the StrataScript First Strand Synthesis System (STRATAGENE, Cedar Greek, TX, USA) with an oligo-dT primer, and sequential PCR was carried out with TaKaRa Ex Taq (TaKaRa). Temperature cycling conditions for each primer consisted of 5 min at 94°C followed by 40 cycles for 1 min at 94°C, 1 min at 55–65°C and 1 min at 72°C, with a final extension for 10 min at 72°C. The sequence specificity of each primer pair was shown in our previous report.[9]

Western blot analysis

Protocols were previously described.[9] We exposed transblotted, blocked proteins for 1–2 h to primary antibodies (1:100), and then probed the proteins with secondary antibodies (1:2000) for 1 h. The membranes were extensively washed and visualized by enhanced chemiluminescence detection reagents (ECL-prime, Amersham, UK).

Transendothelial transport experiments

For transport assays, TY09 and hCMEC/D3 cells were seeded on type I collagen precoated polycarbonate Transwell filters (pore size 0.4 μm, 1.1 cm^2 filter surface) at a density of 5×10^4 cells per cm^2. The TY09 cells were cultured in EC growth medium for 7 days at 33°C and for 1 day at 37°C. The growth medium was changed every 2–3 days. The hCMEC/D3 cells were cultured for 8 days at 37°C in growth factor-depleted medium (EBM-2 supplemented with 1 ng/mL basic fibroblast growth factor (bFGF), 2.5% fetal calf serum (FCS), 0.55 μmol/L hydrocortisone, 10 mmol/L HEPES and penicillin-streptomycin), which was changed every 3–4 days. The cell culture medium was replaced with prewarmed transport buffer (Hank's balanced salt solution [HBSS] supplemented with 10 mmol/L HEPES and 1 mmol/L Na-Pyruvate, pH 7.4) before the beginning of the transport assays. A 1.5-mL aliquot of transport buffer was added to the basolateral side, and 0.5 mL of transport buffer containing the test substances was applied to the apical donor compartment. For the transport studies of the radiolabelled compounds, 0.3 μCi [^{3}H]-sucrose and 0.3 μCi [^{14}C]-epigallocatechin gallate ([^{14}C]-EGCG), [^{14}C]-resveratrol, [^{14}C]-carvacrol or [^{14}C]-thymoquinone were added to the apical donor compartment of a Transwell filter insert. It should be noted that the extracellular marker [^{3}H]-sucrose was always combined with [^{14}C]-test compound in the same experiment to provide a control for cellular tightness. After 5, 10, 20, 30, 45 and 60 min, 100-μL samples were collected from the basolateral acceptor compartment and were replaced by fresh prewarmed transport buffer. Additionally, a sample of 100 μL was taken from the stock solution. Each sample was then mixed with 2 mL of liquid scintillation cocktail (Ultima gold XR scintillation liquid, Perkin Elmer, Waltham, MA, USA) and the radioactivity was measured using a Packard 2000CA

© 2012 Japanese Society for Neuroimmunology

Tri-Carb β-liquid scintillation counter (Perkin Elmer, Boston, MA, USA). The monolayer integrity and paracellular permeability were determined using the extracellular marker, Lucifer yellow, after the indicated number of days after seeding. The transport assays were carried out as described earlier. The initial applied concentration of Lucifer yellow was 10 μmol/L. Lucifer yellow was quantified by fluorescence spectroscopy using a Spectramax M2 spectrophotometer (Molecular Devices, Sunnydale, CA, USA). The excitation and emission wavelengths were set to 430 nm and 535 nm, respectively. Permeability coefficients were calculated according to equations 1 and 2:

$$\text{Clearance (mL)} = \text{CL (mL)} = X/C_d \quad (1)$$

Where X is the cumulative amount of drug transported to the acceptor compartment and C_d is the concentration of the substance in the donor compartment at each time-point. C_d is calculated by subtracting the accumulated transported amount of drug from the initial amount in the donor compartment determined from the stock solution. CL refers to the total cleared volume at each time-point. The permeability-surface area product (PS) is determined by plotting Cl as a function of time. The slope of the curve represents the PS value. The PS values of the cell monolayer plus filter (PS_{total}) and the porous filter (PS_{filter}) were determined and used for the calculation of the permeability coefficient (P_e) according to the following equations:

$$1/PS_e = 1/PS_{total} - 1/PS_{filter}; P_e = PS_e/A \quad (2)$$

A is the surface area of the filter. The P_e ratios were obtained by normalization of the P_e values of the test compound (P_e test) with the corresponding P_e values of the extracellular marker sucrose (P_e sucrose): P_e ratio = P_e test/P_e sucrose.

Statistical analysis

All data are represented as means ± SEM, and the number of experiments, n, is shown each time. Statistical significance was determined by Student's t-test. $P < 0.05$ was considered statistically significant.

Results

Establishment of the TY09 cell line

A new human brain microvascular endothelial cell line, termed TY09, was successfully generated using a retrovirus encoding the open reading frame of *hTERT*. The expression of *hTERT* by TY09 was confirmed by western blot (Fig. 1a) and immunohistochemical analyses (Fig. 1b). TY09 cells were closely packed and showed contact inhibition at confluence. They maintained a spindle-shaped morphology after the acquisition of *hTERT* (Fig. 2a). In addition, they preserved the uptake of DiI-Ac-LDL and expression of vWF antigen at passage 35 and passage 46, respectively (Figs. 2b–d).

Temperature sensitivity of TY09 cells

TY09 cells showed robust proliferation at the permissive temperature of 33°C, with a doubling time of approximately 2 days. One day after the temperature shift from 33°C to 37°C, the cell growth was stopped (Fig. 3a). Two days after the temperature shift from 33°C to 37°C, the amount of large T-antigen in these cells decreased and was further reduced 7 days after the temperature shift (Fig. 3c). The TY09 cells grew stably for more than 60 passages when they were cultured at 33°C, retaining

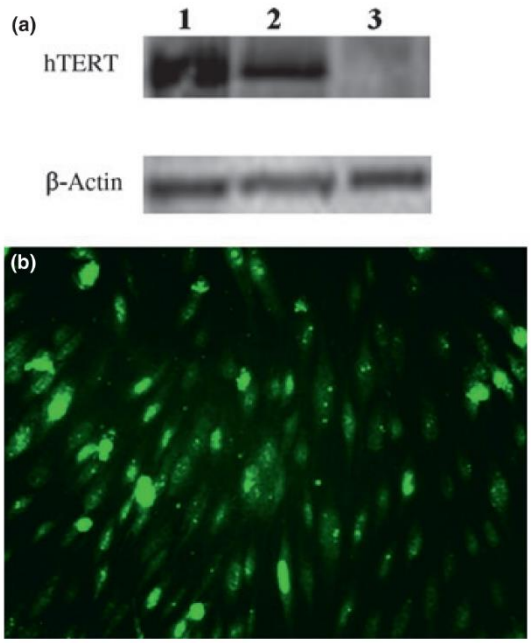

Figure 1 TY09 cells express human telomerase. (a) The result of a western blot analysis for the expression of the human telomerase reverse transcriptase (*hTERT*) protein in TY09 cells (passage 18). The *hTERT* protein was detected in the TY09 cells as well as in HEK293 cells harboring *hTERT* gene. Lane 1, TY09 cells. Lane 2, HEK293 cells transfected with the plasmid harboring the *hTERT* gene as a positive control. Lane 3, HEK293 cells as a negative control. (b) The immunocytochemical staining for the *hTERT* protein in TY09 cells.

© 2012 Japanese Society for Neuroimmunology

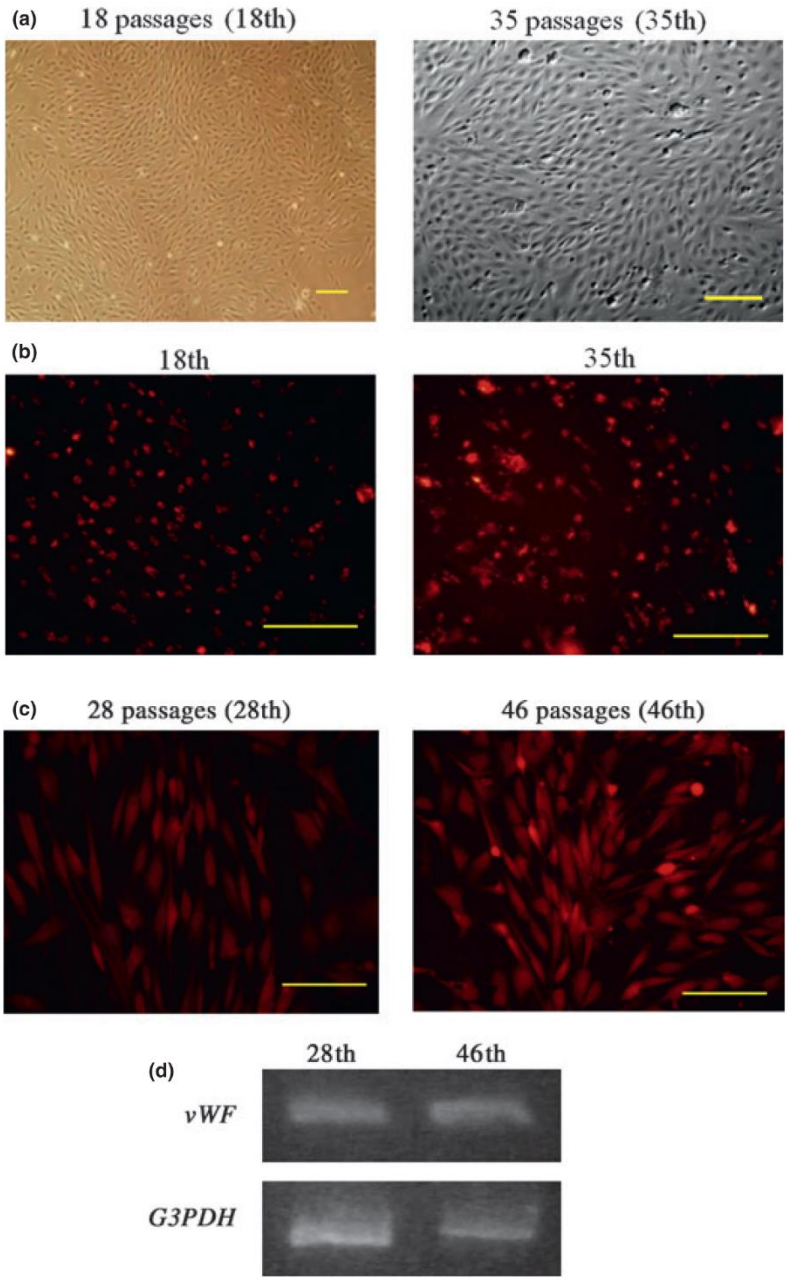

Figure 2 The morphology and the maintenance of the endothelial nature of TY09 cells. (a) Low- and high-passage TY09 cells maintained their spindle-shaped morphology, with contact inhibition at both passages as shown by phase contrast microscopy and differential interference contrast microscopy (DIC), respectively. (b) To label TY09 cells with DiI-Ac-LDL, the cells were incubated with 10 μg/mL DiI-Ac-LDL at 33°C in the culture medium overnight. All of the low- and high-passage cells (passage 18 and 35) were positive for DiI-Ac-LDL. (c) Immunostaining of the TY09 cells (passage 28 and 46) using an anti-von Willebrand factor antibody. (d) The expression of von Willebrand factor mRNA in TY09 cells (passage 28 and 46) was detected by reverse transcription polymerase chain reaction. Bars, 200 μm.

their spindle-shaped morphology (data not shown). However, once the cells were seeded at 37°C, they gradually swelled and never became as confluent as they did when incubated at 33°C (Fig. 3b). In general, primary cultures of HBMEC become swollen after several passages. These results show that TY09 cells grew stably as immortalized cells at the permissive temperature and escaped from their tumor-like features at the non-permissive temperature. This indicates that the TY09 cells preserved their temperature-sensitive nature, despite their expression of *hTERT*, and maintained the ability to revert to endothelial cells that had not been immortalized.

© 2012 Japanese Society for Neuroimmunology

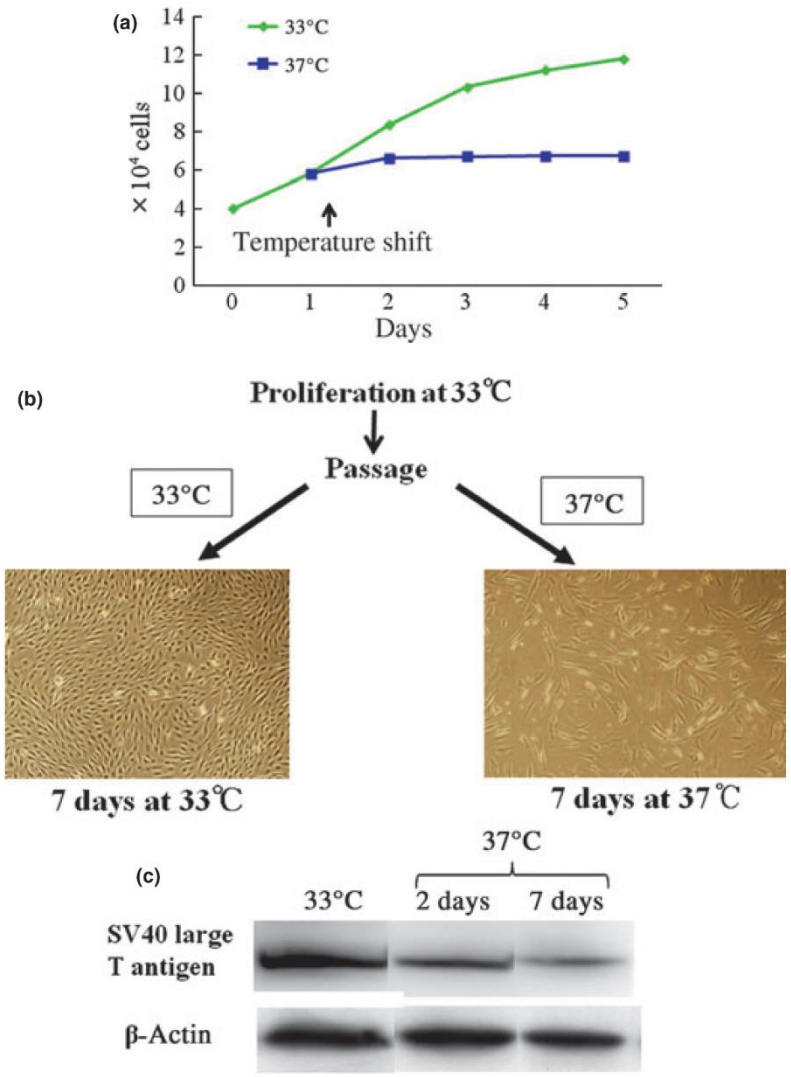

Figure 3 The temperature-sensitive nature of the TY09 cells. (a) TY09 cells (passage 35) proliferated readily at the permissive temperature of 33°C. One day after the temperature shift from 33°C to 37°C, the cell growth was arrested. (b) The morphological difference in the TY09 cells at the permissive and non-permissive temperature. This cell line shows robust proliferation under the permissive temperature, regardless of the passage number, with cells preserving their BBB-specific morphology. Once the cells were spread on dishes at 37°C, however, they gradually lost their capacity for proliferation and thereafter became swollen. As a result, they resemble the cells derived from the central nervous system that have not been immortalized. (c) The amount of the *tsA58* protein expressed in the TY09 cells at permissive and non-permissive temperatures. Two days after the shift to 37°C, the amount of the protein in the TY09 cells began to decrease, and declined further at 7 days. Three independent experiments were carried out. The result from one representative experiment is presented.

Expression of tight junction molecules in the TY09 cells

Several proteins have been reported to be localized at tight junctions, including occludin,[10] claudin-5,[11] claudin-12,[11,12] ZO-1, ZO-2[13] and junctional adhesion molecule A (JAM-A).[14] The expression of claudin-5, claudin-12, occludin, ZO-1 and JAM-A was confirmed in the TY09 cells. It should be noted that ZO-2 mRNA was expressed at very low levels (data not shown). The mRNA quantities of each molecule in high-passage cells (passage 46) were as high as those in the low-passage cells (passage 18; Fig. 4a). Claudin-5[11,12] and occludin[10,15] play a key role in the barrier properties of brain capillary endothelial cells. Therefore, the expression of claudin-5 and occludin was investigated in the TY09 cells at the protein level by western blot analysis. Importantly, the high-passage TY09 cells (passage 50) also maintained their expression of both molecules at the protein level (Fig. 4b). Two bands for occludin were detected, which correspond to two different isoforms of occuldin monomers of 60 and 65 kDa.[16] No significant differences in the expression levels of tight junction-associated molecules between the low- and high-passage TY09 cells were apparent. We further investigated the subcellular localization pattern of these tight junction molecules in the TY09 cells (passage 30) by the immunohistochemical analyses. Claudin-5, occludin and ZO-1 were all localized at the cell–cell boundaries in the TY09 cells (Figs. 4c–e).

© 2012 Japanese Society for Neuroimmunology

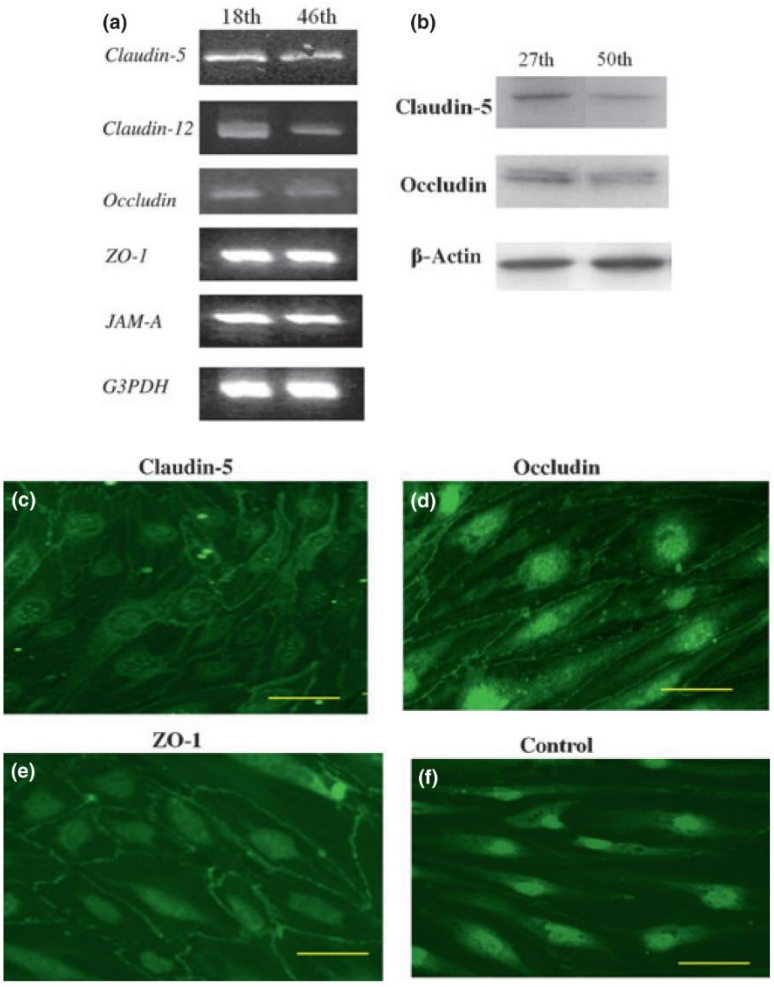

Figure 4 The expression of tight junctional molecules by the TY09 cells. (a) The expression of claudin-5, claudin-12, occludin, ZO-1 and JAM-A mRNA in low-passage (passage 18) and high-passage (passage 46) TY09 cells was analyzed by reverse transcription polymerase chain reaction. G3PDH was used as a control. (b) The western blot analysis of claudin-5 and occludin expression in low-passage (passage 27) and high-passage (passage 50) TY09 cells. β-actin was shown as a reference. (c–f) Immunocytochemical staining of tight junction proteins in confluent TY09 cells (passage 30). Rabbit anti-claudin-5, rabbit anti-occludin and rabbit anti-ZO-1 antibodies were used as primary antibodies and fluorescein isothiocyanate (FITC)-conjugated anti-rabbit immunoglobulin G as secondary antibodies. (c) Claudin-5, (d) occludin and (e) ZO-1 were all continuously detected at the cell–cell boundaries in the TY09 cells. (f) As a negative control, we carried out the staining only with FITC-conjugated anti-rabbit immunoglobulin G secondary antibodies. (c–e) A weak staining of the nuclei is caused by unspecific binding of the secondary antibody, as shown in (f) the corresponding negative control experiment. Bars, 100 μm.

Barrier function of the TY09 cells

To examine the fundamental barrier properties of TY09 cells, their permeability to Lucifer yellow and the TEER across the cell monolayers were tested. The permeability of the extracellular marker, Lucifer yellow, across the TY09 cells was measured at defined time-points after seeding. Furthermore, the impact of the incubation for 1 or 2 days at the non-permissive temperature of 37°C on monolayer tightness was investigated. Figure 5 shows that the lowest permeability (P_e value = $0.82 \pm 0.05 \times 10^{-3}$ cm/min) was observed on day 8 after the cells were cultured for 1 day at 37°C. No significant improvement of the monolayer tightness could be achieved when cells had been cultured for 2 days at 37°C within these 8 days in culture (Fig. 5). Next, we investigated whether the TEER value of the TY09 cells declines with the progression of passages. The TEER of high-passage TY09 cells (passage 54) and that of earlier-passage cells (passage 30) were 25.5 ± 0.3 and $26.3 \pm 0.3\ \Omega \cdot cm^2$ ($P = 0.131$). This constantly low level ($<40\ \Omega \cdot cm^2$) of TEER reflects high ionic permeability. However, this finding is a typical property of immortalized brain endothelial cells as shown and discussed previously for the reference human BBB cell lines, hCMEC/D3[8] and TY08.[9]

Transendothelial transport of the TY09 and hCMEC/D3 cells

To evaluate transendothelial transport across TY09 cell monolayers, the permeability of various reference compounds with different physicochemical properties was determined (Fig. 6a). Using a similar experimental protocol, additional transport studies were carried out with hCMEC/D3 cells (Fig. 6b). To monitor the integrity of the cell monolayers, the

© 2012 Japanese Society for Neuroimmunology

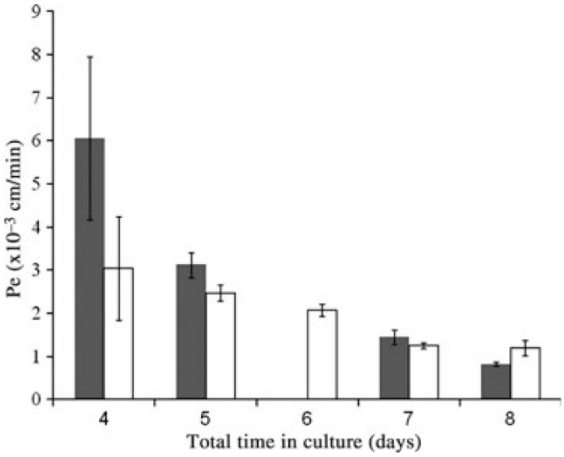

Figure 5 Transendothelial permeability of an extracellular marker (Lucifer yellow) across TY09 cell monolayers. The TY09 cells of passage 31 were cultured at 33°C and differentiated within the total time in culture for either 1 day (black bars) or 2 days (white bars) at 37°C. At defined time-points after seeding, the apical to basolateral transport of Lucifer yellow across the cell monolayers was determined. Differences between the corresponding values at each time-point were statistically not significant ($P > 0.05$). Data represent means ± SEM ($n = 3$).

extracellular marker (sucrose) was used in all experiments. In the hCMEC/D3 cells, the mean P_e value of sucrose was $1.77 \pm 0.25 \times 10^{-3}$ cm/min. This value is in agreement with data published previously.[17] A 30% lower P_e value for sucrose was found in the TY09 cells. Furthermore, the P_e value for Lucifer yellow in the TY09 cells was 40% lower than that of the hCMEC/D3 cells (Table 1). A ranking of the test substances with respect to their transendothelial permeability is shown in Figure 6c and 6d. The P_e values of the test compounds were normalized to the corresponding P_e values of sucrose, and were called the "P_e ratio". In the TY09 cell line, the highly hydrophilic molecule, EGCG, showed the lowest P_e ratio, followed by the less hydrophilic molecule, res-

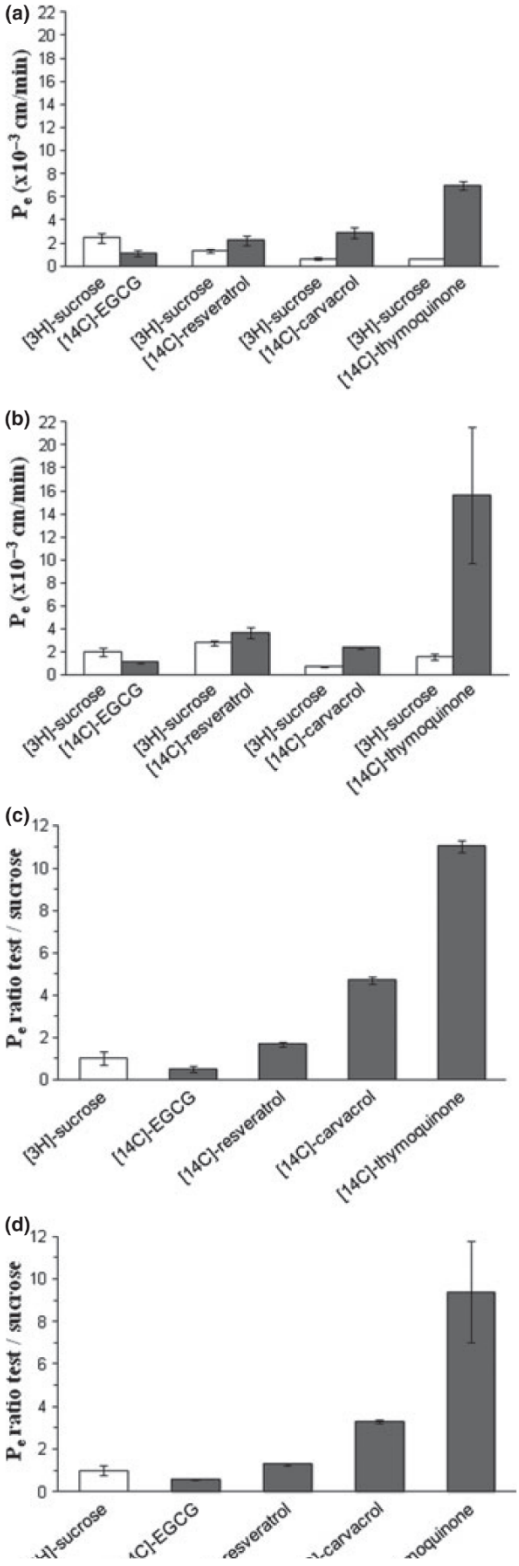

Figure 6 A comparison of two human brain endothelial cell lines, TY09 and hCMEC/D3, with respect to their para- and transcellular permeability. The transendothelial permeation of test compounds of similar molecular weights, but different physicochemical properties, was studied in the presence of the extracellular marker [^{3}H]-sucrose, using TY09 and hCMEC/D3 cell monolayers. Apical to basolateral transport was investigated. Permeability coefficients (P_e) of the test compounds and sucrose were determined in (a) TY09 and (b) hCMEC/D3 cells. In addition, the P_e values of test compounds were normalized to the corresponding P_e values of sucrose in (c) TY09 cells and (d) hCMEC/D3 cells. TY09 cells were of passage 34. White bars represent [^{3}H]-sucrose and dark bars represent test compounds. Values are means ± SEM ($n = 3$).

© 2012 Japanese Society for Neuroimmunology

Table 1 Comparison of the TY09 and hCMEC/D3 cell lines with respect to paracellular permeability of sucrose and Lucifer yellow

	TY09 cells	hCMEC/D3 cells	Ratio TY09/ hCMEC/ D3
P_e sucrose ($\times 10^{-3}$ cm/min)	1.25 ± 0.24, n = 12	1.77 ± 0.25, n = 12	0.7
P_e Lucifer yellow ($\times 10^{-3}$ cm/min)	0.82 ± 0.05, n = 3	1.28 0.05, n = 3	0.6

Values are means ± SEM.

veratrol, and the two highly lipophilic compounds, carvacrol and thymoquinone (Fig. 6c). These data are comparable with results obtained with hCMEC/D3 cells (Fig. 6d). To our knowledge, the permeability to these phytochemicals was investigated for the first time in both of these cell lines.

Expression of transporters even after repeated passages in the TY09

The mRNA expression of various transporters that can mediate blood-to-brain influx in the TY09 cells was examined by a RT–PCR analysis. Both low- (passage 18) and high- (passage 46) passage TY09 cells expressed glucose transporter 1 (GLUT1),[18] System L (LAT1 and 4F2hc),[19] CAT1,[20] MCT1[21] and CRT[22], all of which are major blood-to-brain influx transporters (Fig. 7a). The expression of various brain-to-blood efflux transporters was also examined in both low- (passage 18) and high- (passage 46) passage TY09 cells. These cells expressed multidrug resistance gene 1a (Mdr1a),[23] MRP1, MRP4, MRP5[24] and adenosine triphosphate binding cassette subfamily G member 2 (ABCG2)[25] at the mRNA level (Fig. 7b). The expression of P-gp and MRP4 was also confirmed at the protein level by western blot analysis, whereas the expression level of these proteins was diminished in the high-passage (passage 55) cells compared with the low-passage (passage 24) cells (Fig. 7c).

Functional expression of P-glycoprotein in the TY09 cells

Next, the functionality of P-gp was examined in the TY09 cells at 37°C. The drug accumulation studies with TY09 cells were carried out according to the same methods previously described.[9]

The influence of the P-gp inhibitor, verapamil, on the uptake of the P-gp substrate, rhodamine 123, in the TY09 cells was investigated. Figure 8 shows that verapramil inhibited the function of P-gp, leading to a significantly increased uptake of rhodamine 123 in TY09 cells (Fig. 8). This indicates that the P-gp expressed in the TY09 cells functions as an efflux pump against the P-gp substrates. Importantly, the high-passage cells (passage 56), as well as low-passage cells (passage 22), showed functional expression of P-gp.

Discussion

Normal human cells placed in culture undergo a finite number of divisions and ultimately enter a non-dividing state termed replicative senescence.[26,27] In human cells, replicative senescence is dependent on cumulative cell divisions associated with the progressive shortening of the telomeres, indicating that proliferation is limited by a "mitotic clock".[28,29] When adult somatic cells, such as HBMEC, divide, their telomeres shorten because the cells do not contain functional telomerase. Telomerase is a cellular ribonucleoprotein reverse transcriptase comprising a template RNA (TER) plus *hTERT*, which is absent from adult somatic cells.[30] Consequently, functional telomerase activity can be reconstituted by ectopic expression of *hTERT*.[31]

In a previous study,[9] we developed immortalized TY08 brain capillary endothelial cells. These cells were immortalized using a temperature-sensitive SV40-T antigen (*tsA58*). By this procedure, TY08 cells could gain an additional lifespan of 10–12 passages compared with primary HBMEC. However, these cells did not divide indefinitely. To overcome this limitation, we introduced *hTERT* into the TY08 cells, leading to the development of a new cell line (TY09), which has the ability to divide for at least 60 passages. Interestingly, the TY09 cells maintained their temperature-sensitive nature, even after obtaining functional telomerase activity. The present results are in agreement with those of O'Hare et al., who reported that human mammary microvascular endothelial cells harboring *tsA58* and *hTERT* genes showed temperature-sensitive growth.[32] These results show that the combination of the *tsA58* and *hTERT* in TY09 cells is a good strategy to generate an immortalized human microvascular endothelial cell line. These cells have the advantage of being conditionally immortal, and at the same time, have the potential to differentiate at the non-permissive temperature.

 © 2012 Japanese Society for Neuroimmunology

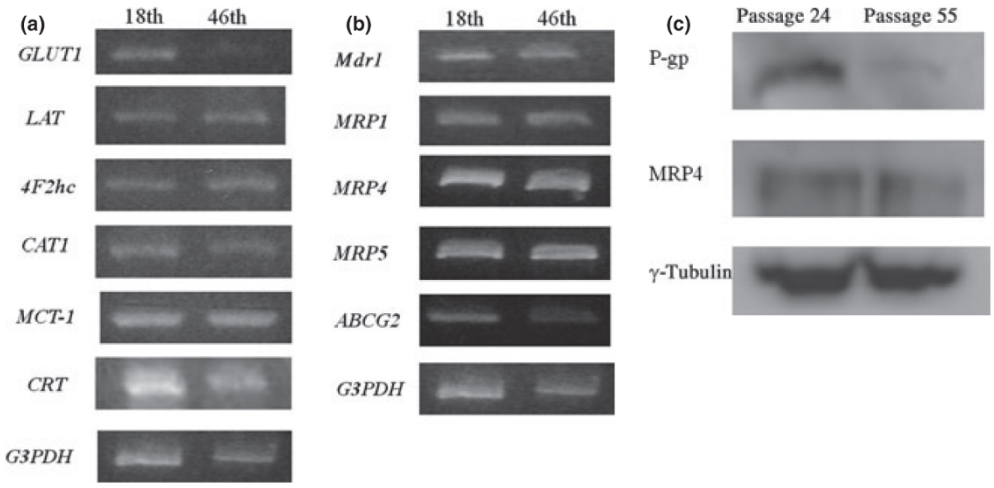

Figure 7 The expression of transporters functioning at the human blood–brain barrier in the TY09 cells. (a) The expression levels of transporters that can mediate influx in the TY09 cells. The expression of GLUT-1, LAT-1, 4F2hc, CAT-1, MCT-1 and CRT mRNA in low-passage (passage 18) and high-passage (passage 46) TY09 cells were examined. G3PDH was used as a control. (b) The expression levels of brain-to-blood efflux transporters in the TY09 cells were also examined. The expression of MDR1 (P-gp), MRP1, MRP4, MRP5 and ABCG2 (BCRP) mRNA in low-passage (passage 18) and high-passage (passage 46) TY09 cells were examined by reverse transcription polymerase chain reaction. G3PDH was used as a control. (c) Western blot analysis of P-gp and MRP4 in low-passage (passage 24) and high-passage (passage 55) TY09 cells. γ-Tubulin was used as a control.

It is noteworthy that the TY09 cells retained BBB-specific properties, and were therefore similar to primary brain endothelial cells. The TY09 cells maintained a spindle-shaped morphology throughout the long-term culture. Active uptake of DiI-Ac-LDL, as well as the expression of vWF, was also observed (Fig. 2). Furthermore, both the low- and high-passage cells expressed important tight junction molecules and various drug transporters, such as P-gp and MRP (Figs 4, 7, 8). We therefore concluded that the TY09 cells maintained the barrier-specific nature and important BBB-specific properties found in TY08 cells, despite the introduction of an additional immortalizing gene, *hTERT*. These properties are constitutively present and are not dependent on the cell passage number.

There is an increasing need for predictive *in vitro* models to study transendothelial drug transport across the blood–brain barrier. Such models can be used for mechanistic investigations or for central nervous system drug screening. Restrictive paracellular permeability is an important criterion for an *in vitro* model to be sensitive enough to discriminate between molecules with high, medium or low permeability across the BBB.[33] The TY09 cells showed restrictive paracellular barrier properties. As shown in Table 1, the permeability values of the extracellular markers were slightly lower compared with those of an established human BBB model, the hCMEC/D3 cell line. The increased tightness of the TY09 cell monolayers allowed for better differentiation between the analyzed substances. The P_e values of

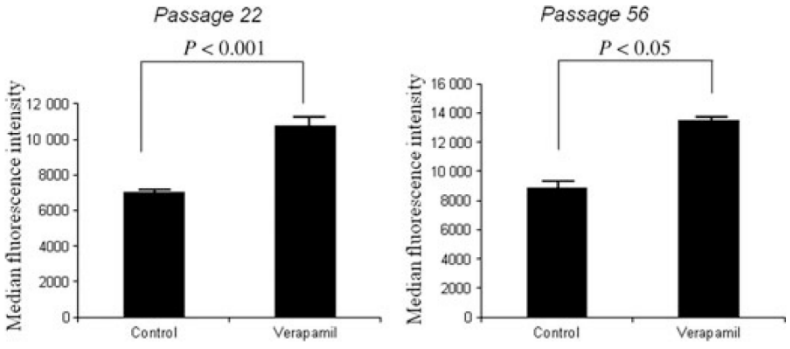

Figure 8 The functionality of the P-gp expressed by TY09 cells (passage 22 and 56). The cellular uptake of rhodamine 123 was measured in the presence or absence of verapamil, a specific inhibitor of P-gp. Verapamil significantly increased the uptake of rhodamine 123 by high-passage (passage 56) cells, as well as low-passage (passage 22) cells. The experiment was carried out in triplicate. The data are presented as the means ± SEM (n = 6).

© 2012 Japanese Society for Neuroimmunology

sucrose obtained using the hCMEC/D3 cells were in agreement with data published previously.[8,16] Therefore, both the TY09 and hCMEC/D3 cell lines can be used to discriminate between molecules with high, intermediate or low BBB permeation rates. In the present study, it was possible to rank a series of test compounds. These compounds included phytochemicals with different physicochemical properties and were predicted to differ with respect to their passive brain permeability.[4,34–36] In particular, their calculated lipophilicity (octanol-to-water partition coefficient, logP) did cover a range from –3.75 (sucrose) to 3.82 (carvacrol). Descriptors were calculated using Molinspiration (www.molinspiration.com).[37] Low transcellular permeability was observed for highly hydrophilic compounds, such as sucrose and epigallocatechin gallate (P_e ratio ≤ 1). Intermediate permeability was determined for resveratrol ($1 < P_e$ ratio < 3). As expected, carvacrol and thymoquinone were characterized by a high permeability (P_e ratio ≥ 3). There was a good correlation between lipophilicity and transcellular permeability. Although there are several *in vitro* BBB models derived from the human brain, the TY09 cells are the only BBB-derived human cell line with *tsA58* and *hTERT*, which possess a temperature-sensitive nature, permitting them to undergo terminal differentiation. This new cell line might be very useful for the development of new therapeutic methods against many inflammatory CNS disorders, and for estimating drug permeability across the human BBB.

Acknowledgements

This study was supported in part by research grants from the Japan Society for the Promotion of Science, Tokyo, Japan (Nos. 21790841 and 23790994).

References

1. Engelhardt B. T cell migration into the central nervous system during health and disease: different molecular keys allow access to different central nervous system compartments. *Clin Exp Neuroimmunol*. 2010; **1**: 79–93.
2. Engelhardt B, Sorokin L. The blood-brain and the blood-cerebrospinal fluid barriers: function and dysfunction. *Semin Immunopathol*. 2009; **31**: 497–511.
3. Joó F. Endothelial cells of the brain and other systems: some similarities and differences. *Prog Neurobiol*. 1996; **48**: 255–73.
4. Pardridge , W.M . The blood-brain barrier: bottleneck in brain drug development. *NeuroRx*. 2005; **2**: 3–14.
5. Perrière N, Yousif S, Cazaubon S, Chaverot N, Bourasset F, Cisternino S, et al. A functional *in vitro* model of rat blood-brain barrier for molecular analysis of efflux transporters. *Brain Res*. 2007; **1150**: 1–13.
6. Terasaki T, Ohtsuki S, Hori S, Takanaga H, Nakashima E., Hosoya K. New approaches to *in vitro* models of blood-brain barrier drug transport. *Drug Discov Today*. 2003; **8**: 944–54.
7. Wilhelm I, Fazakas C, Krizbai IA. *In vitro* models of the blood-brain barrier. *Acta Neurobiol Exp(Wars)*. 2011; **71**: 113–28.
8. Weksler BB, Subileau EA, Perrière N, Charneau P, Holloway K, Leveque M, et al. Blood-brain barrier-specific properties of a human adult brain endothelial cell line. *FASEB J*. 2005; **19**: 1872–4.
9. Sano Y, Shimizu F, Abe M, Maeda T, Kashiwamura Y, Ohtsuki S, et al. Establishment of a new conditionally immortalized human brain microvascular endothelial cell line retaining an *in vivo* blood-brain barrier function. *J Cell Physiol*. 2010; **225**: 519–28.
10. Furuse M, Hirase T, Itoh M, Nagafuchi A, Yonemura S, Tsukita S, et al. Occludin: a novel integral membrane protein localizing at tight junctions. *J Cell Biol*. 1993; **123**: 1777–88.
11. Nitta T, Hata M, Gotoh S, Seo Y, Sasaki H, Hashimoto N, et al. Size-selective loosening of the blood-brain barrier in claudin-5-deficient mice. *J Cell Biol*. 2003; **161**: 653–60.
12. Ohtsuki S, Sato S, Yamaguchi H, Kamoi M, Asashima T, Terasaki T. Exogenous expression of claudin-5 induces barrier properties in cultured rat brain capillary endothelial cells. *J Cell Physiol*. 2007; **210**: 81–6.
13. Biernacki K, Prat A, Blain M, Antel JP. Regulation of cellular and molecular trafficking across human brain endothelial cells by Th1- and Th2-polarized lymphocytes. *J Neuropathol Exp Neurol*. 2004; **63**: 223–32.
14. Yeung D, Manias JL, Stewart DJ, Nag S. Decreased junctional adhesion molecule-A expression during blood-brain barrier breakdown. *Acta Neuropathol*. 2008; **115**: 635–42.
15. Hirase T, Staddon JM, Saitou M, Ando-Akatsuka Y, Itoh M, Furuse M, et al. Occludin as a possible determinant of tight junction permeability in endothelial cells. *J Cell Sci*. 1997; **110**: 1603–13.
16. Liu J, Jin X, Liu KJ, Liu W. Matrix metalloproteinase-2-mediated occludin degradation and caveolin-1-mediated claudin-5 redistribution contribute to blood-brain barrier damage in early ischemic stroke stage. *J Neurosci*. 2012; **32**: 3044–57.
17. Poller B, Gutmann H, Krähenbühl S, Weksler B, Romero I, Courand PO, et al. The human brain endothelial cell line hCMEC/D3 as a human blood-brain barrier model for drug transport studies. *J Neurochem*. 2008; **107**: 1358–68.
18. Cornford EM, Hyman S, Swartz BE. The human brain GLUT1 glucose transporter: ultrastructural localization to

© 2012 Japanese Society for Neuroimmunology

the blood-brain barrier endothelia. *J Cereb Blood Flow Metab*. 1994; **14**: 106–12.
19. Kanai Y, Segawa H, Miyamoto K, Uchino H, Takeda E, Endou H. Expression cloning and characterization of a transporter for large neutral amino acids activated by the heavy chain of 4F2 antigen (CD98). *J Biol Chem*. 1998; **273**: 23629–32.
20. O'Kane RL, Viña JR, Simpson I, Zaragozá R, Mokashi A, Hawkins RA. Cationic amino acid transport across the blood-brain barrier is mediated exclusively by system y+. *Am J Physiol Endocrinol Metab*. 2006; **291**: E412–9.
21. Kido Y, Tamai I, Okamoto M, Suzuki F, Tsuji A. Functional clarification of MCT1-mediated transport of monocarboxylic acids at the blood-brain barrier using *in vitro* cultured cells and *in vivo* BUI studies. *Pharm Res*. 2000; **17**: 55–62.
22. Ohtsuki S, Tachikawa M, Takanaga H, Shimizu H, Watanabe M, Hosoya K, et al. The blood-brain barrier creatine transporter is a major pathway for supplying creatine to the brain. *J Cereb Blood Flow Metab*. 2002; **22**: 1327–35.
23. Schinkel AH, Wagenaar E, Mol CA, Van Deemter L. P-glycoprotein in the blood-brain barrier of mice influences the brain penetration and pharmacological activity of many drugs. *J Clin Invest*. 1996; **97**: 2517–24.
24. Nies AT, Jedlitschky G, König J, Herold-Mende C, Steiner HH, Schmitt HP, et al. Expression and immunolocalization of the multidrug resistance proteins, MRP1-MRP6 (ABCC1-ABCC6), in human brain. *Neuroscience*. 2004; **129**: 349–60.
25. Cisternino S, Mercier C, Bourasset F, Roux F, Scherrmann JM. Expression, up-regulation, and transport activity of the multidrug-resistance protein Abcg2 at the mouse blood-brain barrier. *Cancer Res*. 2004; **64**: 3296–301.
26. Goldstein S. Replicative senescence: the human fibroblast comes of age. *Science*. 1990; **249**: 1129–33.
27. Campisi J. Replicative senescence: an old lives' tale? *Cell*. 1996; **84**: 497–500.
28. Harley CB, Goldstein S. Cultured human fibroblasts: distribution of cell generations and a critical limit. *J Cell Physiol*. 1978; **97**: 509–16.
29. Allsopp RC, Vaziri H, Patterson C, Goldstein S, Younglai EV, Futcher AB, et al. Telomere length predicts replicative capacity of human fibroblasts. *Proc Natl Acad Sci USA*. 1992; **89**: 10114–8.
30. Cerni C. Telomeres, telomerase, and myc An update. *Mutat Res*. 2000; **462**: 31–47.
31. Bodnar AG, Ouellette M, Frolkis M, Holt SE, Chiu CP, Morin GB, et al. Extension of life-span by introduction of telomerase into normal human cells. *Science*. 1998; **279**: 349–52.
32. O'Hare MJ, Bond J, Clarke C, Takeuchi Y, Atherton AJ, Berry C, et al. Conditional immortalization of freshly isolated human mammary fibroblasts and endothelial cells. *Proc Natl Acad Sci USA*. 2001; **98**: 646–51.
33. Gumbleton M, Audus KL. Progress and limitations in the use of *in vitro* cell cultures to serve as a permeability screen for the blood-brain barrier. *J Pharm Sci*. 2001; **90**: 1681–98.
34. Clark DE. In silico prediction of blood-brain barrier permeation. *Drug Discov Today*. 2003; **8**: 927–33.
35. Kelder J, Grootenhuis PD, Bayada DM, Delbressine LP, Ploemen JP. Polar molecular surface as a dominating determinant for oral absorption and brain penetration of drugs. *Pharm Res*. 1999; **16**: 1514–9.
36. Waterhouse RN. Determination of lipophilicity and its use as a predictor of blood-brain barrier penetration of molecular imaging agents. *Mol Imaging Biol*. 2003; **5**: 376–89.
37. Van Damme S, Langenaeker W, Und Bultinck P. Prediction of blood–brain partitioning: a model based on ab initio calculated quantum chemical descriptors. *J Mol Graph Model*. 2008; **26**: 1223–36.

© 2012 Japanese Society for Neuroimmunology

3.2 Pharmacological Characterization of Designer Cathinones *in Vitro*

L.D. Simmler,[1] T.A. Buser,[1] M. Donzelli,[1] Y. Schramm,[2] L.-H. Dieu,[3] J. Huwyler,[3] S. Chaboz,[4] M.C. Hoener[4] and M.E. Liechti[1]

[1]Division of Clinical Pharmacology and Toxicology, Departments of Biomedicine and Internal Medicine, University Hospital and University of Basel, Basel, Switzerland

[2]Department of Chemistry, University of Basel, Basel, Switzerland

[3]Department of Pharmaceutical Sciences, University of Basel, Basel, Switzerland

[4]Pharmaceuticals Division, Neuroscience Research, F. Hoffmann-La Roche Ltd, Basel, Switzerland

British Journal of Pharmacology (2013) **168** 458–470

British Journal of Pharmacology

DOI:10.1111/j.1476-5381.2012.02145.x
www.brjpharmacol.org

RESEARCH PAPER

Pharmacological characterization of designer cathinones *in vitro*

LD Simmler[1], TA Buser[1], M Donzelli[1], Y Schramm[2], L-H Dieu[3], J Huwyler[3], S Chaboz[4], MC Hoener[4] and ME Liechti[1]

[1]*Division of Clinical Pharmacology and Toxicology, Departments of Biomedicine and Internal Medicine, University Hospital and University of Basel, Basel, Switzerland,* [2]*Department of Chemistry, University of Basel, Basel, Switzerland,* [3]*Department of Pharmaceutical Sciences, University of Basel, Basel, Switzerland, and* [4]*Pharmaceuticals Division, Neuroscience Research, F. Hoffmann-La Roche Ltd, Basel, Switzerland*

Correspondence
Dr Matthias E Liechti, Division of Clinical Pharmacology and Toxicology, University Hospital Basel, Hebelstrasse 2, CH-4031 Basel, Switzerland. E-mail: mliechti@uhbs.ch

Keywords
designer drug; cathinone; amphetamine; legal high; monoamine transporter; serotonin; dopamine; noradrenaline

Received
4 July 2012
Revised
30 July 2012
Accepted
8 August 2012

BACKGROUND AND PURPOSE

Designer β-keto amphetamines (e.g. cathinones, 'bath salts' and 'research chemicals') have become popular recreational drugs, but their pharmacology is poorly characterized.

EXPERIMENTAL APPROACH

We determined the potencies of cathinones to inhibit DA, NA and 5-HT transport into transporter-transfected HEK 293 cells, DA and 5-HT efflux from monoamine-preloaded cells, and monoamine receptor binding affinity.

KEY RESULTS

Mephedrone, methylone, ethylone, butylone and naphyrone acted as non-selective monoamine uptake inhibitors, similar to cocaine. Mephedrone, methylone, ethylone and butylone also induced the release of 5-HT, similar to 3,4-methylenedioxymethamphetamine (MDMA, ecstasy) and other entactogens. Cathinone, methcathinone and flephedrone, similar to amphetamine and methamphetamine, acted as preferential DA and NA uptake inhibitors and induced the release of DA. Pyrovalerone and 3,4-methylenedioxypyrovalerone (MDPV) were highly potent and selective DA and NA transporter inhibitors but unlike amphetamines did not evoke the release of monoamines. The non-β-keto amphetamines are trace amine-associated receptor 1 ligands, whereas the cathinones are not. All the cathinones showed high blood–brain barrier permeability in an *in vitro* model; mephedrone and MDPV exhibited particularly high permeability.

CONCLUSIONS AND IMPLICATIONS

Cathinones have considerable pharmacological differences that form the basis of their suggested classification into three groups. The predominant action of all cathinones on the DA transporter is probably associated with a considerable risk of addiction.

Abbreviations

BBB, blood–brain barrier; DA, dopamine; DAT, dopamine transporter; MBDB, 3,4-methlyenedioxyphenyl-N-methyl-2-butanamine; MDEA, 3,4-methylenedioxy-N-ethylamphetamine; MDMA, 3,4-methylenedioxymethamphetamine; MDPV, 3,4-methylenedioxypyrovalerone; NET, NA transporter; P_e, permeability coefficient; SERT, 5-HT transporter; TA receptor, trace amine-associated receptor

Introduction

Stimulant drug abuse remains a major public health issue worldwide. While 'old stimulants', including cocaine, methamphetamine and amphetamine, and 'entactogens', including 3,4-methylenedioxymethamphetamine (MDMA, ecstasy), 3,4-methylenedioxy-N-ethylamphetamine (MDEA) and 3,4-methlyenedioxyphenyl-N-methyl-2-butanamine

© 2012 The Authors
British Journal of Pharmacology © 2012 The British Pharmacological Society

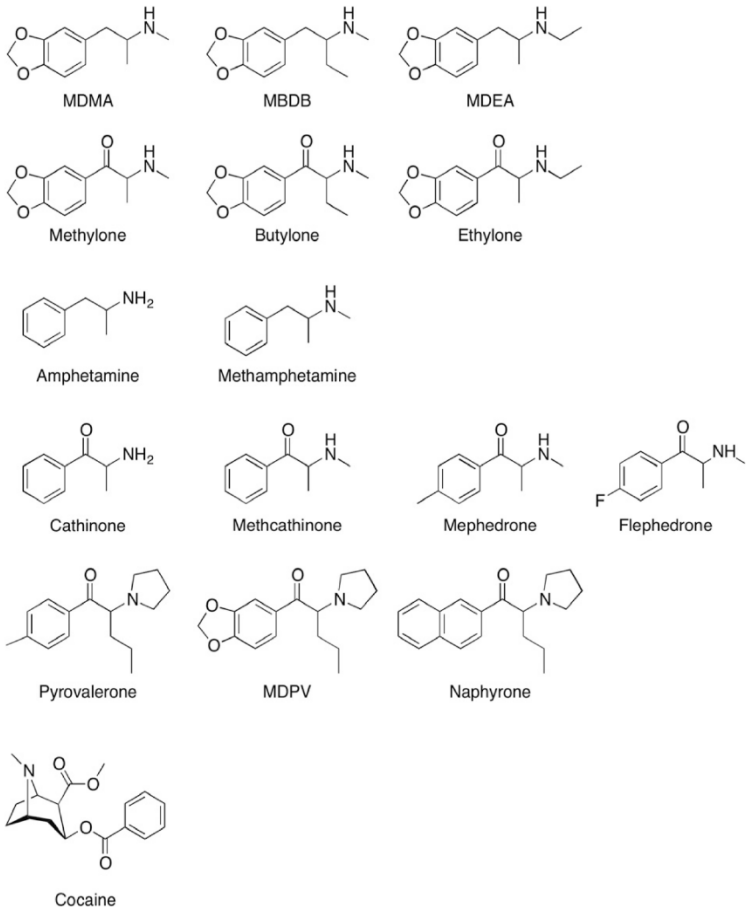

Figure 1
Chemical structures of cathinones, related amphetamines and cocaine.

(MBDB), continue to be used, novel designer cathinones are emerging. Cathinones differ from amphetamines by the presence of a ketone oxygen group at the β-position (Figure 1). The β-keto-amphetamines are distributed as 'bath salts', 'research chemicals' and 'plant food' via the Internet and have been advertised as 'legal highs' with similar psychotropic effects to MDMA or cocaine (Spiller *et al.*, 2011).

As β-keto analogues of amphetamines, cathinones may be expected to have amphetamine-like effects because of their structural similarity. Cathinones enhance DA, NA and 5-HT neurotransmission (Hadlock *et al.*, 2011; Kehr *et al.*, 2011; Baumann *et al.*, 2012; Lopez-Arnau *et al.*, 2012; Martinez-Clemente *et al.*, 2012). However, the molecular pharmacology of this novel class of stimulant drugs is poorly documented. In particular, a systematic comparative characterization of the effects of different cathinones on the human DA, NA and 5-HT transporters and comparisons with classic stimulants are lacking.

In the present study, we assessed the *in vitro* pharmacology of cathinone, methcathinone, mephedrone (4-methylmethcathinone), flephedrone (4-flouromethcathinone), methylone (3,4-methylenedioxymethcathinone, β-keto-MDMA), ethylone (3,4-methylenedioxyethylcathinone, β-keto-MDEA), butylone (β-keto-MBDB), pyrovalerone, 3,4-methylenedioxypyrovalerone (MDPV) and naphyrone (naphthylpyrovalerone). We determined the potencies of these cathinones to inhibit DA, NA and 5-HT transport *in vitro*. We also tested whether cathinones are releasers of DA or 5-HT and characterized the binding affinities of these drugs for monoamine transporters, dopamine D_{1-3} receptors, α_1 and α_2 adrenoceptors, 5-HT_{1A}, 5-HT_{2A} and 5-HT_{2C} receptors, the trace amine-associated receptor 1 (TA_1 receptor) and the histamine H_1 receptor. Finally, blood-brain–barrier (BBB) permeability was assessed using a human *in vitro* model. The pharmacological profiles of the novel cathinones were compared with their non-β-keto amphetamine analogues,

including MDMA, MDEA, MBDB, amphetamine and methamphetamine as well as with cocaine.

Methods

The drug target nomenclature conforms to BJP's *Guide to Receptors and Channels* (Alexander *et al.*, 2011).

Drugs

The hydrochloride salts of the drugs (purity >98.5%) were supplied by Lipomed (Arlesheim, Switzerland), with the exception of naphyrone, which was synthesized according to Meltzer *et al.* (2006). Racemic drugs were used except for D-amphetamine and D-methamphetamine.

Radioligand binding

The radioligand binding assays were performed as described previously (Revel *et al.*, 2011; Hysek *et al.*, 2012c). Briefly, membrane preparations from HEK 293 cells (Invitrogen, Zug, Switzerland) that overexpress the respective human transporters (Tatsumi *et al.*, 1997) or receptors (except for rat/mouse TA_1 receptor) (Revel *et al.*, 2011) were incubated with the radiolabelled selective ligands at concentrations equal to K_d, and ligands displacement by the compounds was measured. Specific binding of the radioligand to the target receptor was defined as the difference between the total binding and nonspecific binding determined in the presence of selected competitors in excess. The following radioligands and competitors were used: *N*-methyl-[^{3}H]-nisoxetine and indatraline (NA transporter [NET]), [^{3}H]-citalopram and indatraline (5-HT transporter [SERT]) and [^{3}H]-WIN35,428 and indatraline (DA transporter [DAT]). [^{3}H]-8-hydroxy-2-(di-*n*-propylamino) tetralin (8-OH-DPAT) and indatraline (5-HT_{1A} receptor), [^{3}H]-ketanserin and spiperone (5-HT_{2A} receptor), [^{3}H]-mesulergine and mianserin (5-HT_{2C} receptor), [^{3}H]-prazosin and risperidone (α_1 adrenoceptor), [^{3}H]-rauwolscine and phentolamine (α_2 adrenergic receptor), [^{3}H]-SCH 23390 and butaclamol (DA D_1 receptor), [^{3}H]-spiperone and spiperone (DA D_2 and D_3 receptors), [^{3}H]-pyrilamine and clozapine (histamine H_1 receptor) and [^{3}H]-RO5166017 and RO5166017 (TA_1 receptor). All radioligands were obtained from Perkin-Elmer (Schwerzenbach, Switzerland), with the exception of [^{3}H]-RO5166017, which was synthesized at Roche (Basel, Switzerland).

Monoamine uptake transporter inhibition

The potencies of the drugs to inhibit the SERT, NET and DAT were evaluated in HEK 293 cells that stably expressed human SERT, NET and DAT (Tatsumi *et al.*, 1997) as previously described (Hysek *et al.*, 2012c). The DAT/SERT ratio was calculated as 1/DAT IC_{50}:1/SERT IC_{50}.

Monoamine release

We assessed DAT- and SERT-mediated DA and 5-HT efflux in HEK 293 cells that overexpressed human DAT or SERT respectively. We cultured the cells in 24-well plates (XF24, Seahorse Biosciences, North Billerica, MA) coated with poly-D-lysine to 70–100% confluency. After removing the culture medium, we added 85 µL release buffer (Krebs–HEPES that contained 130 mM NaCl, 1.3 mM KCl, 2.2 mM $CaCl_2$, 1.2 mM $MgSO_4$, 1.2 mM KH_2PO_4, 10 mM HEPES, 10 mM D-glucose, 0.2 mg·mL^{-1} ascorbic acid and 10 µM pargyline) with 10 nM [^{3}H]-5-HT (SERT cells) or 10 nM [^{3}H]-DA and 1 µM unlabelled DA (DAT cells). We filled the cells with the respective radiolabelled monoamine for 20 min at 37°C. We then removed the buffer and washed twice with warm buffer. We induced [^{3}H]-5-HT and [^{3}H]-DA release by adding 1000 µL release buffer that contained the drugs in different concentrations or controls. We incubated the cells for 15 min at 37°C and shaked at 300 r.p.m. on a rotary shaker. We then stopped the release by removing the buffer and washing the cells twice with ice-cold buffer. The release time was based on the difference between drug-stimulated and spontaneous release (control) over time, which reached its maximum before 15 min. We then added 65 µL lysis buffer and lysed the cells overnight in a refrigerator. We mixed 50 µL of the cell lysate suspension with 2.5 mL UltimaGold and determined radioactivity. The radioactive counts in the cells where no drug was present in the release buffer (control) was defined as 100%, and the percentages of radioactivity that remained in the cells treated with drugs were calculated. Pure uptake transporter inhibitors, including imipramine, citalopram, cocaine and mazindol, have been shown to produce apparent substrate efflux from monoamine-preloaded HEK cells that is explained by inhibition of transporter-mediated re-uptake of the substrate that diffuses out of the cells (Scholze *et al.*, 2000). The DAT inhibitor mazindol and SERT inhibitor citalopram reduced the amount of preloaded DA and 5-HT (mean ± SD) by 15.6 ± 7 and 19.6 ± 8%, respectively, at the maximal concentration of 100 µM (E_{max}) compared with controls. This nonspecific release was subtracted from total release at the maximal drug concentration of 100 µM to yield E_{max} values of specific transporter-mediated release. We considered any drug that produced significantly higher maximal DA efflux compared with mazindol to be a DA releaser and a drug that produced significantly higher maximal 5-HT efflux compared with citalopram as a 5-HT releaser. EC_{50} values were calculated using Prism (GraphPad, San Diego, CA). ANOVA followed by Dunnett's tests were used to compare drug effects with the control condition. Efflux was studied in DAT- and SERT-expressing cells because the action of a drug on the DA and 5-HT system was considered to be relevant for predicting its stimulant-like properties and abuse potential (Rothman and Baumann, 2006).

Cytotoxicity

Cell membrane integrity was verified using the ToxiLight BioAssay Kit (Lonza, Basel, Switzerland) for all of the drugs (10 and 100 µM) after 4 h of incubation at 37°C.

Transendothelial BBB transport

Transendothelial transport was assessed for a selection of compounds using a human *in vitro* BBB permeability model (Sano *et al.*, 2010; 2012). Conditionally immortalized human brain capillary endothelial cells (TY09) were obtained from the Department of Neurology and Clinical Neuroscience, Yamaguchi University, Japan. TY09 cells express the human blood-to-brain influx and brain-to-blood efflux transporters,

form tight cell monolayers and retain BBB-specific properties independent of cell passage number (Sano *et al.*, 2012). The cells were grown in growth medium (EGM-MV BulletKit CC-3125, Lonza, Verviers, Belgium) supplemented with 20% FBS (AMIMED, BioConcept, Allschwil, Switzerland), 100 U·mL^{-1} penicillin (Sigma, Buchs, Switzerland) and 100 mL·mL^{-1} streptomycin (Sigma). The cells were seeded on Transwell polycarbonate membrane inserts (Corning, Baar, Switzerland; 0.4 µm pore size, 12 mm insert diameter) pre-coated with rat tail collagen type 1 solution (Becton Dickinson, Allschwil, Switzerland) at a density of 5×10^4 cells·cm^{-2} and grown to confluence. Before the initiation of the transport studies, the cell culture medium was replaced with pre-warmed transport buffer (HBSS supplemented with 10 mM HEPES and 1 mM Na-Pyruvate, pH 7.4), and 1.5 µM of the test substance was added to the donor compartment of a Transwell filter insert. The extracellular marker Lucifer yellow CH dilithium salt (Sigma) was always combined with the test compound in the same experiment to provide a control for cellular tightness. The initial concentration of Lucifer yellow applied was 10 µM. After 10, 20, 30, 45 and 60 min, 200 µL samples were collected from the acceptor compartment and replaced by buffer. Additionally, a sample of 200 µL was taken from the stock solution and analysed. Lucifer yellow was quantified by fluorescence spectroscopy using a Spectramax M2 spectrophotometer (Molecular Devices, Sunnyvale, CA).

Drug concentrations were determined using HPLC coupled to tandem MS. The analytes were extracted using methanol that contained 0.1 µg·mL^{-1} MDMA-d5 (Lipomed, Arlesheim, Switzerland). Chromatographic separation was performed on a Shimadzu HPLC system (Shimadzu, Reinach, Switzerland). A Reprosil Fluosil 100 PFP column (50 × 2 mm, 2.2 µm, Dr Maisch, Ammerbuch-Entringen, Germany) was used for the separation of the analytes. Eluent A (0.1% formic acid in water) and eluent B (0.1% formic acid in methanol) were used with the following gradient: 5% B for 0–0.4 min, 5–98% B for 0.4–1.9 min, 98% B for 1.9–2.7 min, and 5% B for 2.7–3 min. The mobile phases were delivered at a constant flow rate of 0.35 mL·min^{-1}. The total run time was 3.0 min. The column oven was set at 40°C. The injection volume was 10 µL. MS detection was performed using a triple quadrupole MS (API3200, Applied Biosystems, Rotkreuz, Switzerland) operated in electrospray ionization positive-ion mode. The assays were linear in the concentration range of 1.2–300 ng·mL^{-1} for all of the analytes. The selected mass-to-charge (*m/z*) ratio transitions of the protonated MH$^+$ analyte ions used in selective reaction monitoring mode were the following: MDMA 194 → 163, MDMA-d5 199 → 165, mephedrone 178 → 160, methylone 208 → 160, cocaine 304 → 182, cathinone 150 → 132, methcathinone 164 → 146, amphetamine 136 → 91, methamphetamine 150 → 91, MDPV 276 → 126. The dwell time was set at 20 ms for all of the analytes.

Permeability coefficients were calculated according to Equations 1–3 (Cecchelli *et al.*, 1999):

$$\text{Clearance (mL)} = \text{Cl}^- \text{ (mL)} = X/C_d \quad (1)$$

where X is the cumulative amount of drug transported to the acceptor compartment, and C_d is the concentration of the substance in the donor compartment at each time point. C_{il} is calculated by subtracting the accumulated transported amount of drug from the initial amount in the donor compartment determined from the stock solution. *Cl* refers to the total cleared volume at each time point. The permeability-surface area product (*PS*) is determined by plotting *Cl* as a function of time. The slope of the curve represents the *PS* value. The *PS* values of the cell monolayer plus filter (PS_{total}) and porous filter (PS_{filter}) were determined and used for the calculation of the permeability coefficient (P_e) according to the following equations:

$$1/PS_e = 1/PS_{total} - 1/PS_{filter} \quad (2)$$

$$P_e = PS_e/A \quad (3)$$

where A is the surface area of the filter. The P_e ratios were obtained by normalizing the P_e values of the test compounds (P_e *test*) with the corresponding P_e values of the extracellular marker Lucifer yellow (P_e *Lucifer yellow*): P_e *ratio* = P_e *test*/P_e *Lucifer yellow*. $P_e \leq 1$ indicates low trancellular permeability as observed with highly hydrophilic compounds, such as sucrose. $P_e > 1$ and <3 indicates intermediate permeability, and $P_e \geq 3$ indicates high permeability (Sano *et al.*, 2012). Estimates of partition coefficient (CLogP) values (Ghose *et al.*, 1998) were calculated using ChemDraw Ultra 11 (CambridgeSoft, Cambridge, MA).

Results

Receptor binding profiles

The monoamine transporter and receptor binding affinities are shown in Table 1. Pyrovalerone and MDPV exhibited very high affinity for the DAT and NET in the low nanomolar range (<10 nM), consistent with their high potency as DAT and NET inhibitors (Table 2). Cathinone and methcathinone showed similar monoamine transporter binding profiles to amphetamine and methamphetamine, with binding affinities for the DAT and NET in the low micromolar range (<10 µM) and no affinity for the SERT (>30 µM). Transporter binding affinities for the DAT and SERT were generally lower than the respective potencies as transporter inhibitors for those compounds that also released DA or 5-HT respectively. Mephedrone, flephedrone and methcathinone were the only cathinones that exhibited relevant (<10 µM) 5-HT$_{2A}$ receptor binding. These compounds and cathinone also bound to α_1 adrenoceptors, which was not seen for the other drugs investigated. Cocaine and all of the cathinones showed lower binding affinity for TA$_1$ receptor compared with the non-β-keto analogue amphetamines.

Inhibition of monoamine transporters

The effects of the cathinones and reference substances on monoamine transporter function are shown in Figure 2. IC_{50} values for monoamine transport inhibition and DAT/SERT inhibition ratios are shown in Table 2. Significant differences were observed in the absolute and relative potencies of the cathinones to inhibit monoamine transporter function. Pyrovalerone and its derivative MDPV were the most potent DAT inhibitors, significantly more potent than all of the

Table 1
Monoamine transporter and receptor binding affinities

	NET	DAT	SERT	5-HT$_{1A}$	5-HT$_{2A}$	5-HT$_{2C}$	α_{1A}	α_{2A}	D_1	D_2	D_3	H_1	TA$_{rat}$	TA$_{1mouse}$
MDMA	30.5 ± 8.0	6.5 ± 2.5	13.3 ± 0.6	12.2 ± 0.8	7.8 ± 2.4	>13	>6	15.0 ± 10	>13.6	25.2 ± 12	>17.7	>14.4	0.37 ± 0.12	2.4 ± 1.1
MBDB	11.9 ± 1.4	3.1 ± 0.3	5.80 ± 0.7	15.5 ± 3.8	6.62 ± 1.8	>13	>6	16.9 ± 4	>12.5	NA	>16	>13	1.2 ± 0.1	3.6 ± 1.1
MDEA	6.17 ± 1.4	1.35 ± 0.06	4.32 ± 0.6	18.8 ± 0.78	>13	>13	>6	12.2 ± 0.5	>12.5	NA	>16	>13	0.32 ± 0.6	4.9 ± 1.7
Ethylone	9.89 ± 0.9	1.43 ± 0.4	9.04 ± 0.6	17.0 ± 2.4	>13	>13	>6	>25	>12.5	NA	>16	>13	>12.5	>10
Mephedrone	>25	3.4 ± 0.8	>30	>20	2.1 ± 0.7	>13	3.48 ± 2.2	11.0 ± 5.0	>13.6	>30	>9.2	>14.4	4.3 ± 2.0	>10
Naphyrone	0.18 ± 0.02	0.04 ± 0.01	0.18 ± 0.02	6.00 ± 0.21	11 ± 2.2	>13	>6	8.0 ± 2.8	>12.5	NA	>16	2.28 ± 0.27	>12.5	>10
Butylone	8.13 ± 0.7	0.44 ± 0.03	14.1 ± 4.1	>20	>13	>13	>6	>25	>12.5	NA	>16	>13	>12.5	>10
Cocaine	4.47 ± 2.6	0.28 ± 0.07	1.1 ± 0.09	>20	>13	>13	>6	>20	>13.6	>30	>17.7	>14.4	>10	>10
Methylone	>25	2.73 ± 0.2	>30	>20	>13	>13	>6	>20	>13.6	>30	>9.2	>14.4	>12.5	>10
Flephedrone	>25	12.2 ± 3.1	>30	>20	1.4 ± 0.6	>13	1.52 ± 0.05	>20	>13.6	>30	>17.7	>14.4	5.4 ± 1.7	>10
Cathinone	3.50 ± 2.7	19.8 ± 1.9	>30	>20	>13	>13	5.40 ± 1.1	8.9 ± 2.7	>13.6	>30	>17.7	>14.4	2.2 ± 0.70	2.1 ± 0.73
Methcathinone	1.45 ± 0.7	1.28 ± 0.2	>30	12.7 ± 3.5	3.0 ± 0.6	>13	3.93 ± 1.3	11.9 ± 3.9	>13.6	>30	>9.2	>14.4	4.1 ± 1.2	>10
Amphetamine	1.00 ± 0.6	5.68 ± 3.8	>25	6.74 ± 1.38	>13	>13	>6	2.8 ± 0.8	>13.6	>30	>17.7	>14.4	0.23 ± 0.18	0.09 ± 0.06
Methamphetamine	4.28 ± 2.1	1.85 ± 0.9	26.7 ± 11	8.07 ± 0.75	>13	>13	>6	6.1 ± 1.6	>13.6	>30	>17.7	>14.4	0.35 ± 0.12	0.55 ± 0.2
Pyrovalerone	0.06 ± 0.005	0.03 ± 0.005	4.97 ± 0.3	13.4 ± 2.1	>13	>13	>6	>20	>13.6	>30	>9.2	10.7 ± 1.5	>12.5	>10
MDPV	0.08 ± 0.02	0.01 ± 0.002	2.86 ± 0.1	10.29 ± 4.7	>13	>13	>6	>20	>13.6	>30	>9.2	>14.4	7.2 ± 1.1	>10

Values are K_i given as μM (mean ± SD).
NA, not assessed.

other drugs. The rank order of potency for DAT inhibition was MDPV and pyrovalerone >> naphyrone, cocaine, methamphetamine, amphetamine and methcathinone > butylone, mephedrone, methylone, ethylone, flephedrone and MDEA > cathinone, MDMA and MBDB. The rank order of potency for SERT inhibition was naphyrone, MDEA and MDMA > MBDB, cocaine, ethylone, mephedrone and butylone >> all of the others. The DAT/SERT inhibition ratios ranged from >100 for pyrovalerone and MDPV (mostly DAT inhibition) to 0.08 for MDMA (mostly SERT inhibition). The entactogens MDMA, MBDB and MDEA were the only drugs that blocked the SERT significantly more potently than the DAT (DAT/SERT ratio << 1). Ethylone, mephedrone, naphyrone, butylone and methylone were similar to cocaine, with DAT/SERT selectivity ratios in the range of 1–4. Cathinone and methcathinone were similar to their non-β-keto analogues amphetamine and methamphetamine, with DAT/SERT inhibition ratios >10. The rank order of potency for NET inhibition was pyrovalerone and MDPV > methamphetamine, methcathinone and amphetamine > cathinone, flephedrone, naphyrone and mephedrone > MDMA, cocaine and methylone > MDEA, butylone, ethylone and MBDB. DAT and NET but not SERT inhibition potency (IC_{50}) values were correlated with psychotropic effective doses (Table 2) as reported from experimental studies (Martin *et al.*, 1971) or by recreational users (Derungs *et al.*, 2011) http://www.erowid.org; accessed June 20, 2012). The Spearman rank correlation coefficients were $r_s = 0.73$ and 0.79 respectively (both $P < 0.01$).

Monoamine release

Amphetamine, methamphetamine, cathinone, methcathinone, flephedrone, mephedrone and MDMA released DA through the DAT (Figure 3 and Table 3). However, the potency of MDMA to release DA was low (EC_{50} > 10 μM). The entactogens MDMA, MDEA and MBDB, as well as the cathinones methylone, ethylone, butylone and mephedrone released 5-HT through the SERT. Amphetamine, methamphetamine, methcathinone and flephedrone also released 5-HT, however, only at very high concentrations (EC_{50} > 33 μM). The pyrovalerone derivatives, including pyrovalerone, naphyrone and MDPV, produced no DA or 5-HT efflux similar to cocaine, indicating that these pyrovalerone derivatives act as very potent transporter inhibitors but not substrate releasers.

Cytotoxicity

None of the drugs showed apparent cytotoxicity at the concentrations used in the functional assays.

Transendothelial transport

All of the positively tested drugs exhibited P_e ratios ≥3, indicating high permeability (Table 4). P_e ratios for mephedrone and MDPV were >10, suggesting very high permeability. Additionally, the apical to basolateral transport of MDPV was significantly greater ($P < 0.05$) than basolateral to apical transport, consistent with active transport by one of the blood-to-brain influx carriers. P_e ratios could not be calculated for cocaine and cathinone because of low recovery.

Table 2

Monoamine transport inhibition

	NET IC_{50} (μM) (95% CI)	DAT IC_{50} (μM) (95% CI)	SERT IC_{50} (μM) (95% CI)	DAT/SERT ratio Ratio (95% CI)	Recreational dose* mg
MDMA	0.447 (0.33–0.60)	17 (12–24)	1.36 (1.0–2.0)	0.08 (0.04–0.16)	100
MBDB	2.80 (1.9–4.1)	22 (20–26)	2.04 (1.4–3.0)	0.09 (0.05–0.15)	200
MDEA	1.02 (0.78–1.3)	9.3 (8.0–11)	1.27 (0.93–1.7)	0.14 (0.01–0.21)	125
Ethylone	2.54 (2.0–3.2)	5.68 (4.9–6.5)	4.46 (3.8–5.2)	0.8 (0.6–1.1)	175
Mephedrone	0.254 (0.22–0.30)	3.31 (2.6–4.2)	4.64 (3.7–5.9)	1.4 (0.9–2.4)	150
Naphyrone	0.25 (0.20–0.32)	0.47 (0.40–0.55)	0.96 (0.85–1.09)	2.0 (1.5–2.7)	25
Butylone	2.02 (1.5–2.7)	2.90 (2.5–3.4)	6.22 (4.3–9.0)	2.1 (1.3–3.6)	150
Cocaine	0.451 (0.38–0.59)	0.768 (0.6–1.0)	2.37 (2.0–2.9)	3.1 (2–4.8)	75
Methylone	0.542 (0.39–0.75)	4.82 (3.8–6.1)	15.5 (10–26)	3.3 (1.5–6.8)	150
Flephedrone	0.246 (0.16–0.37)	6.35 (4.2–9.5)	>10	5.8 (0.8–41)	200
Cathinone	0.199 (0.15–0.26)	14.0 (10–20)	>100	>10	50
Methcathinone	0.085 (0.06–0.17)	1.12 (0.83–1.5)	>10	>10	59
Amphetamine	0.094 (0.06–0.14)	1.30 (0.83–2.0)	>10	>10	30
Methamphetamine	0.064 (0.04–0.09)	1.05 (0.74–1.5)	>10	>10	30
Pyrovalerone	0.043 (0.03–0.06)	0.035 (0.03–0.04)	13.0 (10.8–15.8)	>100	20
MDPV	0.044 (0.03–0.07)	0.031 (0.03–0.04)	9.30 (6.8–12.8)	>100	5

Values are means of three to four independent experiments and 95% confidence intervals (CI).
Drugs are ranked according to the DAT/SERT ratio = 1/DAT IC_{50} : 1/SERT IC_{50}.
*Estimated average.

Discussion

All of the cathinones were inhibitors of the monoamine transporters, but their selectivity for the SERT, NET and DAT varied considerably. Further, most of the compounds were substrate releasers. Thus, important pharmacological differences were found between different cathinones. We classified the cathinones into three groups based on, firstly, their relative potency to act as SERT, NET and DAT inhibitors and, secondly, their action as substrate releasers: (1) cocaine-MDMA-mixed cathinones (including mephedrone, methylone, ethylone, butylone and naphyrone, which act as relatively nonselective monoamine uptake inhibitors similar to cocaine and, with the exception of naphyrone, also as MDMA-like 5-HT releasers); (2) methamphetamine-like cathinones (including cathinone, methcathinone and flephedrone, which act as preferential catecholamine inhibitors and DA releasers, similar to amphetamine and methamphetamine); and (3) pyrovalerone–cathinones (including pyrovalerone and MDPV, which act as very potent and selective catecholamine uptake blockers but not substrate releasers).

The potency of drugs of abuse to inhibit the NET and DAT or activate the NA and DA system is associated with their psychostimulant effects and enhanced abuse liability (Rothman *et al.*, 2001). Consistently, we found that the doses of the drugs abused by humans correlated with their potency to inhibit catecholamine transport. In contrast, relatively increased activation of the 5-HT system is linked to a reduction in abuse potential (Wee *et al.*, 2005; Rothman and

Table 3

Monoamine release from monoamine-preloaded cells

	DAT EC_{50} (μM) (95% CI)	SERT EC_{50} (μM) (95% CI)
MDMA	22 (8.9–53)	5.63 (3.5–9.2)
MBDB	>100	2.49 (1.0–6.9)
MDEA	>100	2.88 (1.6–5.0)
Ethylone	>100	9.90 (2.4–40)
Mephedrone	3.75 (1.7–8.4)	5.98 (3.2–11)
Naphyrone	>100	>100
Butylone	>100	5.5 (1.8–17)
Cocaine	>100	>100
Methylone	>100	>10
Flephedrone	12.5 (5.7–28)	>33
Cathinone	5.64 (3.0–10)	>100
Methcathinone	2.36 (1.7–3.3)	>33
Amphetamine	1.76 (1.1–2.9)	>33
Methamphetamine	1.56 (0.9–2.8)	>33
Pyrovalerone	>100	>100
MDPV	>100	>100

Values are means.

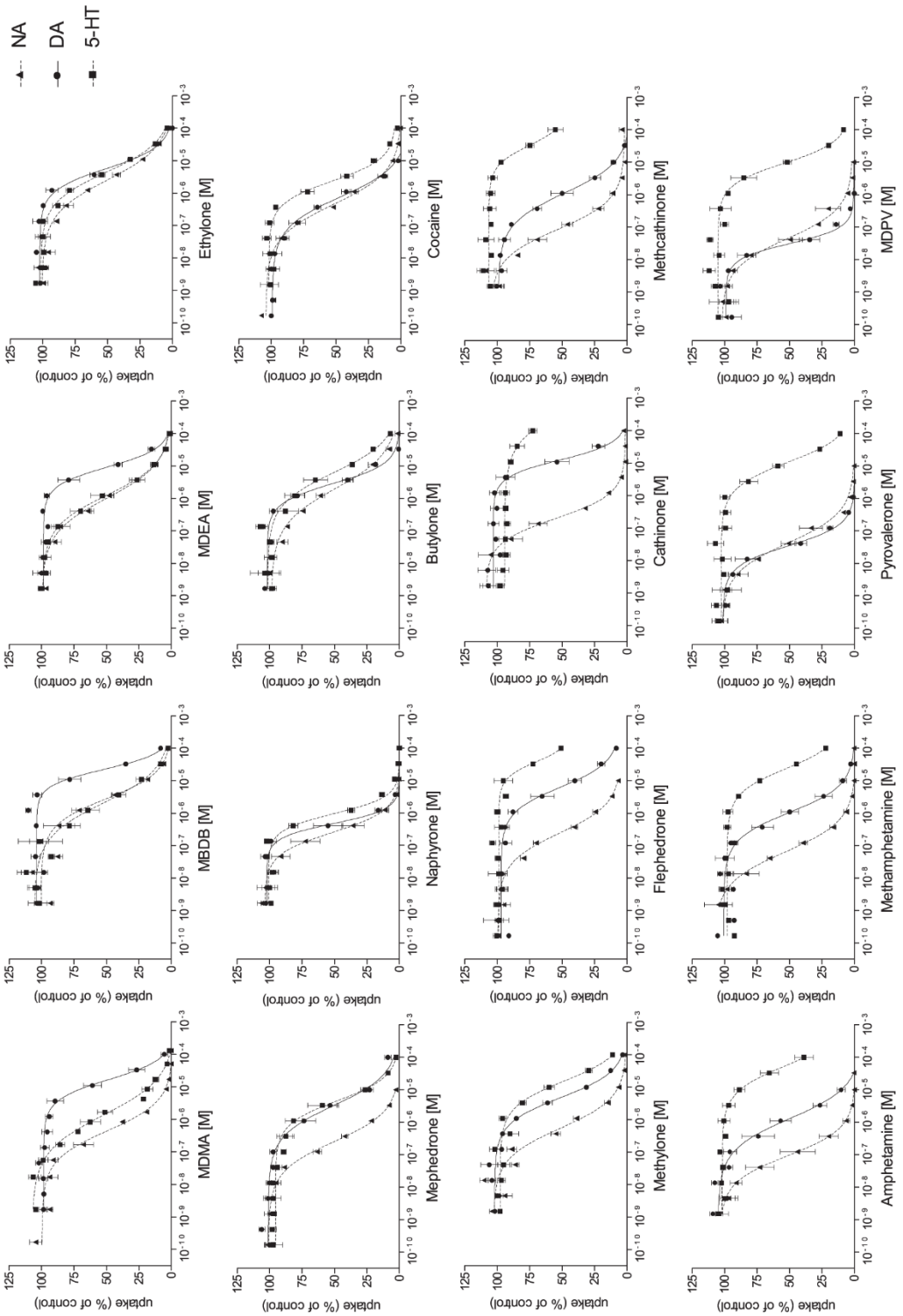

Figure 2
Monoamine uptake inhibition. Potencies of different drug concentrations to inhibit the accumulation of NA, DA and 5-HT into NA, DA and 5-HT transporter-transfected HEK 293 cells respectively. The data are expressed as the mean ± SEM of three to five independent experiments. The lines show the data fit by nonlinear regression. IC_{50} values are presented in Table 2.

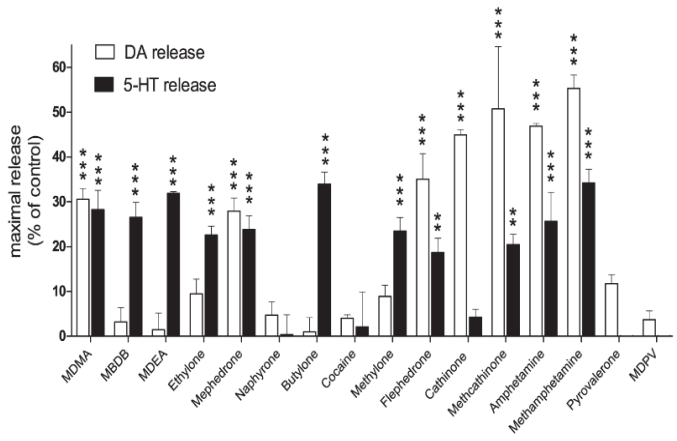

Figure 3

Dopamine and 5-HT release. HEK 293 cells that stably express the DA or 5-HT transporter were preloaded with [^{3}H]-DA or [^{3}H]-5-HT, respectively, washed and incubated with drugs. Transporter-mediated release is expressed as % reduction in monoamine cell content at the maximal drug concentration (100 μM) compared with controls. $^{**}P < 0.01$, $^{***}P < 0.001$, significant effects compared with controls. The EC_{50} values are shown in Table 3. The data are expressed as the mean ± SEM of three independent experiments.

Table 4

Blood-brain barrier permeability

	P_e ratio				
	Apical to basolateral	Basolateral to apical	Permeability	[a]Active transport	[b]CLogP
MDMA	6.0 ± 0.56	7.4 ± 2.4	+	No	1.85
Mephedrone	14.0 ± 10.4	12.2 ± 6.1	++	No	1.67
Methylone	6.1 ± 2.8	5.3 ± 1.3	+	No	1.39
Methcathinone	5.9 ± 2.8	8.5 ± 3.2	+	No	1.19
Amphetamine	6.3 ± 3.7	5.2 ± 1.3	+	No	1.74
Methamphetamine	5.4 ± 1.1	6.4 ± 3.0	+	No	1.74
MDPV	37.2 ± 11.3	12.0 ± 11.2	++	Yes	3.80

Data are expressed as mean ± SD (n = 3–9).
P_e ratios indicate the blood–brain barrier permeability of the drug in relation to the extracellular marker lucifer yellow (P_e = 1).
+, high permeability (P_e ratio >3). ++, very high permeability (P_e ratio >10).
[a]P <0.05 significant difference between apical to basolateral compared with basolateral to apical transport indicating active transport.
[b]CLogP, prediction of partition coefficient (lipophilicity).

Baumann, 2006; Baumann *et al.*, 2011) and more 'entactogenic' MDMA-like subjective drug effects (Liechti *et al.*, 2000a). Thus, the relative *in vitro* effect on the DAT versus SERT is useful to predict drug characteristics *in vivo* and compare novel cathinones with known psychostimulants. MDMA is selective for the SERT, with a DAT/SERT inhibition ratio of 0.08 (present study) and DA/5-HT release potency ratio <1 (Baumann *et al.*, 2012), and produces positive mood effects in humans with little psychostimulation (Liechti *et al.*, 2001). Cocaine has a DAT/SERT ratio close to unity, and methamphetamine is more selective for the DAT, with a DAT/SERT inhibition ratio >10 and DA/5-HT release ratio >100 (Baumann *et al.*, 2012) and has mostly psychostimulant effects in humans.

Cocaine-MDMA-mixed cathinones

Mephedrone, methylone, ethylone, butylone and naphyrone exhibited relative DAT versus SERT inhibition potencies in the range of 1–5, similar to cocaine. Uptake inhibition studies using rat synaptosomes found that mephedrone was equally potent at the DAT and SERT (Hadlock *et al.*, 2011). Methylone and butylone were slightly more potent DAT than SERT inhibitors at the human transporter as previously shown for methylone (Cozzi *et al.*, 1999). Equal uptake inhibition

potencies for the DAT and SERT were shown for methylone and butylone using rat brain synaptosomes (Nagai *et al.*, 2007; Lopez-Arnau *et al.*, 2012). Ethylone was an equipotent inhibitor of all three transporters, and we are not aware of other published data. Compared with methylone, ethylone and butylone, the respective non-β-keto analogue entactogens MDMA, MDEA and MBDB were 10-fold more selective for the SERT versus DAT, consistent with previous data on methylone and MDMA (Cozzi *et al.*, 1999; Nagai *et al.*, 2007). Together the data indicate that the cocaine–MDMA–mixed cathinones are more dopaminergic with regard to monoamine transporter inhibition than their entactogen analogs.

In terms of monoamine release, the cocaine–MDMA–mixed cathinones were comparable with MDMA. Ethylone and butylone released 5-HT, comparable with their non-β-keto entactogen analogues MBDB and MDEA, but with lower potency. Previous studies found that the monoamine release profiles of mephedrone and methylone resembled those of MDMA, with DAT/SERT and NET/DAT ratios close to unity (Nagai *et al.*, 2007; Baumann *et al.*, 2012). However, mephedrone was a more potent releaser of DA than MDMA in the present study and from striatal suspensions preloaded with DA (Hadlock *et al.*, 2011). An *in vivo* microdialysis study in rats showed that mephedrone also produced a rapid and pronounced increase in nucleus accumbens DA levels, comparable with amphetamine and unlike MDMA, which only moderately elevates DA levels (Kehr *et al.*, 2011). Both mephedrone and MDMA also produced strong increases in extracellular 5-HT, whereas amphetamine had only a moderate effect on 5-HT levels (Kehr *et al.*, 2011). Other microdialysis studies showed that mephedrone and methylone elevated extracellular DA and 5-HT levels in the rat nucleus accumbens, with relatively higher effects on 5-HT levels (Aarde *et al.*, 2011; Baumann *et al.*, 2012), similar to MDMA and unlike methamphetamine, which preferentially increases DA (Baumann *et al.*, 2012). Thus, mephedrone shares some of the DA-releasing properties of amphetamine and methamphetamine and 5-HT-releasing property of MDMA. Mephedrone also produced relatively weak motor stimulation similar to MDMA, unlike amphetamine that strongly increases locomotor activity in rats (Kehr *et al.*, 2011), and a preference to move along the walls of the test box (Motbey *et al.*, 2012) as previously described for MDMA. Like MDMA, mephedrone also reduced voluntary wheel running in rats, while running was increased by methamphetamine or MDPV (Huang *et al.*, 2012). Similar to mephedrone, methylone was also reported to be a weak motor stimulant compared with methamphetamine (Baumann *et al.*, 2012). Drug discrimination studies in rats also showed that methylone generalized well to MDMA and at lower potency also to amphetamine (Dal Cason *et al.*, 1997). Mephedrone is self-administered by rats (Aarde *et al.*, 2011; Hadlock *et al.*, 2011), has been reported to produce strong craving in humans (Brunt *et al.*, 2011) and when administered intranasally is rated by users to be more addictive than cocaine (Winstock *et al.*, 2011). Furthermore, mephedrone showed very high BBB permeability in our *in vitro* model, confirming that mephedrone readily enters the brain (Hadlock *et al.*, 2011). Overall, the pharmacological effects of mephedrone and methylone appear to be relatively similar to those of MDMA but share more of the DA system-stimulating properties of amphetamine and methamphetamine and the DAT versus SERT inhibition profile of cocaine. The subjective effects of mephedrone have been reported to be similar to those of cocaine (Winstock *et al.*, 2011) but also MDMA (Carhart-Harris *et al.*, 2011). Importantly, MDMA is mostly used orally, whereas intranasal administration is the most common route of use for mephedrone (Winstock *et al.*, 2011) and cocaine. Users noted that the high obtained with the intranasal use of mephedrone was similar to or better than the high produced by cocaine (Winstock *et al.*, 2011). These observations indicate that the oral use of mephedrone produces overall similar effects to MDMA, whereas intranasal use results in more cocaine-like psychotropic effects. Similar to mephedrone and methylone, ethylone and butylone may be associated with an increased risk of addiction compared to their non-β-keto analogues because of the stronger relative activation of the DA system.

The pyrovalerone derivative naphyrone exhibited a monoamine uptake transporter inhibition profile that was very close to that of cocaine, with equal relative potency at all three transporters. Similar to cocaine, naphyrone was not a monoamine releaser. Naphyrone is distinct from pyrovalerone and its derivative MDPV because of its higher absolute and relative SERT-inhibiting potency. Although the structure would suggest similar pharmacological effects to the other pyrovalerone derivatives, the additional SERT inhibition may indicate more similar effects to cocaine in humans (Derungs *et al.*, 2011).

Methamphetamine-like cathinones

Cathinone and methcathinone exhibited a relative monoamine transporter inhibition profile that was very similar to that of the non-β-keto analogues amphetamine and methamphetamine, with high inhibitory potencies at the DAT and low potencies at the SERT, consistent with previous findings (Cozzi *et al.*, 1999; Fleckenstein *et al.*, 1999). Cathinone and methcathinone were also potent releasers of DA but not 5-HT, similar to amphetamine and methamphetamine. Cathinone and methcathinone have previously been shown to release radiolabelled DA and 5-HT from rat brain preparations with similar DA versus 5-HT selectivity to amphetamine (Kalix, 1990) and methamphetamine (Glennon *et al.*, 1987), but with two- to three-fold lower potency. Methcathinone has been shown to be a substrate for the transporter (Cozzi and Foley, 2003), similar to the classic amphetamines and MDMA (Rothman *et al.*, 2001; Verrico *et al.*, 2007). Cathinone and methcathinone produce amphetamine-like locomotor stimulation in animals (Glennon *et al.*, 1987; Kelly, 2011), and cathinone is self-administered by rats (Gosnell *et al.*, 1996) or rhesus monkeys (Johanson and Schuster, 1981; Woolverton and Johanson, 1984) with reinforcing efficacies comparable to amphetamine and cocaine. Clinically, cathinone and methcathinone have been reported to produce similar toxicity to amphetamine, including hypertension, hyperthermia, euphoria, locomotor activation and hallucinations following higher or repeated doses (Kalix, 1990; Widler *et al.*, 1994). Thus, the pharmacology of cathinone and methcathinone is qualitatively very close to that of amphetamine and methamphetamine.

Flephedrone was a DAT but not a SERT inhibitor, similar to its analogue 4-fluoroamphetamine (Nagai *et al.*, 2007). Flephedrone released DA but not 5-HT (IC_{50} >33 μM). The

DAT/SERT selectivity profile of flephedrone is therefore equal to the methamphetamine-like cathinones. In contrast, flephedrone had higher 5-HT_{2A} receptor binding that was similar to mephedrone and MDMA. We are not aware of any other *in vitro* or *in vivo* data on flephedrone. Agitation and psychosis were reported in a patient who insufflated flephedrone and MDPV powder (Thornton *et al.*, 2012).

Pyrovalerone cathinones

Pyrovalerone and its derivative MDPV were very potent DAT inhibitors as previously shown (Meltzer *et al.*, 2006) and at least 10-fold more potent than cocaine and methamphetamine. In contrast to the pyrovalerone derivative naphyrone, MDPV and pyrovalerone are weak inhibitors of the SERT, resulting in high DAT selectivity, with DAT/SERT inhibition ratios >100. MDPV and pyrovalerone were also the most potent NET inhibitors. Despite the high potency to block the DAT, pyrovalerone and MDPV did not produce DA efflux. Thus, pyrovalerone derivative cathinones are pure transporter uptake inhibitors. Consistent with the potent effect on catecholamine carriers, MDPV, compared with mephedrone, produced behavioural effects in animals at lower doses (Aarde *et al.*, 2011) and has been reported to produce mostly sympathomimetic toxicity and psychotic reactions in humans (Spiller *et al.*, 2011). Similar to methamphetamine, MDPV and pyrovalerone did not exhibit affinity for the 5-HT_{2A} receptor and exhibited low affinity for TA_1 receptors, consistent with the other cathinones.

Pyrovalerone derivatives have been suggested to easily cross the BBB because of their high lipophilicity (Meltzer *et al.*, 2006; Coppola and Mondola, 2012). All of the cathinones and non-β-keto amphetamine analogues showed good membrane permeation in our *in vitro* BBB model, but we indeed documented very high transmembrane permeability of MDPV and a potential active transport. Although the high brain uptake may contribute to the higher potency of MDPV compared with the non-pyrovalerone cathinones, the high potency at the NET and DAT is more likely to be responsible for the psychotropic effects at low doses in humans. In fact, we found that the potencies to inhibit the NET and DAT were significantly correlated with the doses reported to produce psychotropic effects in recreational users. Consistently, pyrovalerone and MDPV are at least 10-fold more potent inhibitors of the NET or DAT compared with mephedrone; this was demonstrated in the present study and previously (Meltzer *et al.*, 2006), and are used recreationally at approximately 10-fold lower doses than mephedrone (Derungs *et al.*, 2011), whereas both MDPV and mephedrone exhibited very high BBB penetrance in our study. The potency of the pyrovalerone derivatives at the DAT and NET and high brain penetrance could result in high sympathomimetic toxicity and risk of addiction in humans. MDPV has also been shown to be a potent reinforcer in rats, similar to methamphetamine (Watteron *et al.*, 2011).

Structure–activity relationship and binding to monoamine receptors

β-Keto-amphetamines appear to have similar effects on plasma membrane monoamine transporters compared with their non-β-keto analogues, with slightly higher selectivity for the DAT over the SERT. β-Keto-analogue cathinones also exhibited approximately 10-fold lower affinity for the TA_1 receptor compared with their respective non-β-keto amphetamines. TA_1 receptors play an important role in the modulation of dopaminergic and 5-hydroxytryptaminergic activity (Lindemann *et al.*, 2008; Revel *et al.*, 2011). Activation of TA_1 receptors negatively modulates dopaminergic neurotransmission. Importantly, methamphetamine decreased DAT surface expression via a TA_1 receptor-mediated mechanism and thereby reduced the presence of its own pharmacological target (Xie and Miller, 2009). MDMA and amphetamine have been shown to produce enhanced DA and 5-HT release and locomotor activity in TA_1 receptor knockout mice compared with wild-type mice (Lindemann *et al.*, 2008; Di Cara *et al.*, 2011). Because methamphetamine and MDMA auto-inhibit their neurochemical and functional effects via TA_1 receptors, low affinity for these receptors may result in stronger effects on monoamine systems by cathinones compared with the classic amphetamines. The higher selectivity of the cathinones for the DAT and lack of TA_1 receptor binding may result in an increased risk of dependence compared with classic non-β-keto analogue stimulants (Rothman and Baumann, 2006). Because 5-HT release dampens the stimulant effects of amphetamine-type drugs, the lower activity of the cathinones at the SERT would be expected to result in more stimulant-like effects (Baumann *et al.*, 2011) compared with the non-β-keto analogues. The α-ethyl-substituted compounds MBDB and butylone exhibited fivefold lower absolute and relative NET inhibition potencies than their α-methyl-analogues MDMA and methylone, in line with previous studies (Montgomery *et al.*, 2007). The lower affinity for NET has been associated with the low stimulant and euphorigenic properties of MBDB (Montgomery *et al.*, 2007).

Several of the drugs evaluated in the present study exhibited moderate direct affinity for 5-HT receptors and adrenoceptors, with K_i values in the 1–10 μM range. Direct interactions between MDMA and 5-HT_2 receptors rather than indirect agonist effects via 5-HT release have been suggested to contribute to MDMA-induced excitation and hallucinogen-like perceptual alterations at higher doses (Liechti *et al.*, 2000b; 2001). MDMA, MBDB, mephedrone, flephedrone and methcathinone bound to 5-HT_{2A} receptors, consistent with previous data on mephedrone, methylone and MDMA (Lopez-Arnau *et al.*, 2012; Martinez-Clemente *et al.*, 2012). Stimulation of 5-HT_{2A} receptors has also been shown to enhance DA release (Gudelsky *et al.*, 1994), potentially increasing abuse liability. Although flephedrone and methcathinone show low potency at the SERT, these drugs may have direct effects on the 5-HT system via 5-HT_{2A} receptor activation at higher doses. Amphetamine and methamphetamine bound to 5-HT_{1A} receptors, potentially resulting in behavioural effects that are opposite to those induced by 5-HT_{2A} receptor stimulation (Nichols, 2004; Gatch *et al.*, 2011). Mephedrone, flephedrone, cathinone and methcathinone exhibited affinity for α_{1A} adrenoceptors, which have been implicated in stimulant-induced vasoconstriction, hyperthermia (Hysek *et al.*, 2012b) and euphoria (Newton *et al.*, 2012). Finally, amphetamine and methamphetamine bound to α_{2A} receptors, which modulate NA release and sympathomimetic toxicity (Hysek *et al.*, 2012a).

It is important to note that we assessed the effects of racemic cathinones, whereas stereoselective and drug-specific interactions have been demonstrated for amphetamines (Lyon *et al.*, 1986; Steele *et al.*, 1987; Acquas *et al.*, 2007). Furthermore, we did not investigate drug interactions with intracellular targets such as monoamine oxidase or the vesicular monoamine transporter.

In summary, considerable differences were found in the pharmacology of the different cathinones. Mephedrone, methylone, ethylone, butylone and naphyrone acted as non-selective monoamine uptake inhibitors, similar to cocaine and, with the exception of naphyrone, also induced the release of 5-HT, similar to MDMA. Cathinone and methcathinone were found to be selective catecholamine uptake inhibitors and releasers, similar to their non-β-keto analogues amphetamine and methamphetamine. Pyrovalerone and MDPV were shown to be highly potent and selective catecholamine transporter inhibitors but not substrate releasers.

Acknowledgements

We thank V Metzler and A van der Klooster for technical assistance and Prof A Pfaltz for providing support for the synthesis of naphyrone. This work was supported by the Swiss National Science Foundation (no. 323230_126231 and 3232B_144996) and the Translational Medicine Hub Innovation Fund of F Hoffmann-La Roche and the University of Basel.

Conflict of interest

None.

References

Aarde SA, Wright MJ, Buczynski MW, Angrish D, Parsons LH, Houseknecht KL *et al.* (2011). Behavioral and termoregulatory effects of novel cathinone derivative drugs 4-MMC and MDPV. Neuropsychopharmacology 36: S441.

Acquas E, Pisanu A, Spiga S, Plumitallo A, Zernig G, Di Chiara G (2007). Differential effects of intravenous R,S-(+/–)-3,4-methylenedioxymethamphetamine (MDMA, Ecstasy) and its S(+)- and R(–)-enantiomers on dopamine transmission and extracellular signal regulated kinase phosphorylation (pERK) in the rat nucleus accumbens shell and core. J Neurochem 102: 121–132.

Alexander SP, Mathie A, Peters JA (2011). Guide to Receptors and Channels (GRAC), 5th edition. Br J Pharmacol 164 (Suppl. 1): S1–S324.

Baumann MH, Clark RD, Woolverton WL, Wee S, Blough BE, Rothman RB (2011). In vivo effects of amphetamine analogs reveal evidence for serotonergic inhibition of mesolimbic dopamine transmission in the rat. J Pharmacol Exp Ther 337: 218–225.

Baumann MH, Ayestas MA Jr, Partilla JS, Sink JR, Shulgin AT, Daley PF *et al.* (2012). The designer methcathinone analogs, mephedrone and methylone, are substrates for monoamine transporters in brain tissue. Neuropsychopharmacology 37: 1192–1203.

Brunt TM, Poortman A, Niesink RJ, van den Brink W (2011). Instability of the ecstasy market and a new kid on the block: mephedrone. J Psychopharmacol 25: 1543–1547.

Carhart-Harris RL, King LA, Nutt DJ (2011). A web-based survey on mephedrone. Drug Alcohol Depend 118: 19–22.

Cecchelli R, Dehouck B, Descamps L, Fenart L, Buee-Scherrer VV, Duhem C *et al.* (1999). In vitro model for evaluating drug transport across the blood-brain barrier. Adv Drug Deliv Rev 36: 165–178.

Coppola M, Mondola R (2012). 3,4-methylenedioxypyrovalerone (MDPV): chemistry, pharmacology and toxicology of a new designer drug of abuse marketed online. Toxicol Lett 208: 12–15.

Cozzi NV, Foley KF (2003). Methcathinone is a substrate for the serotonin uptake transporter. Pharmacol Toxicol 93: 219–225.

Cozzi NV, Sievert MK, Shulgin AT, Jacob P 3rd, Ruoho AE (1999). Inhibition of plasma membrane monoamine transporters by beta-ketoamphetamines. Eur J Pharmacol 381: 63–69.

Dal Cason TA, Young R, Glennon RA (1997). Cathinone: an investigation of several N-alkyl and methylenedioxy-substituted analogs. Pharmacol Biochem Behav 58: 1109–1116.

Derungs A, Schietzel S, Meyer MR, Maurer HH, Krahenbuhl S, Liechti ME (2011). Sympathomimetic toxicity in a case of analytically confirmed recreational use of naphyrone (naphthylpyrovalerone). Clin Toxicol (Phila) 49: 691–693.

Di Cara B, Maggio R, Aloisi G, Rivet JM, Lundius EG, Yoshitake T *et al.* (2011). Genetic deletion of trace amine 1 receptors reveals their role in auto-inhibiting the actions of ecstasy (MDMA). J Neurosci 31: 16928–16940.

Fleckenstein AE, Haughey HM, Metzger RR, Kokoshka JM, Riddle EL, Hanson JE *et al.* (1999). Differential effects of psychostimulants and related agents on dopaminergic and serotonergic transporter function. Eur J Pharmacol 382: 45–49.

Gatch MB, Forster MJ, Janowsky A, Eshleman AJ (2011). Abuse liability profile of three substituted tryptamines. J Pharmacol Exp Ther 338: 280–289.

Ghose AK, Viswanadhan VN, Wendoloski JJ (1998). Prediction of hydrophobic (lipophilic) properties of small organic molecules using fragment methods: an analysis of ALogP and CLogP methods. J Phys Chem A 102: 3762–3772.

Glennon RA, Yousif M, Naiman N, Kalix P (1987). Methcathinone: a new and potent amphetamine-like agent. Pharmacol Biochem Behav 26: 547–551.

Gosnell BA, Yracheta JM, Bell SM, Lane KE (1996). Intravenous self-administration of cathinone by rats. Behav Pharmacol 7: 526–531.

Gudelsky GA, Yamamoto BK, Nash JF (1994). Potentiation of 3,4-methylenedioxymethamphetamine-induced dopamine release and serotonin neurotoxicity by 5-HT_2 receptor agonists. Eur J Pharmacol 264: 325–330.

Hadlock GC, Webb KM, McFadden LM, Chu PW, Ellis JD, Allen SC *et al.* (2011). 4-Methylmethcathinone(mephedrone): neuropharmacological effects of a designer stimulant of abuse. J Pharmacol Exp Ther 339: 530–536.

Huang PK, Aarde SM, Angrish D, Houseknecht KL, Dickerson TJ, Taffe MA (2012). Contrasting effects of

d-methamphetamine, 3,4-methylenedioxymethamphetamine, 3,4-methylenedioxypyrovalerone, and 4-methylmethcathinone on wheel activity in rats. Drug Alcohol Depend 126: 168–175.

Hysek CM, Brugger R, Simmler LD, Bruggisser M, Donzelli M, Grouzmann E *et al.* (2012a). Effects of the a_2-adrenergic agonist clonidine on the pharmacodynamics and pharmacokinetics of 3,4-methylenedioxymethamphetamine in healthy volunteers. J Pharmacol Exp Ther 340: 286–294.

Hysek CM, Schmid Y, Rickli A, Simmler LD, Donzelli M, Grouzmann E *et al.* (2012b). Carvedilol inhibits the cardiostimulant and thermogenic effects of MDMA in humans. Br J Pharmacol 166: 2277–2288.

Hysek CM, Simmler LD, Nicola V, Vischer N, Donzelli M, Krähenbühl S *et al.* (2012c). Duloxetine inhibits effects of MDMA ('ecstasy') in vitro and in humans in a randomized placebo-controlled laboratory study. Plos ONE 7: e36476.

Johanson CE, Schuster CR (1981). A comparison of the behavioral effects of l- and dl-cathinone and d-amphetamine. J Pharmacol Exp Ther 219: 355–362.

Kalix P (1990). Pharmacological properties of the stimulant khat. Pharmacol Ther 48: 397–416.

Kehr J, Ichinose F, Yoshitake S, Goiny M, Sievertsson T, Nyberg F *et al.* (2011). Mephedrone, compared to MDMA (ecstasy) and amphetamine, rapidly increases both dopamine and serotonin levels in nucleus accumbens of awake rats. Br J Pharmacol 164: 1949–1958.

Kelly JP (2011). Cathinone derivatives: a review of their chemistry, pharmacology and toxicology. Drug Test Anal 3: 439–453.

Liechti ME, Baumann C, Gamma A, Vollenweider FX (2000a). Acute psychological effects of 3,4-methylenedioxymethamphetamine (MDMA, 'ecstasy') are attenuated by the serotonin uptake inhibitor citalopram. Neuropsychopharmacology 22: 513–521.

Liechti ME, Saur MR, Gamma A, Hell D, Vollenweider FX (2000b). Psychological and physiological effects of MDMA ('Ecstasy') after pretreatment with the 5-HT_2 antagonist ketanserin in healthy humans. Neuropsychopharmacology 23: 396–404.

Liechti ME, Gamma A, Vollenweider FX (2001). Gender differences in the subjective effects of MDMA. Psychopharmacology (Berl) 154: 161–168.

Lindemann L, Meyer CA, Jeanneau K, Bradaia A, Ozmen L, Bluethmann H *et al.* (2008). Trace amine-associated receptor 1 modulates dopaminergic activity. J Pharmacol Exp Ther 324: 948–956.

Lopez-Arnau R, Martinez-Clemente J, Pubill D, Escubedo E, Camarasa J (2012). Comparative neuropharmacology of three psychostimulant cathinone derivatives: butylone, mephedrone and methylone. Br J Pharmacol 167: 407–420.

Lyon RA, Glennon RA, Titeler M (1986). 3,4-Methylenedioxymethamphetamine (MDMA): stereoselective interactions at brain 5-HT1 and 5-HT2 receptors. Psychopharmacology (Berl) 88: 525–526.

Martin WR, Sloan JW, Sapira JD, Jasinski DR (1971). Physiologic, subjective, and behavioral effects of amphetamine, methamphetamine, ephedrine, phenmetrazine, and methylphenidate in man. Clin Pharmacol Ther 12: 245–258.

Martinez-Clemente J, Escubedo E, Pubill D, Camarasa J (2012). Interaction of mephedrone with dopamine and serotonin targets in rats. Eur Neuropsychopharmacol 22: 231–236.

Meltzer PC, Butler D, Deschamps JR, Madras BK (2006). 1-(4-Methylphenyl)-2-pyrrolidin-1-yl-pentan-1-one (Pyrovalerone) analogues: a promising class of monoamine uptake inhibitors. J Med Chem 49: 1420–1432.

Montgomery T, Buon C, Eibauer S, Guiry PJ, Keenan AK, McBean GJ (2007). Comparative potencies of 3,4-methylenedioxymethamphetamine (MDMA) analogues as inhibitors of [3H]noradrenaline and [3H]5-HT transport in mammalian cell lines. Br J Pharmacol 152: 1121–1130.

Motbey CP, Hunt GE, Bowen MT, Artiss S, McGregor IS (2012). Mephedrone (4-methylmethcathinone, 'meow'): acute behavioural effects and distribution of Fos expression in adolescent rats. Addict Biol 17: 409–422.

Nagai F, Nonaka R, Satoh Hisashi Kamimura K (2007). The effects of non-medically used psychoactive drugs on monoamine neurotransmission in rat brain. Eur J Pharmacol 559: 132–137.

Newton TF, De La Garza R 2nd, Brown G, Kosten TR, Mahoney JJ 3rd, Haile CN (2012). Noradrenergic a_1 receptor antagonist treatment attenuates positive subjective effects of cocaine in humans: a randomized trial. Plos ONE 7: e30854.

Nichols DE (2004). Hallucinogens. Pharmacol Ther 101: 131–181.

Revel FG, Moreau JL, Gainetdinov RR, Bradaia A, Sotnikova TD, Mory R *et al.* (2011). TAAR1 activation modulates monoaminergic neurotransmission, preventing hyperdopaminergic and hypoglutamatergic activity. Proc Natl Acad Sci U S A 108: 8485–8490.

Rothman RB, Baumann MH (2006). Balance between dopamine and serotonin release modulates behavioral effects of amphetamine-type drugs. Ann N Y Acad Sci 1074: 245–260.

Rothman RB, Baumann MH, Dersch CM, Romero DV, Rice KC, Carroll FI *et al.* (2001). Amphetamine-type central nervous system stimulants release norepinephrine more potently than they release dopamine and serotonin. Synapse 39: 32–41.

Sano Y, Shimizu F, Abe M, Maeda T, Kashiwamura Y, Ohtsuki S *et al.* (2010). Establishment of a new conditionally immortalized human brain microvascular endothelial cell line retaining an in vivo blood-brain barrier function. J Cell Physiol 225: 519–528.

Sano Y, Kashiwamura Y, Abe M, Dieu L, Huwyler J, Shimizu F *et al.* (2012). A stable human brain microvascular endothelial cell line retaining its barrier-specific nature, independent of the passage number. Clin Exp Neuroimmunol (in press).

Scholze P, Zwach J, Kattinger A, Pifl C, Singer EA, Sitte HH (2000). Transporter-mediated release: a superfusion study on human embryonic kidney cells stably expressing the human serotonin transporter. J Pharmacol Exp Ther 293: 870–878.

Spiller HA, Ryan ML, Weston RG, Jansen J (2011). Clinical experience with and analytical confirmation of 'bath salts' and 'legal highs' (synthetic cathinones) in the United States. Clin Toxicol (Phila) 49: 499–505.

Steele TD, Nichols DE, Yim GK (1987). Stereochemical effects of 3,4-methylenedioxymethamphetamine (MDMA) and related amphetamine derivatives on inhibition of uptake of [3H]monoamines into synaptosomes from different regions of rat brain. Biochem Pharmacol 36: 2297–2303.

Tatsumi M, Groshan K, Blakely RD, Richelson E (1997). Pharmacological profile of antidepressants and related compounds at human monoamine transporters. Eur J Pharmacol 340: 249–258.

Thornton SL, Gerona RR, Tomaszewski CA (2012). Psychosis from a bath salt product containing flephedrone and MDPV with serum, urine, and product quantification. J Med Toxicol 8: 310–313.

Verrico CD, Miller GM, Madras BK (2007). MDMA (ecstasy) and human dopamine, norepinephrine, and serotonin transporters: implications for MDMA-induced neurotoxicity and treatment. Psychopharmacology 189: 489–503.

Watteron LR, Kufahl PR, Nemirovsky NE, Sewalia K, Olive MF (2011). Potent reinforcing effects of the synthetic cathinone methylenedioxypyrovalerone (MDPV) in rats. Neuropsychopharmacology 36: S440.

Wee S, Anderson KG, Baumann MH, Rothman RB, Blough BE, Woolverton WL (2005). Relationship between the serotonergic activity and reinforcing effects of a series of amphetamine analogs. J Pharmacol Exp Ther 313: 848–854.

Widler P, Mathys K, Brenneisen R, Kalix P, Fisch HU (1994). Pharmacodynamics and pharmacokinetics of khat: a controlled study. Clin Pharmacol Ther 55: 556–562.

Winstock AR, Mitcheson LR, Deluca P, Davey Z, Corazza O, Schifano F (2011). Mephedrone, new kid for the chop? Addiction 106: 154–161.

Woolverton WL, Johanson CE (1984). Preference in rhesus monkeys given a choice between cocaine and d,l-cathinone. J Exp Anal Behav 41: 35–43.

Xie Z, Miller GM (2009). A receptor mechanism for methamphetamine action in dopamine transporter regulation in brain. J Pharmacol Exp Ther 330: 316–325.

3.3 Polymersomes Conjugated to 83-14 Monoclonal Antibodies: *in Vitro* Targeting of Brain Capillary Endothelial Cells

Le-Ha Dieu,[1] Dalin Wu,[2] Cornelia Palivan,[2] Vimalkumar Balasubramanian,[1] Jörg Huwyler[1]

[1]Department of Pharmaceutical Sciences, Division of Pharmaceutical Technology, University of Basel, Klingelbergstrasse 50, 4056 Basel, Switzerland

[2]Department of Chemistry, University of Basel, Klingelbergstrasse 80, 4056 Basel, Switzerland

Submitted

ABSTRACT

The blood-brain barrier (BBB) remains an obstacle for many drugs to reach the brain. A strategy to cross the BBB is to modify nanocarrier systems with ligands that bind to endogenous receptors expressed at the BBB to induce receptor-mediated endocytosis and transcytosis. The aim of the present study was to investigate the potential of polymersomes composed of the amphiphilic diblock copolymer poly(dimethylsiloxane)-block-poly(2-methyl-2-oxazoline), PDMS-*b*-PMOXA, for active BBB targeting. We conjugated PDMS-*b*-PMOXA polymersomes to the anti-human insulin receptor antibody 83-14 (83-14 mAb) and studied their uptake by brain capillary endothelial cells. Transmission electron micrography and light scattering measurements revealed the self-assembly of the block copolymers into 200 nm vesicles after extrusion. Fluorescence correlation spectroscopy was employed to calculate the number of antibodies coupled to one polymersome. Binding and uptake of the polymersomes conjugated to 83-14 mAb were studied in the human BBB *in vitro* model hCMEC/D3 expressing the human insulin receptor. Competitive inhibition with an excess of free 83-14 mAb demonstrated the specificity of cellular binding and uptake. Our results suggest that PDMS-*b*-PMOXA polymersomes conjugated to 83-14 mAb may be suitable nanocarriers for drug delivery to the brain.

KEYWORDS Polymersomes, PDMS-*b*-PMOXA diblock copolymers, Blood-brain barrier, Insulin receptor, Anti-human insulin receptor antibody 83-14, Active targeting

INTRODUCTION

A major obstacle in the development of drugs targeted to the brain remains the blood-brain barrier (BBB) which prevents many drugs from entering the brain. Most macromolecules and many small molecules are excluded from the central nervous system (Pardridge, 2003). One strategy to overcome the BBB is to encapsulate a drug into a nanoparticulate system decorated with a ligand. This complex binds to an endogenous receptor expressed at the BBB, thus mediating cellular uptake and transcytosis upon interaction. Transport of ligand-conjugated liposomes across the BBB has been successfully demonstrated *in vivo* (Cerletti et al., 2000; Huwyler et al., 1996).

In the past years, delivery systems for drug targeting using polymersomes have received much attention. Polymersomes are vesicles which spontaneously form by self-assembly of amphiphilic block copolymers in dilute aqueous solutions. Similar to liposomes, polymersomes can encapsulate hydrophilic compounds in their aqueous core and lipophilic substances in their membrane (Discher and Eisenberg, 2002). Depending on the molecular weight of the block copolymers, their vesicle membrane thickness ranges between 8 and 21 nm (Bermudez et al., 2002), which explains their increased mechanical stability compared to liposomes (Balasubramanian et al., 2010). The large variety of amphiphilic copolymers supports formation of polymersomes with a membrane permeability ranging from impermeable to small molecules (Kumar et al., 2007) up to porous membranes that allow a molecular exchange with the environment (van Dongen et al., 2009). Moreover, by choosing a suitable copolymer with appropriate chemical nature of each polymer block or hydrophilic-to-hydrophobic ratio, a broad range of tunable carrier properties with specific advantages (e.g. encapsulation efficiency, stimuli-responsiveness, multifunctionality) can be achieved (Cabane et al., 2012; Gaitzsch et al., 2012; Najer et al., 2013; De Oliveira et al., 2012).

Polymersomes prepared from poly(2-methyl-2-oxazoline)-poly(dimethylsiloxane)-poly(2-methyl-2-oxazoline) [PMOXA-PDMS-PMOXA] triblock copolymers have shown low toxicity and low immune response in different cell lines (Broz et al., 2005; Ranquin et al., 2005; Tanner et al., 2011). In addition, they combine a high stability in oxidative environments with a tight membrane, which does not allow escape of encapsulated molecules (Kumar et al., 2007). Polymersomes based on PDMS-*b*-PMOXA

diblock copolymers have recently been used for cellular targeting. PDMS-*b*-PMOXA polymersomes functionalized with trastuzumab bind specifically to HER2-positive breast cancer cells (SKBR3) and mediate cellular uptake (Egli et al., 2011).

The present study aimed to assess the potential of polymersomes based on PDMS-*b*-PMOXA diblock copolymers for active drug targeting to the brain. To implement an active and physiological targeting strategy, the human insulin receptor expressed by brain capillary endothelial cells was used as a model system. Such an *in vitro* system allows studying the molecular mechanisms of cellular interactions between target cells and polymersomes. The insulin receptor is enriched at the BBB and is known to mediate transcytosis of insulin across the BBB (Pardridge et al., 1985). In addition, *in vivo* receptor binding of the anti-human insulin receptor antibody 83-14 (83-14 mAb) is followed by receptor-mediated endocytosis and transcytosis (Pardridge et al., 1995) with a nearly 10-fold higher BBB transport than an anti-transferrin receptor antibody (Wu et al., 1997). Therefore, targeting the insulin receptor is a promising approach to deliver drugs to the brain.

We conjugated the 83-14 mAb to the polymersomes during the polymer film rehydration process in a fast, one-step conjugation reaction. To the best of our knowledge, this was the first time to functionalize polymersomes with the high-affinity anti-insulin receptor antibody 83-14 mAb for drug targeting.

Brain delivery of ligand-targeted polymersomes has already been described *in vivo* in animals (Pang et al., 2011). However, to improve polymersome uptake by the brain, the underlying molecular mechanisms of transport at the cellular level have to be understood. In the present work, we first tested the functional expression of the human insulin receptor by the human brain capillary endothelial cell lines hCMEC/D3 and TY09 (Poller et al., 2008; Sano et al., 2012). Subsequently, we studied binding, cellular uptake, and intracellular trafficking of polymersomes conjugated to 83-14 mAb in brain endothelial cells.

EXPERIMENTAL PROCEDURES

MATERIALS

Triethylamine (≥99%), 4-(dimethylamino)pyridine (≥99%), succinic anhydride (≥99%), N-hydroxysuccinimide (≥98%), N, N'-dicyclohexylcarbodiimide (99%), and anhydrous dichloromethane (≥99.8%, containing 50-150 ppm amylene as stabilizer) were purchased from Sigma-Aldrich (Schnelldorf, Germany). Regenerated cellulose dialysis membranes (3.5k Da molecular weight cut-off [MWCO]) were obtained from Spectrum Labs (Breda, Netherlands). 5(6)-carboxyfluorescein diacetate N-hydroxysuccinimidyl (NHS) ester, ethanol puriss. and sodium bicarbonate were purchased from Sigma-Aldrich (analytical grade, Schnelldorf, Germany). Milli-Q water was obtained from Millipore (Billerica, Massachusetts, USA). A hybridoma cell line producing the mouse monoclonal antibody against the human insulin receptor (83-14 mAb) was kindly provided by Professor Ken Siddle (Department of Clinical Biochemistry, University of Cambridge, UK). DyLight 488 NHS ester and goat polyclonal anti-rabbit antibody DyLight 633 were obtained from ThermoFischer Scientific (Waltham, MA, USA). Rabbit polyclonal anti-early endosome-associated protein 1 (EEA1) antibody and rabbit polyclonal anti-lysosome-associated membrane protein 1 (Lamp1) antibody were purchased from Abcam (Cambridge, UK). Suppliers of the cell-culture reagents and chemicals are indicated below. All other chemicals were obtained from Sigma-Aldrich (Schnelldorf, Germany).

METHODS

Synthesis and characterization of block copolymers

Synthesis of hydroxyl functionalized poly(dimethylsiloxane)-block-poly(2-methyl-2-oxazoline) block copolymers (PDMS$_{65}$-b-PMOXA$_{14}$-OH).

PDMS$_{65}$-*b*-PMOXA$_{14}$-OH diblock copolymer (Figure 1) was synthesized according to the procedure reported by Egli and coworkers (Egli et al., 2011).

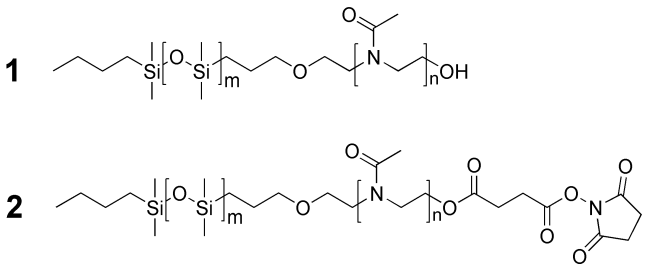

Figure 1: Chemical structures of $PDMS_{65}$-*b*-$PMOXA_{14}$-OH (1) and $PDMS_{65}$-*b*-$PMOXA_{32}$-NHS (2) diblock copolymers.

Synthesis of monocarboxyl acid modified poly(dimethylsiloxane)-block-poly(2-methyl-2-oxazoline) block copolymers ($PDMS_{65}$-b-$PMOXA_{32}$-COOH).

Succinic anhydride (39 mg, 0.39 mmol), triethanolamine (TEA, 50 µL, 0.36 mmol), and 4-(dimethylamino) pyridine (DMAP, 6.9 mg, 0.06 mmol) were added to the anhydrous dichloromethane solution of $PDMS_{65}$-*b*-$PMOXA_{32}$-OH (500 mg, 0.07 mmol) at 0°C under argon. The reaction was maintained for 24 h. Finally, the reaction solution was dialyzed against dichloromethane for two days while changing dichloromethane four times.

Synthesis of NHS activated ester modified poly(dimethylsiloxane)-block-poly(2-methyl-2-oxazoline) block copolymers ($PDMS_{65}$-b-$PMOXA_{32}$-NHS) [Figure 1].

N-Hydroxysuccinimide (NHS, 30 mg, 0.26 mmol) and *N*, *N'*-dicyclohexylcarbodiimide (DCC, 35 mg, 0.17 mmol) were added to the anhydrous dichloromethane solution of $PDMS_{65}$-*b*-$PMOXA_{32}$-COOH (300 mg, 0.04 mmol) at room temperature under argon. The reaction was maintained in this condition for 24 h. Finally, the reaction solution was dialyzed against dichloromethane for two days while changing dichloromethane four times. Figure S1 shows the route of synthesis.

Characterization of the synthesized $PDMS_{65}$-b-$PMOXA_{32}$-COOH block copolymers

The synthesized $PDMS_{65}$-*b*-$PMOXA_{32}$-COOH block copolymer was characterized using proton nuclear magnetic resonance (^{1}H NMR; Figure S2). Fourier transform infrared spectroscopy (FTIR) was used to characterize the presence of specific chemical groups. Polymer samples were placed on the detector and measured with 256 scans and

2 cm^{-1} resolution. FTIR spectra were obtained from 400 to 4000 cm^{-1} (PerkinElmer Spectrum 100 FTIR Spectrometer) [Figure S3].

Preparation and characterization of polymersomes

Preparation

Polymersomes composed of a mixture of amphiphilic diblock copolymers PDMS-*b*-PMOXA (95% $PDMS_{65}$-*b*-$PMOXA_{14}$-OH and 5% $PDMS_{65}$-*b*-$PMOXA_{32}$-NHS) were prepared using the film rehydration method as described previously (Egli et al., 2011). In brief, block copolymer (5 mg) was dissolved in absolute ethanol (1 mL). To form a thin film, the solution was transferred to a round-bottom flask, and the solvent was evaporated at 40°C and 100 mbar using a rotary vacuum evaporator (Buchi Rotavapor R-124 with vacuum controller B-721, Flawil, Switzerland). This film was then further dried overnight in a vacuum oven (ThermoFischer Scientific, Waltham, MA, USA). Bicarbonate buffer (1 mL, 0.1 M, pH 8.3) was added drop-wise to the film and stirred constantly (600 rpm) overnight. Copolymer solution was extruded with an Avanti mini-extruder (Avanti Polar Lipids, Alabama, US) through polycarbonate membranes with pore-size diameters of 400 nm and 200 nm (Whatman GmbH, Bottmingen, Switzerland) 11 times each to homogenize the size distribution of the polymersomes.

Morphology and assemblies size

Morphology and size distribution of polymersomes were analyzed using transmission electron microscopy (TEM) and light scattering (dynamic light scattering, DLS, and static light scattering, SLS). For TEM analysis, 5 µL of non-conjugated polymersomes and polymersomes conjugated to 83-14 mAb were negatively stained with freshly prepared 2% uranyl acetate solution, mounted on a carbon-coated copper grid, and air-dried overnight before analysis. The samples were readily visualized with a Philips Morgagni 268D transmission electron microscope at 293 K.

DLS measurements of the samples (5 mg/mL in phosphate-buffered saline [PBS] 1X) were performed using Delsa Nano C Particle Sizer (Beckman Coulter, Brea, California, USA). The angle for the measurements was set to 165° (back scattering mode). Size distribution was calculated using the CONTIN algorithm.

To confirm the vesicular structure of the assembled block copolymers in solution, further light scattering measurements were performed. DLS and SLS experiments were performed on an ALV goniometer (ALV GmbH, Germany), equipped with an ALV He-Ne laser (λ = 632.8 nm). Light scattering measurements were performed in 10 mm cylindrical quartz cells at angles of 30 – 150° at 293 K. The obtained data were processed using ALV static & dynamic fit and plot software (version 4.31 10/01). SLS data were processed according to the Guinier model, and DLS data by using the Williams-Watts function.

Fluorescent labeling of 83-14 mAb

83-14 mAb (1 mg/mL in PBS 1X) was incubated with a molar excess of NHS ester-functionalized 5(6)-carboxyfluorescein or DyLight 488 for 2 h at 4°C. The sample was then extensively dialyzed using a Spectra Por 4 dialysis membrane with MWCO of 12,000-14,000 Da (Spectrum Labs, Breda Netherlands) against PBS 1X at pH 7.4. The fluorophore to protein (F/P) labeling molar ratio was calculated according to the manufacturer's instruction using the Beer-Lambert Law. In brief, absorbance of the sample was measured at wavelengths of 280 nm and 493 nm to obtain the protein and dye concentration in the sample, respectively. Absorbance of the protein at 280 nm was corrected for the absorbance at 280 nm caused by the dye (manufacturer's recommended correction factor = 0.147). The extinction coefficient was 210,000 M^{-1} cm^{-1} for the protein and 70,000 M^{-1} cm^{-1} for the dye. To calculate the F/P ratio, the molar concentration of the dye was divided by the molar protein concentration. Absorbance measurements were carried out with Spectramax M2e (Molecular Devices LLC, Sunnyvale, California).

Conjugation of the polymersomes to fluorescently labeled 83-14 mAb

Polymersomes conjugated to 83-14 mAb were prepared with fluorescently labeled 83-14 mAb. On average, one antibody was labeled with five DyLight 488 molecules. For conjugation, $PDMS_{65}$-*b*-$PMOXA_{14}$-OH (95%) and $PDMS_{65}$-*b*-$PMOXA_{32}$-NHS (5%) were dissolved in anhydrous ethanol and then dried to form a thin film. Monoclonal antibody in bicarbonate buffer (9.4 µM, pH 8.3) was added to the film and stirred overnight (600 rpm). The ratio of NHS-functionalized block copolymer to mAb was 4:1.

The conjugated polymersomes were then extruded 11 times each with 400 nm and 200 nm filters, and free antibodies were separated by size-exclusion chromatography using Sepharose CL-2B column (GE Healthcare, Little Chalfont, Buckinghamshire, UK) eluting with PBS 1X pH 7.2.

Fluorescence correlation spectroscopy

The number of fluorescently labeled 83-14 mAb per polymersome was determined by fluorescence correlation spectroscopy (FCS). Measurements were carried out as described previously using a laser-scanning microscope (Zeiss LSM 510-META/Confcor2) equipped with different laser lines (488, 458, 477, 488, 514, 543, and 633 nm) and a 40X water immersion objective lens (Zeiss C-Apochromat 40X, NA 1.2) (Egli et al., 2011). Samples of DyLight 488 dye, DyLight-labeled 83-14 mAb, and polymersomes conjugated to DyLight 488-labeled 83-14 mAb were measured at room temperature on a thin cover glass (Huber & Co AG, Reinach, Switzerland). In FCS mode, fluctuations in fluorescence intensity were analyzed in terms of an autocorrelation function. To reduce the number of free fitting parameters, diffusion times for free dye (DyLight 488) and DyLight 488-labeled antibodies were independently determined. The fluorescence intensity signal was detected in real time and calculated by a software correlator (LSM 510 META - ConfoCor 2 System) using an autocorrelation function as well as brightness measurements. Autocorrelation curves were obtained by taking the average of 10 measurements over 30 s.

Cell culture

Immortalized human brain capillary endothelial cells, hCMEC/D3 cells, were obtained under license from the Institut National de la Santé et de la Recherche Médicale, Paris, France (Weksler et al., 2005). Passages from 30 to 35 were used for the experiments. Cells were cultured in endothelial cell basal medium (Provitro GmbH, Berlin, Germany) supplemented with 5% fetal bovine serum (FBS; AMIMED BioConcept, Allschwil, Switzerland), 1 ng/mL basic fibroblast growth factor (PeproTech, Hamburg, German), 5 µg/mL ascorbic acid, 1.4 µM hydrocortisone (Sigma-Aldrich, Schnelldorf, Germany), chemically defined lipid concentrate 1:100 dilution, 10 mM HEPES, 2 mM glutamax

(Gibco Life Technologies, Carlsbad, CA, USA), 100 U/mL penicillin, and 100 mg/mL streptomycin (Sigma-Aldrich, Schnelldorf, Switzerland).

Conditionally immortalized human brain endothelial cells, TY09, were obtained under license from the Department of Neurology and Clinical Neuroscience, Yamaguchi University, Japan. The cells were maintained in culture as described previously (Sano et al., 2012; Simmler et al., 2013). In brief, cells were grown in growth medium (EGM-MV BulletKit CC-3125, Lonza, Verviers, Belgium) supplemented with 20% FBS (AMIMED BioConcept, Allschwil, Switzerland), 100 U/mL penicillin, and 100 mg/mL streptomycin (Sigma-Aldrich, Schnelldorf, Switzerland).

Cells were passaged every 3 to 4 days. Before cell seeding, all culture flasks were coated with 0.1 mg/mL rat tail collagen (BD Biosciences, San Jose, CA, US) for 1 h at 37°C.

Receptor expression, cellular uptake, and subcellular localization

Flow cytometry

Receptor expression

To analyze cell receptor expression, hCMEC/D3 cells and TY09 cells were washed with Dulbecco's Phosphate-buffered Saline 1X (DPBS) [Sigma-Aldrich, Schnelldorf, Switzerland] and then detached from the culture flask with Accutase (Gibco Life Technologies, Carlsbad, CA, USA). The reaction was stopped using medium containing 10% FBS, and the cells were centrifuged and washed two times to remove Accutase. The cells were incubated with mouse 83-14 mAb (1.25 µg/mL) for 20 min at 4°C in staining buffer (DPBS 1X, 0.05% NaN_3, 1% FBS, 2.5 mM EDTA), washed, and further incubated with the 2nd anti-mouse Alexa 488 antibody, 1:500 dilution (Invitrogen Life Technologies, Carlsbad, CA, USA) for 20 min at 4°C. Control cells were only treated with the 2nd anti-mouse Alexa 488 antibody. To exclude dead cells, all samples were treated with 7-AAD before the measurements. The cells were analyzed using FACS Calibur flow cytometer (BD Biosciences, San Jose, CA). The results represented the percentages of cells with positive fluorescence signals after gating to exclude the autofluorescence signal of the control cells. Samples were excited at 488 nm. The green fluorescence signal was detected in FL1 after passing 530/30 nm bandpass filter, and the

7-AAD signal was detected in FL3 after 670 nm LP filter. The data were analyzed using FlowJo analysis software version V9/X (TreeStar, Ashland, OR, USA). Cell count was normalized to mode by FlowJo algorithm. Therefore, the absolute count is represented by 100% of total (% of maximum).

Cellular uptake

To analyze uptake of polymersomes conjugated to 83-14 mAb, hCMEC/D3 cells were seeded on a 12-well plate (TPP, Trasadingen, Switzerland) at a density of 5 x 10^4 cells/cm^2 and grown for two days in culture medium. Polymersome-antibody conjugates suspended in DPBS 1X were mixed with culture medium and added to the cells to a final concentration of 500 µg/mL. Incubation was performed for 1 h and 2 h at 37°C. Cells were washed with ice-cold DPBS 1X to deplete the free polymersome-antibody conjugates and incubated with 0.25% Trypsin-EDTA (Gibco Life Technologies, Carlsbad, CA, USA) until the cells had detached. Trypsin reaction was stopped with ice-cold DMEM (Sigma-Aldrich, Schnelldorf, Switzerland) supplemented with 10% FBS. The cell suspension of each well was centrifuged for 5 min at 200 *g* (4°C). After washing the pellets with staining buffer (DPBS 1X, 0.05% NaN_3, 1% FBS, 2.5 mM EDTA), the cells were treated with 7-AAD and analyzed using a CYAN flow cytometer. Excitation was performed at 488 nm. The DyLight signal was collected in FL1 (530/40 nm) and the 7-AAD signal in FL4 (680/30 nm). The data were analyzed using FlowJo analysis software as described above.

Confocal laser scanning microscopy

Intracellular localization

HCMEC/D3 cells were seeded on collagen-coated cover glasses at a density of 2.5 x 10^4 cells/cm^2 and grown to 70-80% confluency. The cells were washed with DPBS 1X and incubated with polymersomes (500 µg/mL) for 2 h at 37°C. The nuclei were counterstained with Hoechst 33342 (1 µg/mL). After washing three times with ice-cold DPBS 1X, the cells were fixed with 4% paraformaldehyde (15 min at 4°C). The cells were then incubated with either rabbit polyclonal anti-EEA1 or anti-Lamp1 antibodies for endosomes and lysosomes staining (1:500), respectively. The cells were washed with

DPBS 1X, followed by staining with the 2nd antibody, i.e., goat anti-rabbit polyclonal antibody Dylight 633 (1:1000). Images were captured using an Olympus FV 1000 inverted laser scanning microscope equipped with 40x (NA 1.30) and 60x (NA 1.40) oil immersion objectives (Olympus, Tokyo, Japan). Samples were excited with 488 nm laser for the localization of the fluorescent polymersome-antibody conjugates, 405 nm laser for visualization of the nuclei, and 635 nm laser for the detection of intracellular organelles.

RESULTS AND DISCUSSION

Polymersomes have the potential to be employed as carriers for active drug targeting (Kamaly et al., 2012). In the present study, we used polymersomes composed of the amphiphilic diblock copolymers PDMS-*b*-PMOXA for targeting brain endothelial cells (Figure 1). A previous study showed the spontaneous self-assembly of the hydroxyl-functionalized diblock copolymers, $PDMS_{65}$-*b*-$PMOXA_{13}$, into vesicles in aqueous solution by the film rehydration method (Egli et al., 2011). The mixture of $PDMS_{65}$-*b*-$PMOXA_{14}$ (95%) with NHS ester-modified $PDMS_{65}$-*b*-$PMOXA_{32}$ copolymers (5%) allowed to conjugate the polymersomes with 83-14 mAb, which binds with high affinity to the human insulin receptor and subsequently mediates cellular uptake and transcytosis *in vivo* (Pardridge et al., 1995).

Synthesis and characterization of PDMS-b-POMXA diblock copolymers

Synthesis and characterization of hydroxyl-functionalized PDMS-*b*-PMOXA diblock copolymer has been described previously (Egli et al., 2011). The NMR spectra of hydroxyl-functionalized $PDMS_{65}$-*b*-$PMOXA_{32}$ diblock copolymer before and after modification to carboxyl acid-functionalized copolymer revealed an additional peak with a chemical shift of 2.55 ppm (Figure S2, Ha). This demonstrates the successful addition of the carboxyl acid group on the $PDMS_{65}$-*b*-$PMOXA_{32}$ diblock copolymer. Moreover, FTIR results showing an additional peak with wave number of 1728 cm^{-1} for the carbonyl group of the carboxylic acid (Figure S3) further confirmed the reaction to $PDMS_{65}$-*b*-$PMOXA_{32}$-COOH. This copolymer was further treated with *N*-hydroxysuccinimide and

N, N'-dicyclohexylcarbodiimide in anhydrous dichloromethane. The appearance of a white precipitate during the reaction was indicative of successful esterification. After purification, the final product was used without any additional treatment.

Preparation and characterization of polymersomes conjugated to 83-14 mAb

Fluorescently labeled 83-14 mAb

The antibody was first labeled with NHS ester-functionalized fluorescent dye. This functional group reacts with primary amines on the antibody forming amid bonds leading to stable antibody-dye conjugates. Reaction of the fluorophore with primary amines on the binding site may reduce antibody functionality and may even lead to inactivation of the antibody (Vira et al., 2010). Therefore, labeling was optimized in order to achieve a strong fluorescence signal while retaining antibody functionality. We systematically modified the 83-14 mAb with the fluorescent dye 5(6)-carboxyfluorescein NHS ester and tested its functionality after labeling using flow cytometry. We used hCMEC/D3 cells that express much larger quantities of insulin receptor than TY09 cells (Figure 4A). With increasing amount of dye, the fluorophore to protein (F/P) labeling ratios increased linearly. Moreover, flow cytometry analysis revealed increasing fluorescence intensity with increasing F/P ratios. This indicated that the antibody retained its functionality even after modification with an average of 9.4 dye molecules per mAb molecule (Table 1). Higher labeling ratios were not studied since over-labeling can increase non-specific background signals and lead to inactivation of the targeting protein (Vira et al., 2010). Our results confirm previous reports indicating that a final labeling with 2-8 moles of fluorophore per mole antibody is optimal (Haugland, 1995; Vira et al., 2010).

For further conjugation of the fluorescently labeled 83-14 mAb to polymersomes, antibodies with an average of five dye molecules per mAb molecule were used. This ratio was chosen because it did not affect the antibody functionality and in addition, free accessible primary amines on the antibody for coupling to the polymersomes were still available (Table 1). For further experiments, 5(6)-carboxyfluorescein NHS ester was replaced by the photostable dye DyLight 488 NHS ester.

Table 1: Flow cytometry analysis of the fluorescently labeled 83-14 mAb with 5(6)-carboxyfluorescein NHS ester. Molar excess of dye applied, resulting F/P ratio, and median fluorescence intensity (MFI) are listed. F/P ratio: dye to protein labeling ratio. Calculation of this ratio is described in the Materials and Methods section. Absorbance measurements were carried out with Spectramax M2e. HCMEC/D3 cells were used for this analysis.

Molar excess of dye to 83-14 mAb	F/P ratio	MFI
5	2.9	9
10	5	11.2
20	9.4	13.2

Polymersomes conjugated to fluorescently labeled 83-14 mAb

Morphology and size

By combining static and dynamic light scattering data, it is possible to study the structure of the supramolecular assemblies in aqueous solution (Stauch et al., 2002). Light scattering measurements of non-functionalized diblock copolymer assemblies revealed dimensions of 109 nm for radius of gyration (R_g) and 115 nm for radius of hydration (R_h). The ρ-value ($\rho=R_g/R_h$) of 0.95 indicated a hollow sphere structure of the assemblies (Stauch et al., 2002) (Table 2, Figure S4). This observation is in line with findings from a previous study, where a ρ-value of 0.92 was obtained for the $PDMS_{65}$-*b*-$PMOXA_{13}$ diblock copolymer (Egli et al., 2011). Addition of 5% $PDMS_{65}$-*b*-$PMOXA_{32}$-NHS diblock copolymer did not alter the polymersomes structure as confirmed with light scattering data (Table 2). Upon antibody conjugation, the hydrodynamic size of the polymersomes was 117 nm in radius. The polymersomes exhibited a monodisperse size distribution (polydispersity index 0.13). These particles were bigger than liposomes and polymersomes previously used for receptor-mediated brain drug delivery (Huwyler et al., 1996; Pang et al., 2011). However, 200 nm ApoE-coated nanoparticles have recently been shown to cross the BBB (Zensi et al., 2009), and it has been demonstrated that this active process is mediated by the low-density lipoprotein receptor-related protein

(Wagner et al., 2012). We therefore did not consider size to be a limiting factor for our polymersomes to cross cellular barriers *in vivo*.

Table 2: Light scattering data of polymersomes purely composed of $PDMS_{65}$-*b*-$PMOXA_{14}$-OH block copolymer and polymersomes composed of $PDMS_{65}$-*b*-$PMOXA_{14}$-OH (95%) and $PDMS_{65}$-*b*-$PMOXA_{32}$-NHS (5%) block copolymers in aqueous solution.

Block copolymer	**[a] R_g (nm)**	**[b] R_h (nm)**	**ρ ($\rho = \frac{Rg}{Rh}$)**
$PDMS_{65}$-*b*-$PMOXA_{14}$-OH (100%)	109 ± 0.2 nm	115	0.95
$PDMS_{65}$-*b*-$PMOXA_{14}$-OH (95%) $PDMS_{65}$-*b*-$PMOXA_{32}$-NHS (5%)	102 ± 0.2 nm	114	0.89

[a] $R_{g:}$ radius of gyration

[b] $R_{h:}$ radius of hydration

TEM showed the spherically shaped vesicular morphology of non-conjugated polymersomes and polymersomes conjugated to 83-14 mAb (Figure 2). Five percent of NHS ester-functionalized $PDMS_{65}$-*b*-$PMOXA_{32}$ block copolymer served for the conjugation. This molar percentage of functionalized copolymers is in a similar range as the one that was previously used (Egli et al., 2011) and did not affect the self-assembly process as shown in TEM pictures (Figure 2B).

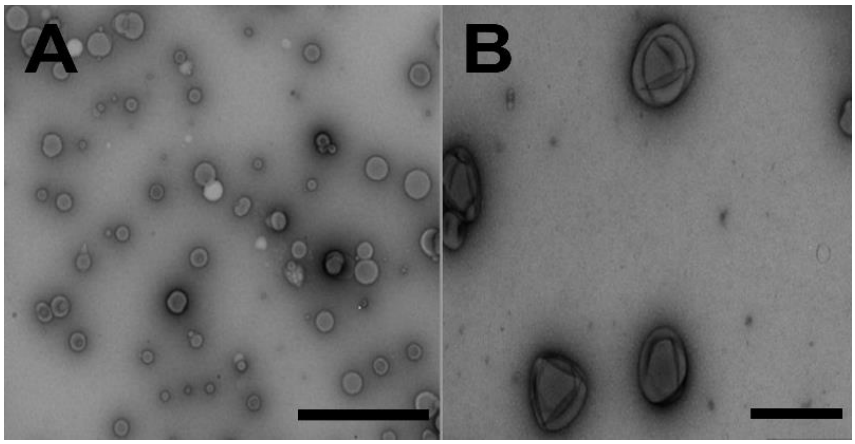

Figure 2: TEM images of PDMS-*b*-PMOXA diblock copolymers with non-conjugated polymersomes (A) and polymersomes conjugated to 83-14 mAb (B). Size bars in A: 2000 nm and B: 500 nm.

Conjugation of antibody

To calculate the number of labeled antibodies attached to one polymersome, we used FCS. Figure 3 shows the normalized FCS autocorrelation curves of free DyLight 488 dye, antibodies labeled with DyLight 488 dye, and polymersomes conjugated to antibodies labeled with DyLight 488. Diffusion times (τ_D) of free DyLight 488 dye, free DyLight 488-labeled antibodies, and polymersomes conjugated to DyLight 488-labeled antibodies were 53 µs, 384 µs, and 12 ms, respectively. Significant differences in diffusion times indicated the association of the antibodies to polymersomes. Molecular brightness of free DyLight 488 dye, free DyLight 488-labeled antibodies, and polymersomes conjugated to DyLight 488 dye-labeled 83-14 mAb allowed to estimate the number of free DyLight 488 dye per antibody, and also the number of antibodies per polymersome. On average, each 83-14 mAb was labeled by five DyLight 488 molecules. This result is in line with the F/P ratio obtained by the absorbance measurements. In total, 13 antibodies were attached to one polymersome. Because the conjugation reaction of amine-functionalized antibody with NHS ester-functionalized diblock copolymers was performed during the self-assembly process, topological orientation of antibody was not predefined.

Recently, polymersomes composed of PDMS-b-PMOXA diblock copolymers were modified with an antibody to specifically target HER2-positive breast cancer cells, SKBR3 (Egli et al., 2011). The antibody-polymersome conjugation technique used by the authors comprised two steps. First, the surface of the polymersomes and antibody were modified with two different functionalities, i.e., 4-succinimidyl 4-formylbenzoate and succinimiyl 6-hydrazinonicotinate acetone hydrazone. In a second step, the modified reactants were allowed to react resulting in a bis-aryl hydrazone bond (Egli et al., 2011). This conjugation led to a stable covalent bond. However, this method involves multiple purification steps that may impact on the overall recovery of samples (GE Healthcare, 2010). In contrast, our approach offers a rapid one-step preparation of polymersomes and simultaneous conjugation to antibodies. This method is straightforward and simple since it is a “one-pot” reaction and only needs one purification step to remove unbound antibody.

Vesicles composed of similar block copolymers, i.e., PMOXA-*b*-PDMS-*b*-PMOXA, are stable in buffer over a period of four months (Litvinchuk et al., 2009). Nevertheless,

we have used the conjugated polymersomes immediately after preparation in order to ascertain the integrity of the polymersome-antibody conjugates for all cell experiments.

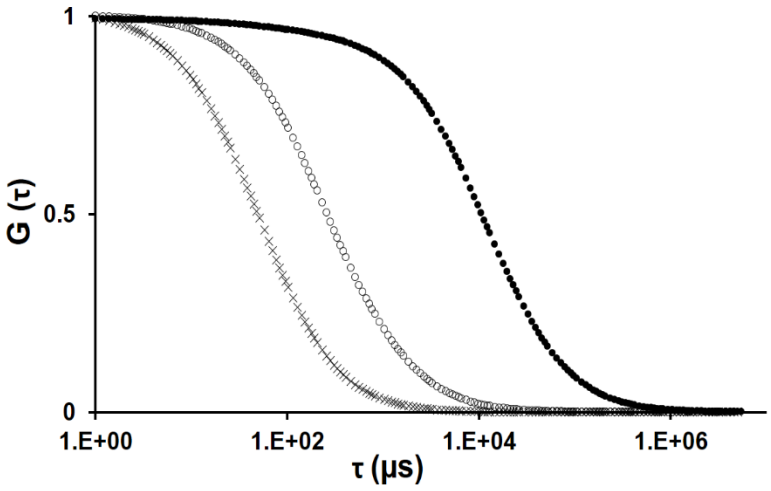

Figure 3: Fluorescence correlation spectroscopy analysis of polymersomes conjugated to fluorescently labeled 83-14 mAb. Normalized autocorrelation curves of free DyLight 488 dye (X), DyLight 488-labeled 83-14 mAb (O), and polymersomes conjugated to DyLight 488-labeled 83-14 mAb (●). Different diffusion times of free DyLight 488 (53 µs), DyLight 488-labeled 83-14 mAb (384 µs), and polymersomes conjugated to DyLight 488-labeled 83-14 mAb (12 ms) indicated the successful conjugation of the polymersomes. Autocorrelation curves represent the averages of 10 measurements over 30 s.

Expression of insulin receptor by brain capillary endothelial cells

High expression of the targeted receptor is a prerequisite for the study of receptor-mediated cellular uptake of particles in *in vitro* models. We have quantified the expression of insulin receptor in two human BBB *in vitro* models, i.e., hCMEC/D3 and TY09. The hCMEC/D3 cell line is a well-characterized BBB *in vitro* model which retains typical BBB characteristics (Poller et al., 2008; Weksler et al., 2005). TY09 is a human conditionally immortalized BBB cell model that shows barrier-specific properties even after repeated passages (Sano et al., 2012).

Flow cytometry analysis revealed high expression of the human insulin receptor by hCMEC/D3 cells. Approximately 94% of the cell population expressed this receptor on the cell surface. In contrast, only 13.4% of the TY09 cell population expressed the insulin

receptor (Figure 4A). Therefore, our result revealed the preservation of insulin receptor functionality in culture conditions in hCMEC/D3 cells and support previous observations that the insulin receptor is expressed at gene and protein levels (Ohtsuki et al., 2013; Urich et al., 2012). Consequently, we used the hCMEC/D3 cell line for further investigations.

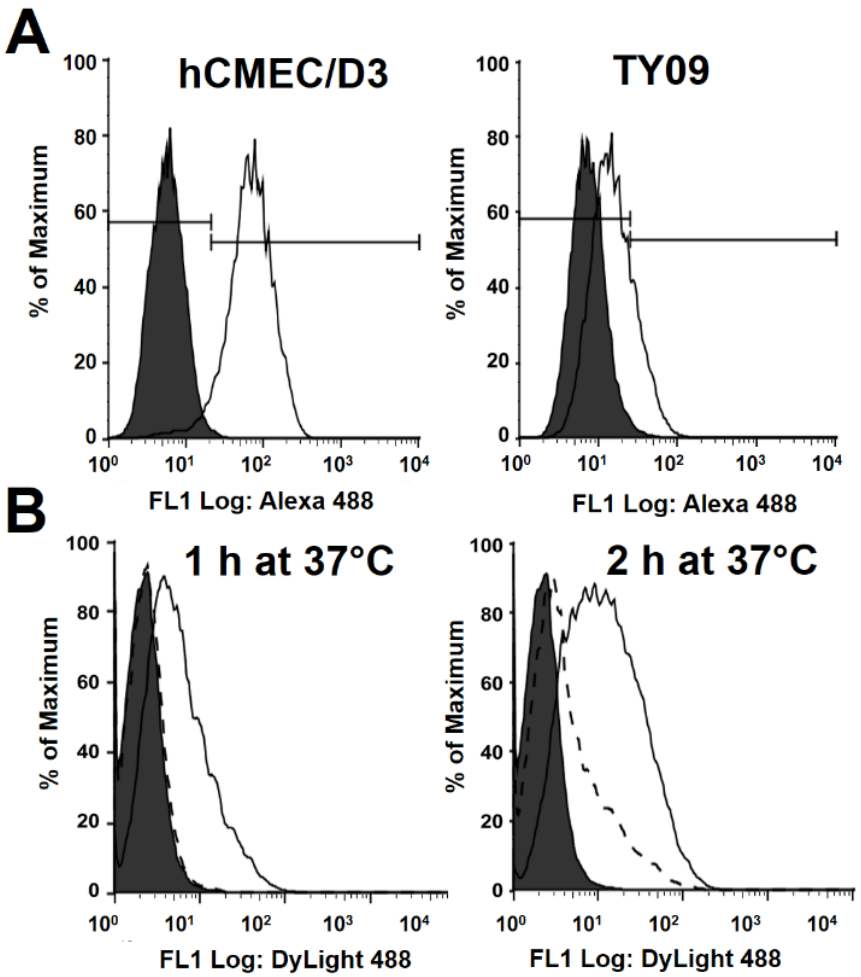

Figure 4: Flow cytometry analysis of insulin receptor expression and uptake of polymersomes conjugated to 83-14 mAb by brain endothelial cells. **A**: Human insulin receptor expression by hCMEC/D3 and TY09 cells. Solid line, shaded area: negative control, cells only stained with anti-mouse Alexa 488 2nd antibody. Solid line, white area: cells stained with 83-14 mAb and 2nd anti-mouse antibody Alexa 488. **B**: Uptake of polymersomes conjugated to 83-14 mAb by hCMEC/D3 cells. Solid line, shaded area: negative control (untreated cells); solid line, white area: cells incubated with polymersomes conjugated to 83-14 mAb for 1 h or 2 h. Dashed line: competitive inhibition of uptake with an excess of free 83-14 mAb. FL 1 Log: Fluorescence signal was collected in FL1 detector as described in the Materials and Methods section and is expressed in logarithmic unit.

Endocytosis of polymersomes conjugated to 83-14 mAb by hCMEC/D3 cell line

Cellular uptake

To investigate cellular interactions, hCMEC/D3 cells were incubated with polymersomes conjugated to 83-14 mAb for predefined times at 37°C. Flow cytometry analysis revealed cellular uptake of polymersomes conjugated to 83-14 mAb by hCMEC/D3 cells. Median fluorescence intensity (MFI) increased from control level by a factor of 2.6 to 5.6 after 1 h and to 10.8 after 2 h of incubation (Figure 4B). To further analyze the specificity of uptake, we treated the cells with polymersomes conjugated to 83-14 mAb in the presence of an excess of free 83-14 mAb. The MFI values decreased to the level of control cells after incubation for 1 h and to 3.5 after incubation for 2 h. Thus, competitive inhibition of uptake indicated the specificity of this process and the involvement of a receptor-mediated uptake mechanism for polymersomes conjugated to 83-14 mAb.

To further confirm these results, cellular uptake of polymersomes conjugated to 83-14 mAb by hCMEC/D3 cells was visualized using confocal laser scanning microscopy after 2 h of incubation at 37°C. This demonstrated intracellular localization of polymersomes conjugated to 83-14 mAb (Figure 5B). For comparison, the cells were incubated with DyLight 488-labeled 83-14 mAb at 37°C for 20 min leading to a similar green fluorescent signal in perinuclear regions (Figure 5A).

Intracellular localization

To elucidate the intracellular trafficking of polymersomes conjugated to 83-14 mAb in endothelial cells, EEA1 and Lamp1 were stained for visualization of early endosomes and lysosomes, respectively. In order to investigate whether polymersomes conjugated to 83-14 mAb followed the same intracellular trafficking mechanism as 83-14 mAb alone, the cells were incubated with free labeled 83-14 mAb and polymersomes conjugated to 83-14 mAb. After 20 min of incubation, 83-14 mAb showed a colocalization with a subpopulation of early endosomes and lysosomes (Figure 5C). Intracellular localization of polymersomes conjugated to 83-14 mAb in hCMEC/D3 cells could be observed after to 2 h of incubation. Again, polymersomes conjugated to 83-14 mAb showed colocalization with a subpopulation of early endosomes and lysosomes after exposure for

2 h at 37°C (Figure 5D). However, the colocalization signal of the targeted polymersomes with intracellular organelles was much weaker than the signal obtained with labeled 83-14 mAb. This is in line with a previous study where only few intracellular PMOXA-*b*-PDMS-*b*-PMOXA-based polymersomes were detected in endolysosomal compartments (Tanner et al., 2013). Previous findings suggested that nanoparticle conjugation influences the mechanism of antibody-mediated receptor endocytosis and subsequent trafficking (Bhattacharyya et al., 2010). Therefore, the different intracellular localization of the polymersome-antibody conjugates relative to the antibody alone may be due to altered trafficking upon conjugation. In addition, the slower accumulation of polymersomes conjugated to 83-14 mAb in these organelles as compared to free mAb can be attributed to the size of the polymersomes since the time needed for cellular uptake and intracellular trafficking of particles is influenced by particle size (Albanese et al., 2012). Although receptor-mediated endocytosis and subsequent intracellular trafficking to the endosomes and lysosomes of antibody is rapid (Smith and Gumbleton, 2006), larger particles may require longer for this transport process (Rejman et al., 2004). For this reason, previous uptake studies with nanoparticles used prolonged incubation times (Balasubramanian et al., 2011; Massignani et al., 2009). However, an incubation time exceeding 2 h might result in non-specific uptake (Egli et al., 2011). Thus, in our experiment, the exposure of particles to cells was limited to 2 h. Nevertheless, this period allowed comparing intracellular trafficking between free antibody and antibody conjugated to polymersomes.

CONCLUSION

In summary, we have successfully functionalized PDMS-*b*-PMOXA-based polymersomes with the high-affinity anti-insulin receptor antibody 83-14 via a one-step reaction. This method allowed to rapidly prepare polymersome-antibody conjugates for investigations of cellular nanoparticle interactions. *In vitro* experiments demonstrated endocytosis of the ligand-targeted polymersomes by human brain capillary endothelial cells. Competitive inhibition of uptake indicated the specificity of this process. Therefore, polymersome-83-14 mAb conjugates based on PDMS-*b*-PMOXA block copolymers may be useful to deliver drugs to the brain. The exact molecular mechanism for the uptake of

large particles by brain endothelial cells has not yet been elucidated. We observed altered intracellular trafficking of the polymersome-antibody conjugates compared to free 83-14 mAb. Particle size seems to critically affect the kinetics of cellular uptake and trafficking (Massignani et al., 2009). Further investigations are required to elucidate if other factors may be involved in this distinct trafficking pattern for the polymersomes conjugated to 83-14 mAb compared to antibody alone and if these findings can be confirmed in animal experiments.

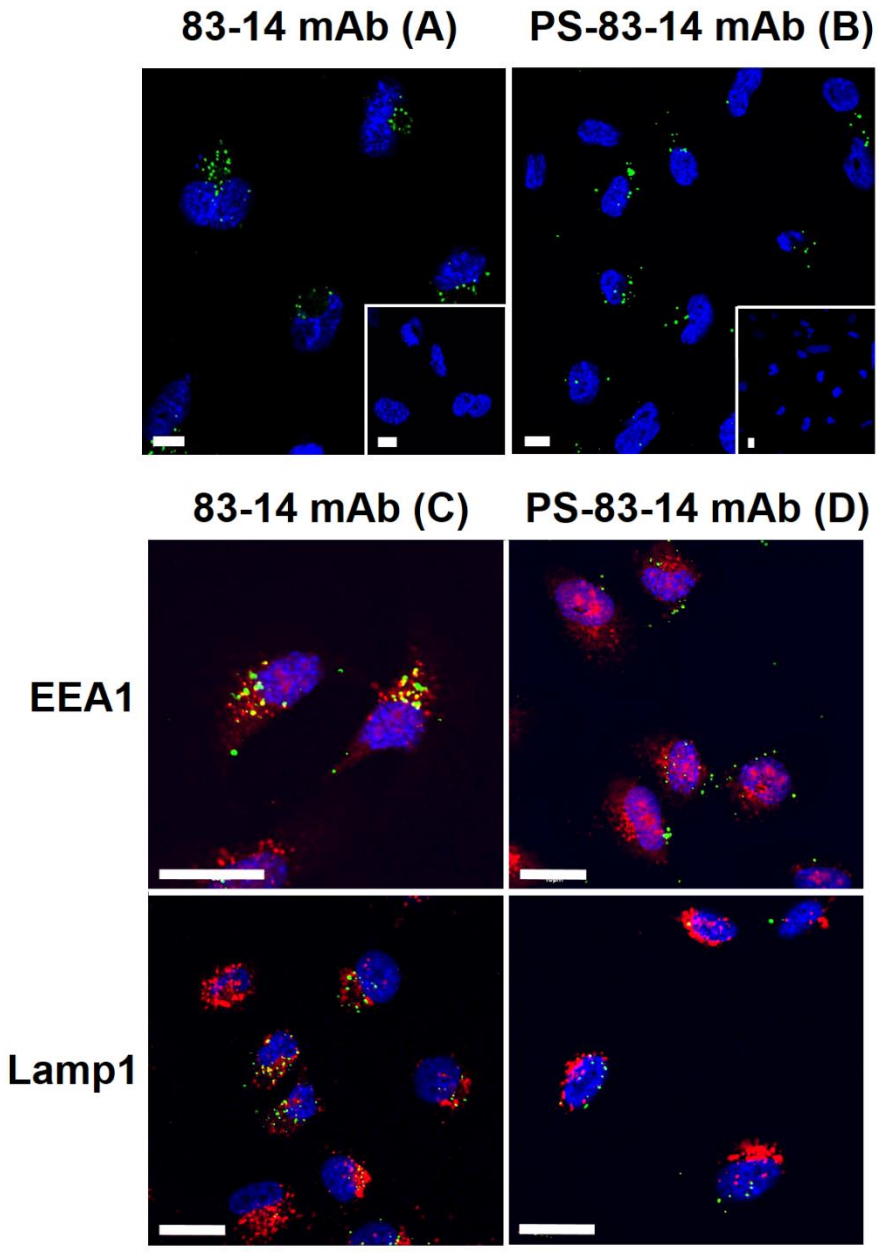

Figure 5: Intracellular localization of 83-14 mAb and polymersomes conjugated to 83-14 mAb (PS-83-14 mAb) in hCMEC/D3 cells. The cells were either exposed to DyLight 488-labeled 83-14 mAb for 20 min (A, C) or to polymersomes conjugated to 83-14 mAb for 2 h (B, D). In C and D, the samples were additionally stained with biochemical organelle markers. Endosomes were visualized with EEA1 staining, and lysosomes with Lamp1 staining. Blue: cell nuclei were stained with Hoechst 33342. Green: 83-14 mAb or 83-14 mAb-PS, yellow: colocalization of the organelles with 83-14 mAb or PS-83-14 mAb. Control samples were stained with Hoechst 33342 and showed no background fluorescence. Size bars: 20 µm.

ACKNOWLEDGEMENTS

We thank Prof. Dr. Wolfgang Meier, Department of Chemistry, University of Basel, for his support with the synthesis of PDMS-*b*-PMOXA block copolymers and useful discussions, Dr. Silvia Rogers for editorial assistance, and the center for microscopy Basel (ZMB) for their support with TEM. The confocal microscope used in the present study was purchased with financial support from the Swiss National Science Foundation (R'Equip).

SUPPORTING INFORMATION

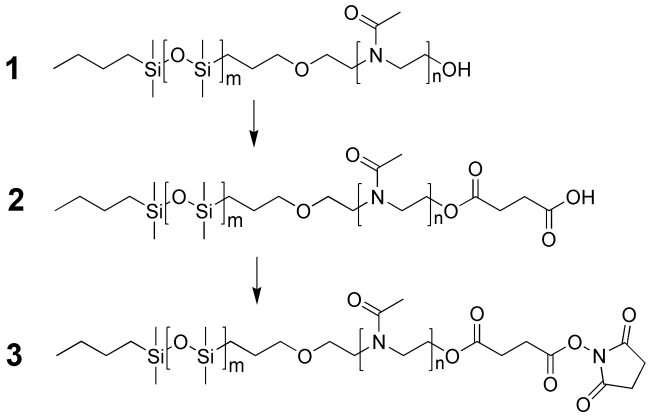

Figure S1: Chemical synthesis of $PDMS_{65}$-*b*-$PMOXA_{32}$-COOH and $PDMS_{65}$-*b*-$PMOXA_{32}$-NHS block copolymers. Reagents and conditions for modification of $PDMS_{65}$-*b*-$PMOXA_{32}$-OH (1) to $PDMS_{65}$-*b*-$PMOXA_{32}$-COOH (2): Succinic anhydride, TEA, DMAP, 0°C to room temperature, 24 h (yield 95%); reagents and conditions for modification of $PDMS_{65}$-*b*-$PMOXA_{32}$-COOH (2) to $PDMS_{65}$-*b*-$PMOXA_{32}$-NHS (3): NHS, DCC, room temperature, 24 h (yield 96%).

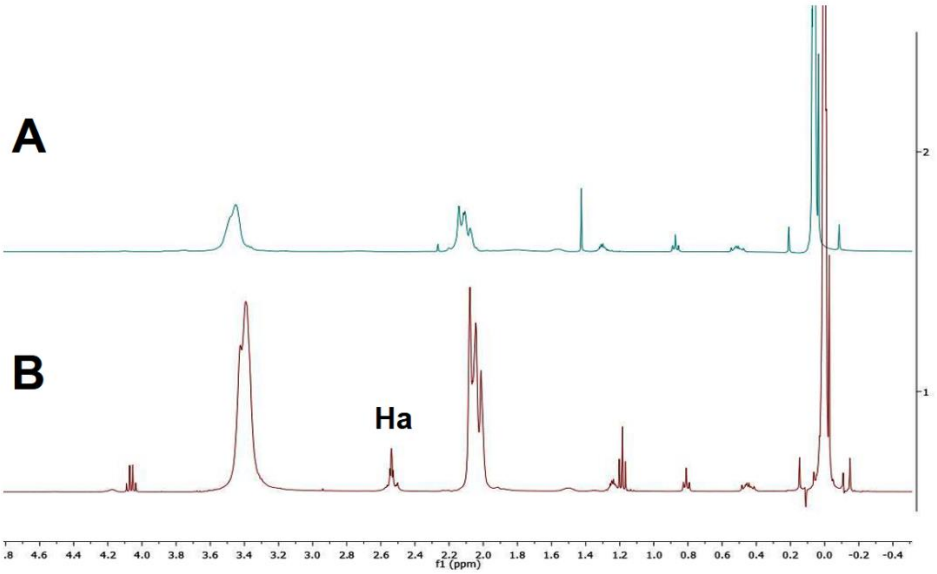

Figure S2: ^{1}H NMR spectra of $PDMS_{65}$-*b*-$PMOXA_{32}$-OH (A) and $PDMS_{65}$-*b*-$PMOXA_{32}$-COOH (B) block copolymers. $PDMS_{65}$-*b*-$PMOXA_{32}$-COOH, Ha: peak corresponds to carboxyl acid. ^{1}H NMR (400 MHz, δ, $CDCl_3$): 0 ppm (m, -Si(CH_3)$_2$), 0.54 ppm (m, -SiCH_2), 0.88 ppm (t, -CH_3), 1.31 ppm (m, CH_3-CH_2-CH_2-), 1.62 ppm (m, -SiCH_2-CH_2-CH_2O-), 2.08-2.21 ppm (m, CH_3-C=O), 2.54 ppm (m, -CH_2-CH_2-COOH), 3.40-3.60 ppm (m, -CH_2-O-CH_2-CH_2-N-CH_2-CH_2-), 4.18 ppm (t, -CH_2-O-C=O).

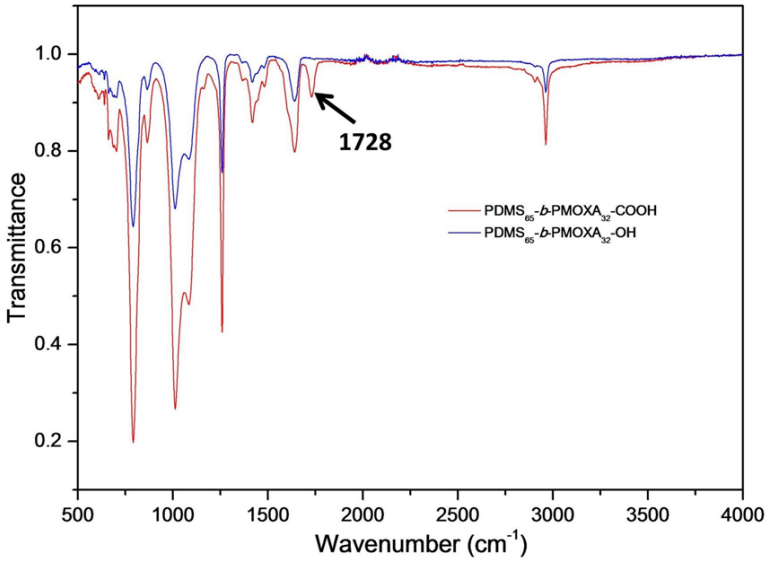

Figure S3: FTIR spectra of $PDMS_{65}$-*b*-$PMOXA_{32}$-OH and $PDMS_{65}$-*b*-$PMOXA_{32}$-COOH block copolymers. Peak at wavelength 1728 cm^{-1} corresponds to carbonyl group of carboxyl acid.

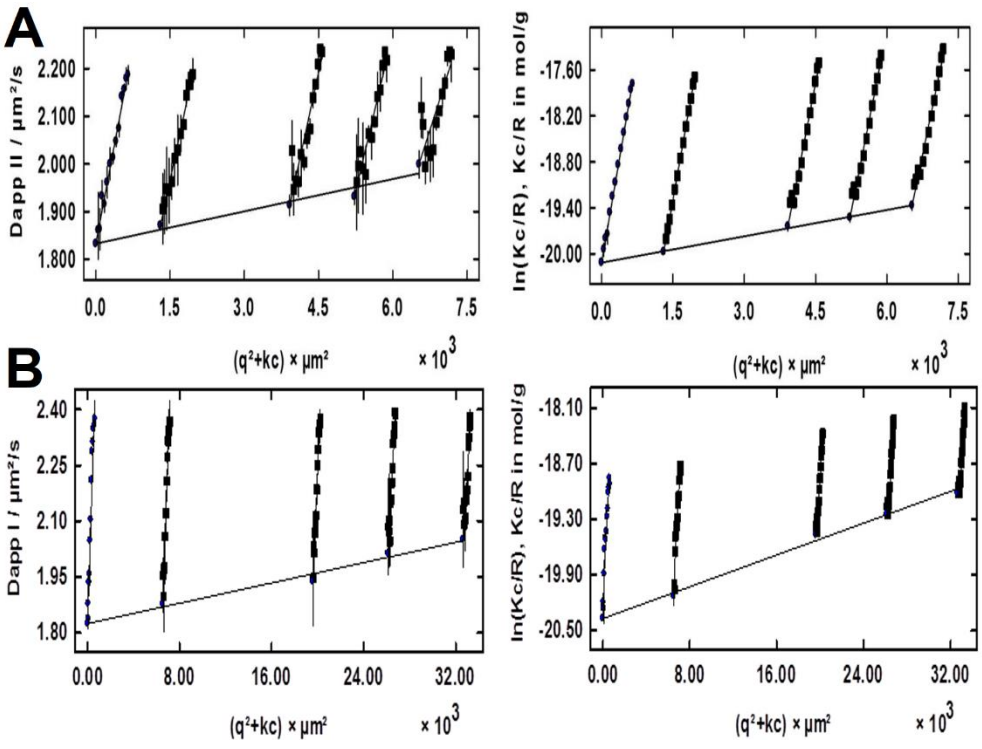

Figure S4: DLS (left) and SLS (right) plots of $PDMS_{65}$-b-$PMOXA_{14}$-OH polymersomes (A) and of $PDMS_{65}$-b-$PMOXA_{14}$-OH polymersomes including 5% of $PDMS_{65}$-$PDMS_{65}$-b-$PMOXA_{32}$-NHS (B). DLS data were calculated by using the Williams-Watts function. Guinier function was employed to fit the SLS data.

REFERENCES

Albanese, A., Tang, P.S., and Chan, W.C.W. (2012). The effect of nanoparticle size, shape, and surface chemistry on biological systems. Annual Review of Biomedical Engineering *14*, 1–16.

Balasubramanian, V., Onaca, O., Enea, R., Hughes, D.W., and Palivan, C.G. (2010). Protein delivery: from conventional drug delivery carriers to polymeric nanoreactors. Expert Opin Drug Deliv *7*, 63–78.

Balasubramanian, V., Onaca, O., Ezhevskaya, M., Doorslaer, S.V., Sivasankaran, B., and Palivan, C.G. (2011). A surprising system: polymeric nanoreactors containing a mimic with dual-enzyme activity. Soft Matter *7*, 5595–5603.

Bermudez, H., Brannan, A.K., Hammer, D.A., Bates, F.S., and Discher, D.E. (2002). Molecular weight dependence of polymersome membrane structure, elasticity, and stability. Macromolecules *35*, 8203–8208.

Bhattacharyya, S., Bhattacharya, R., Curley, S., McNiven, M.A., and Mukherjee, P. (2010). Nanoconjugation modulates the trafficking and mechanism of antibody induced receptor endocytosis. Proc. Natl. Acad. Sci. U.S.A. *107*, 14541–14546.

Broz, P., Benito, S.M., Saw, C., Burger, P., Heider, H., Pfisterer, M., Marsch, S., Meier, W., and Hunziker, P. (2005). Cell targeting by a generic receptor-targeted polymer nanocontainer platform. J Control Release *102*, 475–488.

Cabane, E., Zhang, X., Langowska, K., Palivan, C.G., and Meier, W. (2012). Stimuli-responsive polymers and their applications in nanomedicine. Biointerphases *7*, 9.

Cerletti, A., Drewe, J., Fricker, G., Eberle, A., and Huwyler, J. (2000). Endocytosis and transcytosis of an immunoliposome-based brain drug delivery system. Journal of drug targeting *8*, 435–446.

Discher, D.E., and Eisenberg, A. (2002). Polymer vesicles. Science *297*, 967–973.

Van Dongen, S.F.M., Nallani, M., Cornelissen, J.J.L.M., Nolte, R.J.M., and van Hest, J.C.M. (2009). A three-enzyme cascade reaction through positional assembly of enzymes in a polymersome nanoreactor. Chemistry – A European Journal *15*, 1107–1114.

Egli, S., Nussbaumer, M.G., Balasubramanian, V., Chami, M., Bruns, N., Palivan, C., and Meier, W. (2011). Biocompatible functionalization of polymersome surfaces: a new approach to surface immobilization and cell targeting using polymersomes. J. Am. Chem. Soc. *133*, 4476–4483.

Gaitzsch, J., Canton, I., Appelhans, D., Battaglia, G., and Voit, B. (2012). Cellular interactions with photo-cross-linked and pH-sensitive polymersomes: biocompatibility and uptake studies. Biomacromolecules *13*, 4188–4195.

GE Healthcare (2010). Strategies for protein purification. GE Healthcare Handbook p 40, Chapter 4.

Haugland, R.P. (1995). Coupling of monoclonal antibodies with fluorophores. In Monoclonal Antibody Protocols, W.C. Davis, ed. (Humana Press), pp. 205–221.

Huwyler, J., Wu, D., and Pardridge, W.M. (1996). Brain drug delivery of small molecules using immunoliposomes. PNAS *93*, 14164–14169.

Kamaly, N., Xiao, Z., Valencia, P.M., Radovic-Moreno, A.F., and Farokhzad, O.C. (2012). Targeted polymeric therapeutic nanoparticles: design, development and clinical translation. Chem. Soc. Rev. *41*, 2971–3010.

Kumar, M., Grzelakowski, M., Zilles, J., Clark, M., and Meier, W. (2007). Highly permeable polymeric membranes based on the incorporation of the functional water channel protein Aquaporin Z. Proc. Natl. Acad. Sci. U.S.A. *104*, 20719–20724.

Litvinchuk, S., Lu, Z., Rigler, P., Hirt, T.D., and Meier, W. (2009). Calcein release from polymeric vesicles in blood plasma and PVA hydrogel. Pharm. Res. *26*, 1711–1717.

Massignani, M., LoPresti, C., Blanazs, A., Madsen, J., Armes, S.P., Lewis, A.L., and Battaglia, G. (2009). Controlling cellular uptake by surface chemistry, size, and surface topology at the nanoscale. Small *5*, 2424–2432.

Najer, A., Wu, D., Vasquez, D., Palivan, C.G., and Meier, W. (2013). Polymer nanocompartments in broad-spectrum medical applications. Nanomedicine (Lond) *8*, 425–447.

Ohtsuki, S., Ikeda, C., Uchida, Y., Sakamoto, Y., Miller, F., Glacial, F., Decleves, X., Scherrmann, J.-M., Couraud, P.-O., Kubo, Y., et al. (2013). Quantitative targeted absolute proteomic analysis of transporters, receptors and junction proteins for validation of human cerebral microvascular endothelial cell line hCMEC/D3 as a human blood-brain barrier model. Mol. Pharmaceutics *10*, 289–296.

De Oliveira, H., Thevenot, J., and Lecommandoux, S. (2012). Smart polymersomes for therapy and diagnosis: fast progress toward multifunctional biomimetic nanomedicines. Wiley Interdiscip Rev Nanomed Nanobiotechnol *4*, 525–546.

Pang, Z., Gao, H., Yu, Y., Chen, J., Guo, L., Ren, J., Wen, Z., Su, J., and Jiang, X. (2011). Brain delivery and cellular internalization mechanisms for transferrin conjugated biodegradable polymersomes. Int J Pharm *415*, 284–292.

Pardridge, W.M. (2003). Blood-brain barrier drug targeting: the future of brain drug development. Mol. Interv. *3*, 90–105, 51.

Pardridge, W.M., Eisenberg, J., and Yang, J. (1985). Human blood—brain barrier insulin receptor. Journal of Neurochemistry *44*, 1771–1778.

Pardridge, W.M., Kang, Y.S., Buciak, J.L., and Yang, J. (1995). Human insulin receptor monoclonal antibody undergoes high affinity binding to human brain capillaries in vitro and rapid transcytosis through the blood-brain barrier in vivo in the primate. Pharm. Res. *12*, 807–816.

Poller, B., Gutmann, H., Krähenbühl, S., Weksler, B., Romero, I., Couraud, P.-O., Tuffin, G., Drewe, J., and Huwyler, J. (2008). The human brain endothelial cell line hCMEC/D3 as a human blood-brain barrier model for drug transport studies. J. Neurochem. *107*, 1358–1368.

Ranquin, A., Versées, W., Meier, W., Steyaert, J., and Van Gelder, P. (2005). Therapeutic nanoreactors: combining chemistry and biology in a novel triblock copolymer drug delivery system. Nano Lett. *5*, 2220–2224.

Rejman, J., Oberle, V., Zuhorn, I.S., and Hoekstra, D. (2004). Size-dependent internalization of particles via the pathways of clathrin- and caveolae-mediated endocytosis. Biochem. J. *377*, 159–169.

Sano, Y., Kashiwamura, Y., Abe, M., Dieu, L.-H., Huwyler, J., Shimizu, F., Haruki, H., Maeda, T., Saito, K., Tasaki, A., et al. (2012). Stable human brain microvascular endothelial cell line retaining its barrier-specific nature independent of the passage number. Clinical and Experimental Neuroimmunology *4*, 92–103.

Simmler, L., Buser, T., Donzelli, M., Schramm, Y., Dieu, L.-H., Huwyler, J., Chaboz, S., Hoener, M., and Liechti, M. (2013). Pharmacological characterization of designer cathinones in vitro. British Journal of Pharmacology *168*, 458–470.

Smith, M.W., and Gumbleton, M. (2006). Endocytosis at the blood–brain barrier: from basic understanding to drug delivery strategies. Journal of Drug Targeting *14*, 191–214.

Stauch, O., Schubert, R., Savin, G., and Burchard, W. (2002). Structure of artificial cytoskeleton containing liposomes in aqueous solution studied by static and dynamic light scattering. Biomacromolecules *3*, 565–578.

Tanner, P., Onaca, O., Balasubramanian, V., Meier, W., and Palivan, C.G. (2011). Enzymatic cascade reactions inside polymeric nanocontainers: a means to combat oxidative stress. Chemistry – A European Journal *17*, 4552–4560.

Tanner, P., Balasubramanian, V., and Palivan, C.G. (2013). Aiding nature's organelles: artificial peroxisomes play their role. Nano Lett.

Urich, E., Lazic, S.E., Molnos, J., Wells, I., and Freskgård, P.-O. (2012). Transcriptional profiling of human brain endothelial cells reveals key properties crucial for predictive in vitro blood-brain barrier models. PLoS ONE *7*, e38149.

Vira, S., Mekhedov, E., Humphrey, G., and Blank, P.S. (2010). Fluorescent labeled antibodies - balancing functionality and degree of labeling. Anal Biochem *402*, 146–150.

Wagner, S., Zensi, A., Wien, S.L., Tschickardt, S.E., Maier, W., Vogel, T., Worek, F., Pietrzik, C.U., Kreuter, J., and von Briesen, H. (2012). Uptake mechanism of ApoE-modified nanoparticles on brain capillary endothelial cells as a blood-brain barrier model. PLoS ONE *7*, e32568.

Weksler, B.B., Subileau, E.A., Perrière, N., Charneau, P., Holloway, K., Leveque, M., Tricoire-Leignel, H., Nicotra, A., Bourdoulous, S., Turowski, P., et al. (2005). Blood-brain barrier-specific properties of a human adult brain endothelial cell line. FASEB J. *19*, 1872–1874.

Wu, D., Yang, J., and Pardridge, W.M. (1997). Drug targeting of a peptide radiopharmaceutical through the primate blood-brain barrier in vivo with a monoclonal antibody to the human insulin receptor. J Clin Invest *100*, 1804–1812.

Zensi, A., Begley, D., Pontikis, C., Legros, C., Mihoreanu, L., Wagner, S., Büchel, C., von Briesen, H., and Kreuter, J. (2009). Albumin nanoparticles targeted with Apo E enter the CNS by transcytosis and are delivered to neurones. Journal of Controlled Release *137*, 78–86.

3.4 Bioanalytical Application of Capillary Electrophoresis to Study Transcytosis *in Vitro*

INTRODUCTION

Capillary electrophoresis (CE) is a powerful tool in bioanalytical applications and allows the analysis of a variety of biomolecules (e.g. amino acids, proteins, peptides, nucleic acids and others) (Powell and Ewing, 2005). The minimal sample requirement (nanoliter range) makes this analytical method attractive for several applications, including the investigation of neurological samples and in the context of quantification of transendothelial transport across the BBB (Freed et al., 2002; Powell and Ewing, 2005). The transport of macromolecules, such as monoclonal antibodies, presents a challenge from an analytical point of view, since only small quantities cross the BBB. A sensitive analytical technique is necessary in order to detect the transport of antibody across the BBB *in vitro*. Capillary electrophoresis equipped with a laser-induced fluorescence detector (CE-LIF) is a sensitive analytical method that has already been employed to determine the transport of neuropeptides across the BBB *in vitro* (Freed et al., 2002). Therefore, the present study aimed to evaluate the potential applicability of CE to study transcytosis of macromolecules, i.e. antibodies, *in vitro*.

We used the anti-insulin receptor antibody 83-14 (83-14 mAb) as our model antibody because it binds with high affinity to the insulin receptor and has been shown to cross the BBB *in vivo* (Pardridge et al., 1995). The 83-14 mAb and the extracellular marker albumin were fluorescently labeled. The fluorescent proteins were then applied to a human BBB *in vitro* model expressing the insulin receptor. The extracellular marker monitors the integrity of the cell monolayer during the transport. The quantification of transport of the proteins was performed using CE-LIF.

EXPERIMENTAL PROCEDURES

MATERIALS

Milli Q water was obtained from Millipore (Billerica, Massachusetts, USA). A hybridoma cell line producing the mouse monoclonal antibody against the human insulin receptor (83-14 mAb) was kindly provided by Professor Ken Siddle (Department of Clinical Biochemistry, University of Cambridge, UK). Suppliers of the cell culture reagents and chemicals are indicated in section 3.3. 5(6)-carboxyfluorescein diacetate N-hydroxysuccinimidyl (NHS) ester, sodium bicarbonate, and all other chemicals were obtained from Sigma-Aldrich (Schnelldorf, Germany).

METHODS

Fluorescent labeling of the proteins

Three milligrams of antibody were labeled with 10-fold molar excess of 5(6)-carboxyfluorescein-NHS and 3 mg albumin were modified with 20-fold molar excess of the same dye. The labeling was performed on ice in 0.1 M sodium bicarbonate buffer for 2 h at pH 8.3. The non-reacted dye was removed by size exclusion chromatography using a Sephadex G50 column as described in section 3.3. The end protein concentration was determined using Modified Lowry Protein Assay kit (Thermo Scientific, Waltham, MA, US) according to manufacturer's instructions. Albumin was used as standard for this protein assay. The fluorescent dye to protein ratio (F/P ratio) was quantified for the labeled 83-14 mAb in order to ensure that the fluorescent modification did not exceed the accepted number of dyes per molecule. Previously, we have shown that a F/P ratio up to 10 did not affect the antibody activity. The labeling efficiency was determined according to the manufacturer's instruction using the Beer-Lambert Law (section 3.3). For the transport experiments, the ratio of the fluorescence intensity in the acceptor compartment to that in the donor compartment was determined at each time point. Therefore, it was not necessary to quantify the F/P ratio for albumin.

Capillary electrophoresis

The ProteomeLab PA 800 capillary electrophoresis instrument (Beckman Coulter Inc., Fullerton, CA, USA) equipped with a laser-induced fluorescence detector (CE-LIF) was used for the analysis. A fused-silica capillary (50 µm ID, 375 µm OD, 50 cm to detection window, total length 60 cm; Beckman Coulter) was employed for the separations. Sample was injected into the capillary by pressure (0.5 psi for 20 s). The separation was carried out at 30 kV at 25°C in 50 mM borate buffer, pH 8.8. Excitation was performed using a 488 nm argon-ion laser. Between two runs, the capillary was rinsed 5 min with 1 M NaOH, 5 min with MilliQ water, and another 5 min with borate buffer.

Cell culture

HCMEC/D3 cell line was obtained under license from the Institut National de la Santé et de la Recherche Médicale, Paris, France (Weksler et al., 2005). The cells were maintained in culture as described in section 3.3.

Transport experiments

In the transport experiments, the hCMEC/D3 cells were treated as previously described (Poller et al., 2008). In brief, hCMCE/D3 cells were seeded on polycarbonate Transwell filter inserts (0.4 µm pores, 1.12 cm^2) at a density of 5 x 10^4 cells per cm^2 and cultured for 7 to 10 days. The transport assays were performed in growth-factor-depleted medium (EBM-2 supplemented with bFGF 1 ng/mL, 2.5% FCS, 0.55 µM hydrocortisone, 10 mM HEPES, and 1X penicillin-streptomycin). In the transport studies, 0.1 mg/mL of fluorescently labeled 83-14 mAb was added in presence of the same amount of the extracellular marker albumin to the cell monolayer. Throughout the transport experiment, samples of 20 µL were drawn at 2, 4, 8, and 24 h. The volume was replaced by the same amount of medium. The permeabilities of the test proteins were calculated as described previously and were given as permeability coefficients (P_e). The P_e values of the test compounds across the cell monolayers were corrected by the P_e values of the compounds across blank coated filter inserts without cells (Poller et al., 2008; Sano et al., 2012).

RESULTS AND DISCUSSION

Fluorescent labeling of the proteins

The proteins were fluorescently labeled prior to the transport experiments. The F/P ratio was quantified for the antibody. On average, 5 dyes were labeled to each antibody molecule. This ratio is in the range where the antibody functionality is retained (section 3.3). As mentioned above in ‘methods’, the F/P ratio of the labeled albumin was not determined since the relative fluorescence signals were recorded by comparison with the intrinsic fluorescence intensity of the donor compartment at each time point. Therefore, it was not necessary to quantify the labeling efficiency of albumin.

Capillary electrophoresis

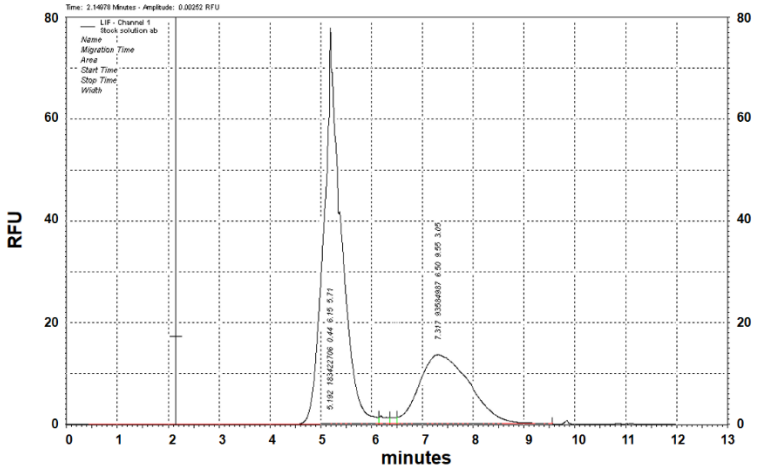

Figure 1: Electropherogram of the stock solution containing 83-14 mAb (t = 5.2 min) and albumin (t = 7.3 min).

The low sample requirement of CE-LIF is of particular advantage when performing transport experiments. A volume of 20 µL was drawn from the acceptor chamber and only few nanoliters were injected into the capillary per run. Therefore, this analytical technique allows multiple sampling during the experiment with only minimal dilution effect because only a small sample volume is replaced by the medium. The transport experiment was performed in transport medium in order to provide the cells with essential nutrients during the period over 24 hours. Moreover, the fetal calf serum in the medium

minimized the sample loss due to potential non-specific adsorption of the antibody to the Transwell chamber. Figure 2 shows the electropherogram of the stock solution containing the fluorescently labeled 83-14 mAb and albumin. The method separated the antibody and albumin in less than 10 min. Using CE-LIF, the labeled antibody reached a low limit of quantification (LLOQ with a signal to noise ratio: 5) of 45 ng/mL (0.3 nM) and albumin 165 ng/mL (2.5 nM) when diluted in transport medium containing serum.

Transcytosis and transendothelial transport

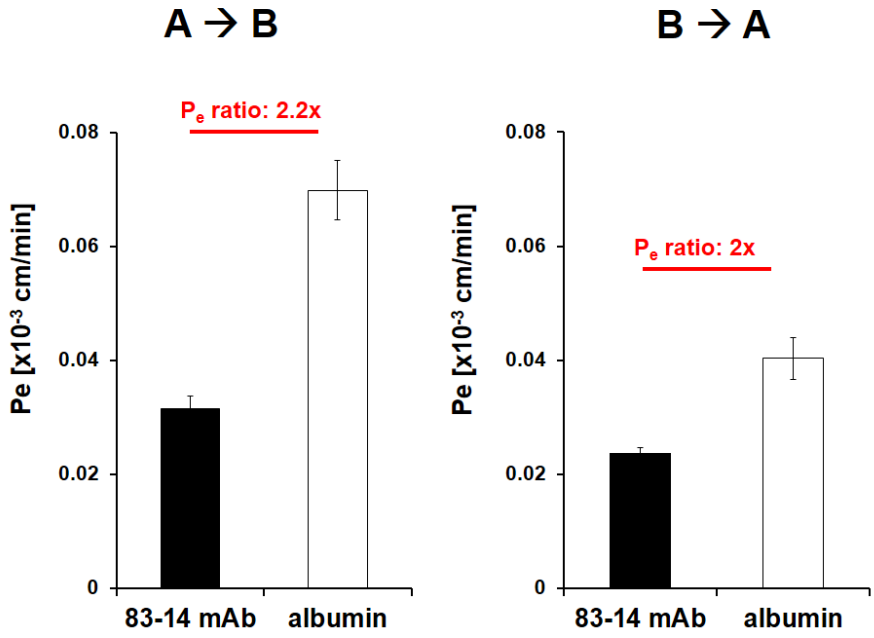

Figure 2: Permeability coefficients of fluorescently labeled 83-14 mAb and albumin. The transport was determined in hCMEC/D3 cell monolayers in apical to basolateral direction (A→B) and basolateral to apical direction (B→A). Values are means ± SEM (n = 3).

To examine whether the 83-14 mAb actively crossed the BBB *in vitro*, we performed bidirectional transport studies. The transport was carried out in presence of the extracellular marker albumin in order to monitor the integrity of the cell monolayers during the experiments. Albumin does not cross the BBB *in vivo* and has been employed as extracellular marker (Bickel, 2005). P_e values of albumin in the experiments were comparable to the permeability coefficient previously observed for Dextran of similar

size (70 kDa) in hCMEC/D3 cell monolayers, indicating monolayer integrity (Weksler et al., 2013). Low permeabilities of 83-14 mAb were determined for both directions (A to B and B to A) with no statistically significant differences. Moreover, the extracellular marker albumin exhibited in both directions a 2-fold higher transport rates across the cell monolayer as compared to 83-14 mAb (Figure 2). This indicates that the detected amount of 83-14 mAb in the receiver side was attributable to passive diffusion enabled by paracellular leakage of our model rather than active transport. The 2-fold higher permeability of albumin compared to the antibody in both directions may be due to the difference in molecular weights of the transported molecules (albumin: 66 kDa, antibody: 150 kDa).

Comparable experiments could not be performed with the TY09 *in vitro* model since the enhanced tightness of this cell line (section 3.1) led to lower signals of the proteins at different time points that were below the detection limit. However, when comparing the transported amount of 83-14 mAb with that of albumin in the receiver compartment at the end of the experiment, similar ratios were obtained as observed in hCMEC/D3 cell line. Similarly, the transport of the 83-14 mAb did not exceed that of albumin. These results suggest that the lack of transcytosis activity was not cell line dependent.

These preliminary experiments indicate that transendothelial transport of fluorescently labeled antibodies can be studied using our cell culture model. Detection limits of the used analytical method, i.e. CE-LIF, allowed for an assessment of the tightness and integrity of the cell monolayers. Passive diffusion of the used antibody across filter membranes could be quantified. However, it was not possible to detect an active transendothelial transport. A possible explanation for the absence of transcytotic activity in our *in vitro* system may be the high-affinity interaction between the 83-14 mAb and the insulin receptor (K_D of 0.45 ± 0.1 nM) (Pardridge, 2001) that competes with the dissociation of the antibody from the receptor. With respect to high-affinity antibody receptor interactions, much research has been focused on the well-known OX26 anti-transferrin receptor antibody. Although the high-affinity OX26 anti-transferrin receptor antibody has been shown to cross the BBB *in vivo*, the antibodies were predominantly associated with the brain capillary endothelial cells and were mainly excluded from the brain parenchyma (Gosk et al., 2004; Moos and Morgan, 2001). Yu et al. recently supported these observations by testing antibodies of different binding affinities against

the transferrin receptor. They showed that high-affinity antibodies mainly remained bound to the brain vasculature and only a limited amount reached the brain parenchyma, whereas low-affinity antibodies were more likely to dissociate from the receptor leading to a higher accumulation in the brain parenchyma (Yu et al., 2011).

In vitro transcytosis has been reported for the FcRn receptor (Dickinson et al., 1999; Stapleton et al., 2011). However, this was observed in epithelial cell lines and the results are not directly comparable with endothelial cells. Moreover, the antibodies used for these studies exhibited at least 1000 times lower affinity to the receptor than the 83-14 mAb.

Furthermore, methodological limitations may also contribute to the lack of transcytosis. Our *in vitro* system consists of brain endothelial cells grown on porous filter inserts that were placed in Transwell chambers filled with medium. This commonly used set-up is convenient and facilitates the sampling procedures during the whole period of the transport experiment. However, the question arises whether this simplified experimental set-up is suitable to detect transcytosis activities of the BBB. *In vivo*, the brain endothelial cells are in close proximity to other cells, i.e. astrocytes, pericytes, microglia, and neurons. For instance, 99% of the surface of the BBB *in vivo* is surrounded by astrocyte foot processes (Pardridge, 1999). This close contact of the BBB to other brain cells may favor the dissociation of the antibody from the receptor at the basolateral side. *In vivo*, once an antibody crosses the BBB, it can immediately interact with acceptor cells. Therefore, further studies can be done with a co-culture system in order to mimic the close cell association *in vivo*.

All these possible explanations may contribute to the discrepancy between the *in vitro* and *in vivo* data. However, these hypotheses need to be verified in the future.

To the best of our knowledge, the transport of the 83-14 mAb across BBB cell monolayers has not yet been documented *in vitro*. The mechanism by which 83-14 mAb reaches the brain remains unresolved. Mechanistic studies in brain endothelial cells to elucidate the molecular mechanism of the transport of the 83-14 mAb might contribute to the understanding of the transcytosis process and the discrepancy between the *in vivo* and *in vitro* data.

With respect to the analytical technique used in the present study, CE-LIF provides a sensitive analytical method for protein quantifications. The high sensitivity in the

picomolar to nanomolar range, combined with the low sample volume requirement, renders this technique attractive for the use in transport studies.

REFERENCES

Bickel, U. (2005). How to measure drug transport across the blood-brain barrier. NeuroRx *2*, 15–26.

Freed, A.L., Audus, K.L., and Lunte, S.M. (2002). Investigation of substance P transport across the blood-brain barrier. Peptides *23*, 157–165.

Pardridge, W.M. (1999). Blood-brain barrier biology and methodology. J. Neurovirol. *5*, 556–569.

Pardridge, W.M., Kang, Y.S., Buciak, J.L., and Yang, J. (1995). Human insulin receptor monoclonal antibody undergoes high affinity binding to human brain capillaries in vitro and rapid transcytosis through the blood-brain barrier in vivo in the primate. Pharm. Res. *12*, 807–816.

Poller, B., Gutmann, H., Krähenbühl, S., Weksler, B., Romero, I., Couraud, P.-O., Tuffin, G., Drewe, J., and Huwyler, J. (2008). The human brain endothelial cell line hCMEC/D3 as a human blood-brain barrier model for drug transport studies. J. Neurochem. *107*, 1358–1368.

Powell, P.R., and Ewing, A.G. (2005). Recent advances in the application of capillary electrophoresis to neuroscience. Anal. Bioanal. Chem. *382*, 581–591.

Sano, Y., Kashiwamura, Y., Abe, M., Dieu, L.-H., Huwyler, J., Shimizu, F., Haruki, H., Maeda, T., Saito, K., Tasaki, A., et al. (2012). Stable human brain microvascular endothelial cell line retaining its barrier-specific nature independent of the passage number. Clin. Exp. Neuroimmunol. *4*, 92–103.

Weksler, B.B., Subileau, E.A., Perrière, N., Charneau, P., Holloway, K., Leveque, M., Tricoire-Leignel, H., Nicotra, A., Bourdoulous, S., Turowski, P., et al. (2005). Blood-brain barrier-specific properties of a human adult brain endothelial cell line. FASEB J. Off. Publ. Fed. Am. Soc. Exp. Biol. *19*, 1872–1874.

Yu, Y.J., Zhang, Y., Kenrick, M., Hoyte, K., Luk, W., Lu, Y., Atwal, J., Elliott, J.M., Prabhu, S., Watts, R.J., et al. (2011). Boosting brain uptake of a therapeutic antibody by reducing its affinity for a transcytosis target. Sci. Transl. Med. *3*, 84ra44–84ra44.

3.5 High-Throughput Viscosity Measurement Using Capillary Electrophoresis Instrumentation

Andrea Allmendinger,[1,2] Le-Ha Dieu,[1] Stefan Fischer,[2] Robert Mueller,[2] Hanns-Christian Mahler,[2] Jörg Huwyler[1]

[1] Division of Pharmaceutical Technology, Department of Pharmaceutical Sciences, University of Basel, Klingelbergstrasse 50, 4056 Basel, Switzerland

[2] Late Stage Pharmaceutical and Processing Development, Pharmaceutical Development & Supplies, Pharma Technical Development Biologics EU, F. Hoffmann-La Roche Ltd, Grenzacherstrasse 124, 4070 Basel, Switzerland

Manuscript in preparation

ABSTRACT

Characterization of viscosity of protein formulations is of utmost importance for the development of subcutaneously administered formulations. However, viscosity determinations are time-consuming and require large sample volumes in the range of hundreds of microliters to a few milliliters, depending on the method used. In this article, we describe an automated, high-throughput method to determine dynamic viscosity of Newtonian fluids using standard capillary electrophoresis (CE) equipment. CE is an analytical method routinely used for the separation and characterization of proteins. The capillary is filled with the test sample, and a constant pressure is applied. Migration time of a riboflavin peak moving through the filled capillary is converted to the viscosity by applying the Hagen-Poiseuille's law. The instrument is operated without using an electrical field. Repeatability, robustness, linearity, and reproducibility were demonstrated for different capillary lots and instruments, as well as for different capillary lengths and diameters. Accuracy was verified by comparing the viscosity data obtained by CE instrumentation with those obtained by plate/cone rheometry. The suitability of the CE method for protein formulations was demonstrated, and advantages and limitations of the method were explored in comparison to different rheological methods used in protein formulation development (plate/cone rheometry, capillary viscosimeters, falling ball viscosimeter). Typical viscosities in the range of 2 to 40 mPas were reliably measured with the CE method. Advantages of the CE method included short measurement times (1 – 15 min) and small sample volumes (few microliters) for a capillary with a diameter of 50 μm and a length of 20.5 cm. Our method promises to be suitable for high-throughput measurements.

INTRODUCTION

Viscosity of protein formulations is a key challenge during formulation development of biologics, such as monoclonal antibodies, for subcutaneous use. At high protein concentrations (>50 – 100 mg/mL), antibodies form viscous solutions due to volume exclusion, protein-protein interactions, and macromolecular crowding (Harris et al., 2004). The viscosity increases exponentially with increasing protein concentration leading to limitations during manufacture (e.g., filtration) and drug administration/injection (Shire, 2009; Shire et al., 2004). Therefore, it is essential to characterize viscosity during formulation and process development. However, only a limited number of rheological methods suitable for viscosity characterization of protein formulations are available. Preferably, viscosity determination should require small amounts of material (in the microliter range) as only limited quantities tend to be available during formulation development. Moreover, viscosity determination should cover a broad viscosity range (preferably between 1 and ~100 mPas) (Jezek et al., 2011), and the method should be manageable in an automated, high-throughput mode. Current methods are sample- and time-consuming and allow a throughput of only a few samples per hour.

Capillary viscosimeters have been used for over a century. The best-known and most frequently used capillary viscosimeters are instruments based on the Ostwald-viscosimeter, the Ubbelohde, and the Canon-Fenske-viscosimeter (Cannon et al., 1960; Mezger, 2010; Ostwald, 1899, 1911; Ubbelohde, 1936; Ubbelohde and Göttner, 1965). These viscometers consist of a glass capillary which is filled with the sample fluid. The sample flows through the capillary driven by gravity, and the migration time for a defined sample volume is measured. The migration time can be converted into the dynamic viscosity of the sample by applying the Hagen-Poiseuille's law. However, large sample volumes in the milliliter range are needed for the commercially available instruments (Jezek et al., 2011; Macosko, 1994; Mezger, 2010). In the recent decades, various efforts have been made to optimize capillary viscometers for smaller sample consumption (Grupi and Minton, 2012; Han et al., 2007; Mach and Arvinte, 2011; Pipe and McKinley, 2009; Pipe et al., 2008; Srivastava et al., 2005). However, these methods do not fulfill all requirements for protein preparations.

The present study aimed to establish an automated, high-throughput method to determine the dynamic viscosity of Newtonian liquids using standard capillary electrophoresis (CE) equipment.

MATERIALS AND METHODS

MATERIALS

Aqueous sucrose and glycerol solutions

For calibration of the CE instrument, standard solutions with defined viscosities consisting of 0% to 60% (w/v) sucrose (Ferro Pfanstiehl, Waukegan, IL, USA) were prepared. The aqueous sucrose solutions covered a viscosity range from 1 to 75 mPas. Viscosity was verified by plate/cone rheometry. For accuracy testing, glycerol/water mixtures were produced by diluting glycerol (99.9%; Acros Organics, Morris Planes, NJ, USA) with water for injection to achieve concentrations between 0% and 80% (w/w) covering a viscosity range of 1 to 65 mPas.

Commercial protein therapeutics

Five commercial protein therapeutics (CPT) were used. These were obtained as either prefilled syringes for CPT 1 (IgG, 60 mg/mL), CPT 2 (IgG, 100 mg/mL), CPT 3 (IgG, 50 mg/mL), and CPT 4 (fusion protein, 50 mg/mL), or as a lyophilisate for CPT 5 (IgG, 100 mg/mL). The products were stored at 2 – 8°C and were used before expiry.

Monoclonal antibody formulation

The purified monoclonal antibody mAb1 (IgG1, pI = 8.5; Mw = ~150 kDa; kD = 5.97 mL/g determined according to Lehermayr et al. 18) was provided by F. Hoffmann-La Roche Ltd (Basel, Switzerland), and was formulated in a 20 mM histidine-acetate buffer (Ajinomoto, Louvain-la-Neuve, Belgium) pH 5.5 at concentrations of 20 to 150 mg/mL.

METHODS

Viscosity measurement using a capillary electrophoresis instrument

A ProteomeLab PA 800 CE instrument (Beckman Coulter Inc., Fullerton, CA, USA) equipped with a photodiode array detector was used. The temperature for sample storage and the capillary was set to 20°C. Bare fused-silica capillaries eCapTM with inner diameters of 50 µm and 75 µm were obtained from Beckman Coulter Inc. (Brea, CA, USA). The instrument was operated without application of an electric field. After rinsing steps with water, 0.1 M HCl, and 0.1 M NaOH at 70 psi (5 min), the capillary was filled with the test sample at high pressure (80 psi) during 5 min. The dye consisting of a 0.02% riboflavin 5' phosphate sodium salt hydrate solution (Sigma Aldrich, St. Louis, MO, USA) was loaded into the capillary by applying pressure (1 psi) for 15 s. Before and after loading, the inlet of the capillary was placed in a vial filled with water to remove remaining dye/sample from the surface of the capillary inlet. After performing an autozero, constant pressure was applied to the system (4 ± 0.05 psi) with the sample vial positioned at the capillary entrance. The dye moved towards the detection window and was detected at 445 nm. Migration time was recorded and related to viscosity. The sample volume for a single measurement was dependent on the capillary properties. A volume of 100 µL in the storage vial with a sample consumption of a few microliters was found to be sufficient for the tested viscosities and set-ups.

The method was tested for repeatability, robustness, linearity, accuracy, and reproducibility using different capillary lots, instruments, capillary lengths, and diameters. Aqueous sucrose and glycerol solutions with defined viscosities showing Newtonian behavior were used. After calibration of the equipment set-up with the sucrose solutions (1 – 75 mPas), dynamic viscosity data for different glycerol concentrations (1 – 65 mPas) were compared to viscosity data obtained by plate/cone rheometry.

Plate/cone rheometry

For comparison, dynamic viscosity was measured on a MCR 301 plate and cone rheometer (Anton Paar AG Switzerland, Zofingen, Switzerland) at 20°C (N = 2). The rheometer was equipped with a measuring cone with an angle of 0.5° and a diameter of 25 mm (Anton Paar AG Switzerland, Zofingen, Switzerland), and a sample volume of

80 µL was used. After equilibration of the sample at a shear rate of 100 s^{-1} for 1 min, the shear rate was increased from 100 s^{-1} to 2,000 s^{-1} over 1 min Dynamic viscosity was determined as the mean of 6 consecutive measurements at a shear rate of 2,000 s^{-1}.

Measuring principle

Figure 1 shows the instrumental set-up and measuring principle based on a capillary electrophoresis with an inner diameter D and total length L.

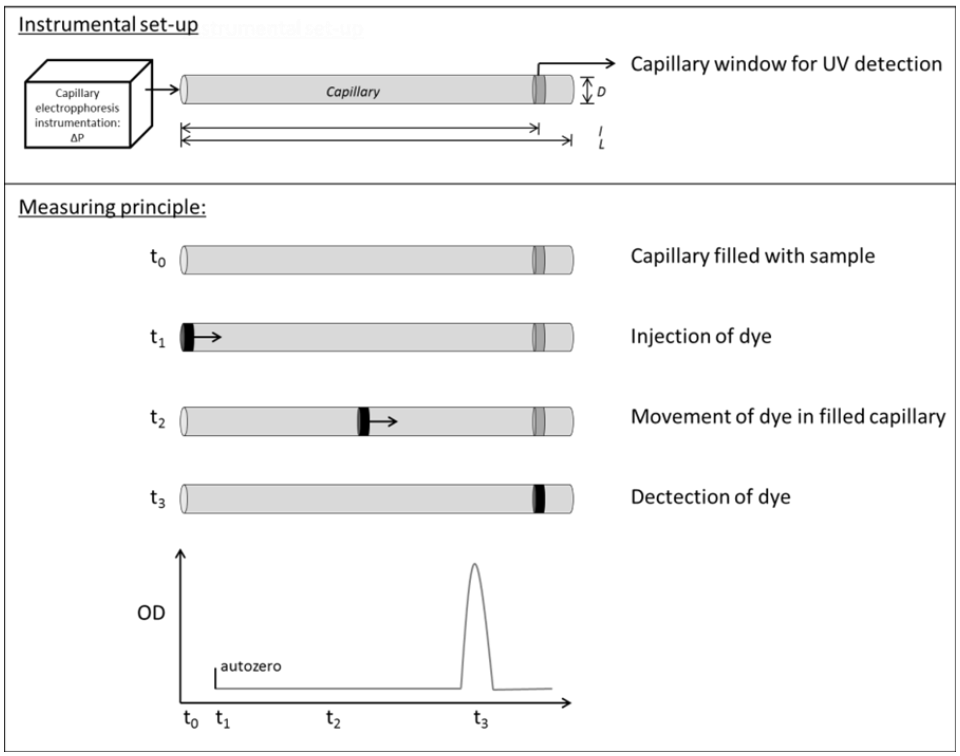

Figure 1: Instrumental set-up and measuring principle of viscosity measurement using CE instrumentation. ΔP = applied pressure [Pa], L = total length of capillary [m], l = length of capillary from inlet to detection window [m], D = inner capillary diameter [m]. (OD = optical density)

The distance between the capillary entrance and window for UV detection corresponds to the capillary length l. At time zero (t0), the capillary is completely filled with the sample. A small amount of dye (riboflavin) is injected into the capillary by applying constant pressure by the CE apparatus (t1). The instrument is operated without use of an electrical field. The volume of the dye is considered negligible compared to the sample volume in the capillary. When applying a constant pressure ΔP, the dye migrates through

the capillary. During this time period, the fluid is continuously drawn up into the capillary which remains completely filled (t2). At t3, the dye is detected as a peak at the capillary window. The migration time t is converted into dynamic viscosity as follows:

The flow of a fluid through a capillary driven by a constant pressure can be described by the Hagen-Poiseuille's law (Equation 1) (Hagen, 1839; Mezger, 2010; Pipe and McKinley, 2009; Poiseuille, 1840; Schiller, 1933; White, 1991). Equation 1 describes the dynamic viscosity η [Pa s] as a function of the applied pressure ΔP [Pa], inner capillary diameter D [m], and time t [s] that the sample takes to flow through the capillary with the length l [m].

$$\boldsymbol{\eta = \frac{\Delta P\, D^2}{32\ l^2} \cdot t} \qquad \textbf{Equation 1}$$

In our set-up, the migration time t was equal to the migration time of the dye, representing the time needed for the sample to flow from the inlet of the capillary to the detection window. This distance is equal to the capillary length l. Equation 1 shows that the dynamic viscosity η of the fluid is directly proportional to the migration time t. To ensure consistent flow and applicability of the Hagen-Poiseuille's law, special attention has to be paid to the completely filled capillary during the measurement. The Hagen-Poiseuille's equation is valid for laminar flow in a tube defined by a Reynolds number Re << 2300 (Mezger, 2010; Reynolds, 1883, 1895). For all tested set-ups, the Reynolds number was equal to 4.5 or smaller and was calculated for the worst case as follows: Re = $\frac{l\, D\, \rho}{\eta\, t}$ = 4.5 with l = 30 cm, D = 50 µm, density $\rho_{20\,°C}$ = 1 g/mL, $\eta_{20\,°C}$ = 1 mPas, and migration time t = 33 s. Figure 2 shows the migration time of the dye as a function of dynamic viscosity determined by plate/cone rheometry for different concentrations of sucrose solutions.

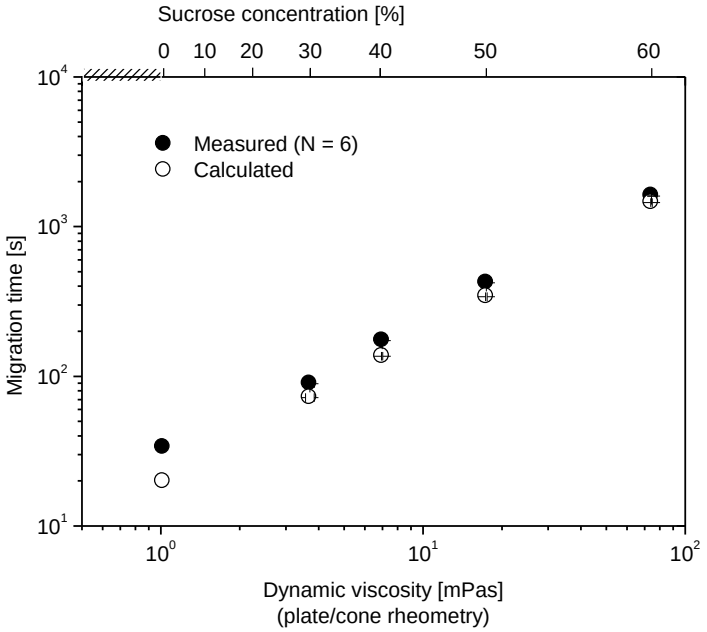

Figure 2: Comparison of measured and calculated migration times based on Hagen-Poiseuille's law for different concentrations of sucrose solutions as a function of dynamic viscosity determined by plate/cone rheometry (2,000 s 1; 20°C). Mean values and standard deviation are reported.

With increasing viscosity, the migration time increased linearly. Figure 2 compares the measured and calculated migration times based on Equation 1. A shift to higher values was found for the measured values due to a lag phase at the beginning of the measurement where the pressure is built up. Therefore, calibration of the system is required before start of the measurement.

Figure 3 (A) shows representative examples of riboflavin peaks with corresponding migration times for different glycerol and sucrose solutions with viscosities between 1 and 25 mPas (D = 50 µm and l = 20.5 cm). The migration time increases with increasing viscosity. The symmetrical peaks are broadening and their intensity decreases with increasing migration time due to Taylor dispersion (Chapman and Goodall, 2008; Lewandrowska et al., 2013). This leads to an upper viscosity limit of the method. Exceeding this limit leads to detection of asymmetrical peaks. Representative examples are shown in Figure 3 (B) for viscosities of 41, 63, and 74 mPas (D = 50 µm, l = 20.5 cm).

However, the viscosity limit changes depending on the capillary diameter and capillary length as described below.

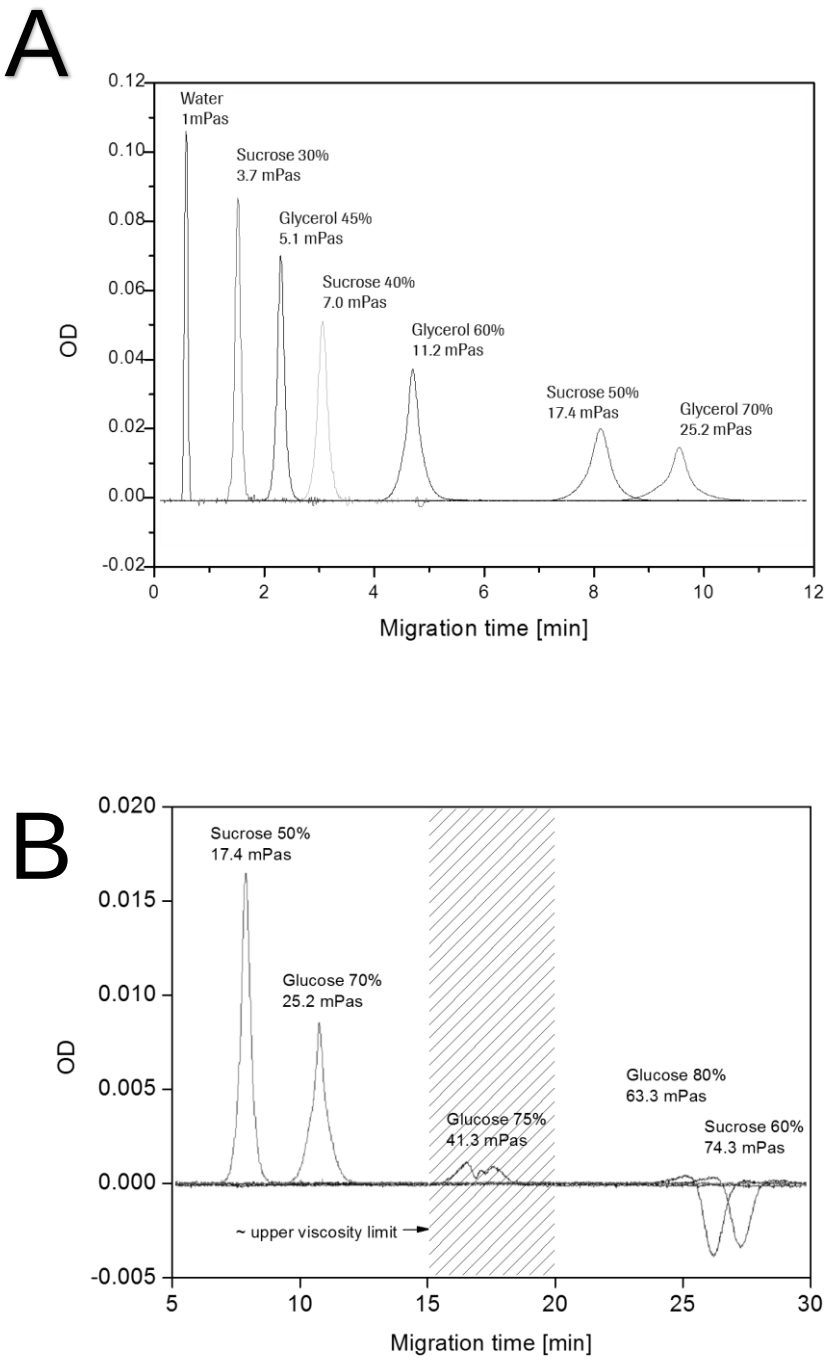

Figure 3: (A) Representative examples of dye peaks (445 nm) for viscosities between 1 and 25 mPas at 20°C. (B) Representative examples of dye peaks (445 nm) below and above the viscosity limit of approximately 40 mPas at 20°C. (Capillary: l = 20.5 cm, D = 50 µm)

The sample volume required for one measurement depends on the diameter and length of the capillary. A volume of 100 µL (storage vial) with a sample consumption of a few microliters was found to be sufficient for the tested viscosities and set-ups.

RESULTS

Figure 4 shows the repeatability, linearity, accuracy, and limit of viscosity measurements at 20°C for different capillaries (A), instruments (B), capillary lengths (C), and capillary diameters (D).

Linearity

In all set-ups used, migration time and dynamic viscosity for the different sucrose solutions (0 – 60% / 1 – 75 mPas) correlated in a linear fashion (Figure 4). The correlation coefficients were between R2 = 0.9988 and 0.9998 (for details see 'Supporting Information', Table S-1). This confirms the direct proportionality of viscosity and migration time in accordance with Hagen-Poiseuille's law.

Repeatability (intra-assay precision) and robustness

Repeatability and robustness were tested by triplicate measurements of different sucrose solutions using three different capillary lots (D = 50 µm, l = 20.5 cm, 20°C; Figure 4, A). Deviations between 0.2 – 1.4% ± 0.2 – 1.9% (average ± standard deviation) were found for the three different capillary lots and different sucrose solutions (intra-capillary repeatability), with the inter-capillary repeatability (robustness) amounting to 1.2 ±1.3% (for details see 'Supporting Information', Table S-1).

Accuracy and viscosity limit

Figure 4 (A) shows the correlation between CE and plate/cone viscosity data for the glycerol solutions and the three different capillary lots. Good agreement between viscosity data obtained from plate/cone rheometry and CE instrumentation was found for viscosities between 2 and 40 mPas. The upper viscosity limit was defined at approximately 40 mPas due to the irregular shape of the riboflavin peak. Accuracy varied

between 1.9% – 5.6% ± 1.9 – 3.5% for the three tested capillaries with a minimum deviation of <0.1% and a maximum deviation of 9.4% (for details see 'Supporting Information', Table S-1).

Reproducibility

For reproducibility testing, measurements were performed on two different CE instruments in different laboratories on different days. Sucrose calibration curves were almost identical for the two CE instruments, (Figure 4, B). Accuracies of 3.2% ± 2.9% (first instrument) and 3.1% ± 2.3% (second instrument) were found for the glycerol samples when comparing the viscosity data obtained by CE and plate/cone instrumentation with a minimum accuracy of 0.1% and 0.3%, and a maximum accuracy of 8.3% and 6.2% for instruments 1 and 2, respectively. The viscosity range ensuring accurate measurements was 2 to 40 mPas as shown also for the first set-up (Figure 4, A).

Optimization: Capillary length

To optimize the method in terms of a shorter measuring time and larger viscosity range, two different capillary lengths (Figure 4, C) and capillary diameters (Figure 4, D) were tested. Figure 4 (C) shows the results for two different capillary lengths, namely 20.5 cm and 30 cm (D = 50 μm, 20°C). The shorter capillary (20.5 cm) was the shortest length feasible and had the smallest distance between inlet vial and the detection window of the capillary. Comparison of the calibration curves showed that elongation of the capillary led to a shift of the calibration curve to longer migration times, in accordance with Equation 1 indicating that the migration time t is directly proportional to the capillary length l. Comparison of viscosity data of the glycerol solutions obtained by plate/cone rheometry and the CE instrument showed good agreement in the range of 2 to 40 mPas (20.5 cm) and 2 – 60 mPas (30 cm), respectively. Although migration time for the 30 cm capillary increased leading to peak broadening and lower intensity, the upper viscosity limit increased to approximately 60 mPas. For the 30 cm capillary, an accuracy of 4.7% ± 2.1% with a minimum of 1.5% and a maximum of 6.6% was found.

Optimization: Capillary diameter

Figure 4 (D) shows the comparison of two different capillary diameters, i.e., 50 µm and 75 µm (l = 20.5 cm, 20°C). The calibration curve for the 75 µm capillary shifted to shorter migration times. This is explained by the Hagen-Poiseuille's equation (Equation 1) as the capillary diameter D is inversely proportional to the migration time t. Comparison of viscosity data of the glycerol solutions obtained by plate/cone rheometry and the CE method revealed good agreement in the viscosity range of 2 to 40 mPas for the 50 µm capillary. However, the upper viscosity limit decreased to approximately 15 mPas when using the 75 µm capillary. An accuracy of 5.9% ± 1.9% was found for the 75 µm capillary with a minimum of 4.5% and a maximum of 8.3%.

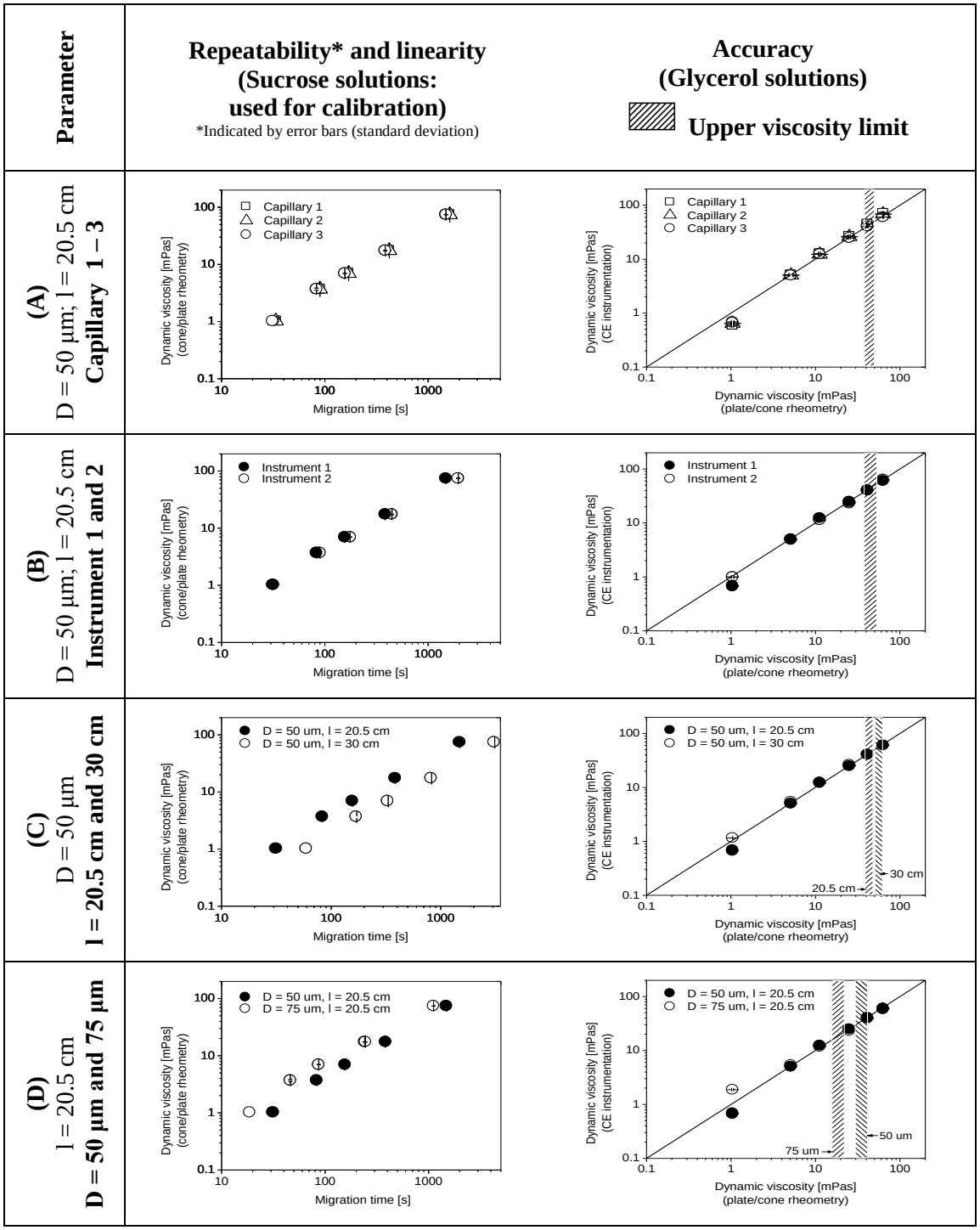

Figure 4: Repeatability, linearity, accuracy, and limit of viscosity measurements at 20°C for different (A) capillaries, (B) instruments, (C) capillary lengths, and (D) capillary diameters. Measurements were performed in triplicates (CE) or duplicates (plate/cone), and mean values and standard deviation are reported. (D = inner capillary diameter, l = capillary length from inlet to detection window)

Application of the CE method to protein formulations

The method to measure viscosity using a CE instrument (D = 50 µm, l = 20.5 cm, 20°C) was applied to protein formulations. As outlined, riboflavin was chosen as a dye which has an absorption maximum at 445 nm. At this wavelength, the absorption of proteins and protein formulations was tested and is considered negligible. Therefore, the proteins and their matrices (formulation) do not interfere with the detection of the dye during UV absorption measurement.

Commercial protein therapeutics

Table 1 compares the viscosity data obtained by plate/cone rheometry with those obtained by the CE instrumentation for the CPT 1 to 5. Good agreement was found between the two methods. Maximum deviation between the viscosity data obtained by the two methods was found for CPT 5 (3.5 mPas) with a deviation of 0.7 mPas.

Table 1: Viscosity of commercial protein therapeutics: Comparison of viscosity data using a CE instrument and plate/cone viscosimeter (20°C). Measurements were performed in triplicates (CE) or duplicates (plate/cone), and mean values and standard deviation are reported.

Product	**Protein concentration [mg/mL]**	**Dynamic viscosity (CE) [mPas]**	**Dynamic viscosity (plate/cone) [mPas]**
CPT 1	60	2.1 ± 0.1	2.0 ± 0.1
CPT 2	100	3.2 ± 0.0	3.0 ± <0.1
CPT 3	50	1.6 ± 0.0	1.6 ± <0.1
CPT 4	50	3.9 ± 0.1	3.7 ± <0.1
CPT 5	100	4.2 ± 0.0	3.5 ± 0.1

CPT = commercial protein therapeutic; CE = capillary electrophoresis

Concentration series of a monoclonal antibody formulation

Viscosity of a monoclonal antibody formulation (mAb1) was determined by the CE method and plate/cone rheometry at different protein concentrations. Figure 5 (A) shows representative riboflavin peaks obtained by the CE instrument with the corresponding migration times for the different protein concentrations. With increasing protein concentration and viscosity, migration time increased as expected; the peaks were broadening, and the intensity decreased. As an example, a migration time of 7.8 min was measured for the highest protein concentration of 151 mg/mL with a viscosity of 13.1 mPas. Figure 5 (B) shows the correlation between the viscosity data obtained by the CE method and plate/cone rheometry. Generally, the data for the measured protein concentrations obtained by CE agreed well with that obtained by plate/cone rheometry, although a small systematic deviation was found for higher viscosities and higher migration times.

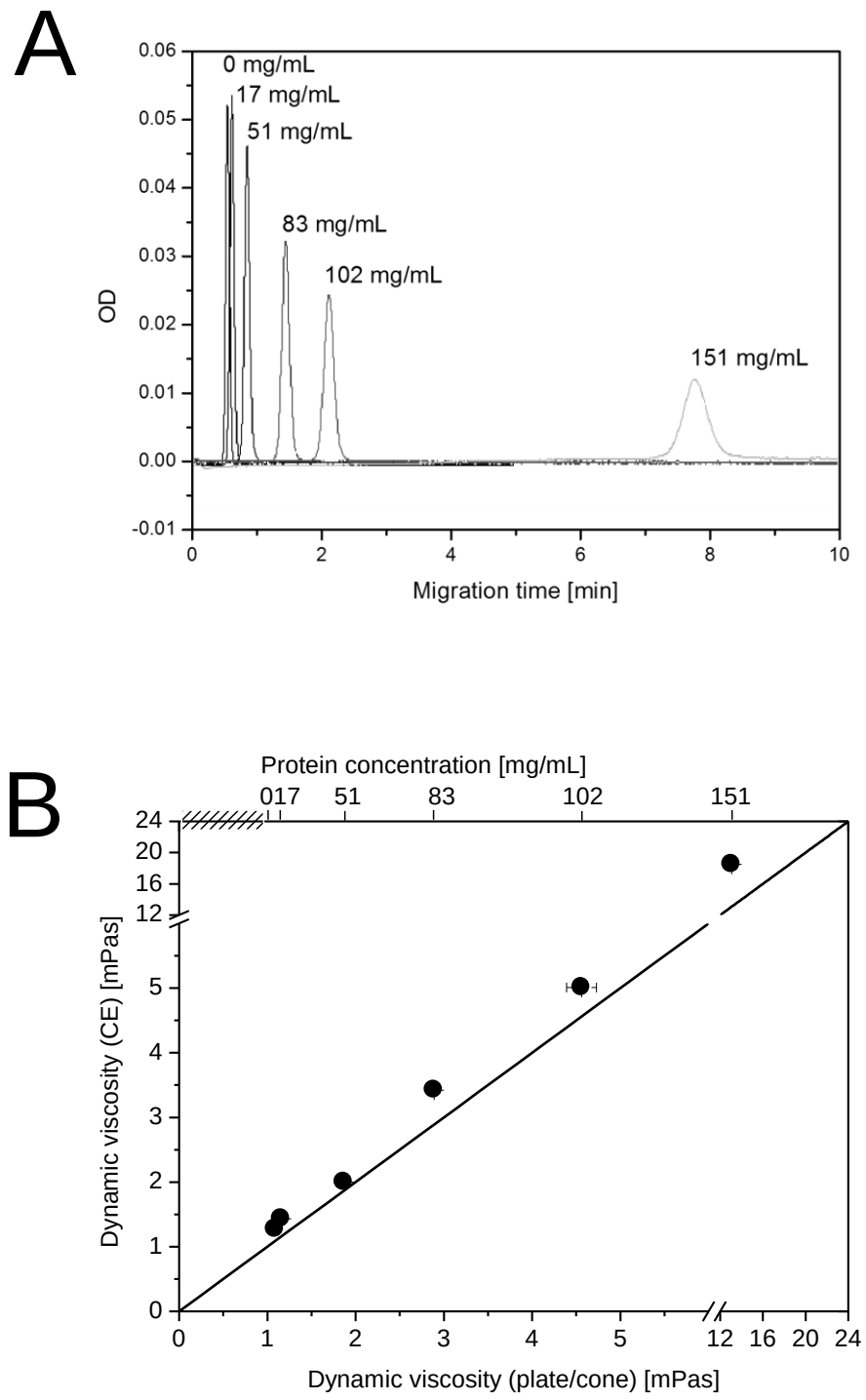

Figure 5: Dynamic viscosity of mAb1. (A) Representative examples of riboflavin peaks (445 nm) during viscosity measurement (CE) for different concentrations of mAb1 at 20°C. (B) Correlation of dynamic viscosity determined by plate/cone rheometry (N=2) and CE instrumentation (N=3) for different concentrations of mAb1. Mean values and standard deviation are reported.

DISCUSSION

The present study aimed to establish an automated method for high-throughput measurement of dynamic viscosity using standard CE equipment. CE is routinely used for the separation and characterization of macromolecules, such as monoclonal antibodies for example (Cianciulli et al., 2012; Stackhouse et al., 2011; Wacker et al., 2011; Zhang et al., 2010). In 1993, Bello et al. have described a method to determine the viscosity using CE instrumentation. They determined the migration time of a boundary between the test liquid and a reference fluid, which was related to the dynamic viscosity of the sample. However, accurate results were only obtained for viscosities up to 3 mPas due to non-linearity (Bello et al., 1994). This limitation was overcome in our set-up by the completely filled capillary thus complying with Hagen-Poiseuille's law. We showed the method to be reproducible, robust, and accurate.

Our data indicated that a short capillary with a larger inner diameter should be chosen for optimization/reduction of measuring time. However, expansion of the viscosity range requires longer capillaries with a small inner diameter. Therefore, a capillary with a diameter of 50 µm and a length of 20.5 cm represents a good compromise of short measuring time (1 – 15 min) and a viscosity range relevant for protein formulations. Aqueous glycerol solutions did not reveal any difference in viscosity values between the established method and standard plate/cone rheometry for viscosities in the range of 2 to 40 mPas. The upper viscosity limit was defined by the irregular shape of the dye peak.

Application of the CE method to different commercial protein therapeutics revealed good agreement of viscosity data with those obtained using plate/cone rheometry. However, a monoclonal antibody formulation with increasing protein concentration exhibited systematic discrepancy between CE data and plate/cone data. One explanation might be an increase/change in capillary wall – protein interaction. We speculate that this increase might have resulted from a change in protein-protein interaction (PPI) with increasing protein concentration. As reported in the literature, attractive PPIs become predominant with increasing protein concentration. Even a change from repulsive forces at low protein concentration to the predominant attractive forces at high protein concentration was reported (Saluja and Kalonia, 2008; Yadav et al., 2010a, 2010b, 2012a, 2012b). The interaction parameter kD between two molecules can be determined by

dynamic light scattering (DLS) experiments, as was previously described by our group (Lehermayr et al., 2011). This was found to be positive (5.97 mL/g) for mAb1, indicating repulsive interaction at low protein concentration. Therefore, the change from repulsive interaction at low protein concentration to predominating attractive forces at higher protein concentration might be responsible for the altered interaction between capillary wall and protein sample. As the deviation was systematic, it can be overcome by calibration with the drug product or ranking experiments. Another possibility is the use of differently coated capillaries, which is the subject of ongoing research.

Viscosity characterization is essential during protein formulation and process development. Methods involving low material consumption (in the microliter range) and a high throughput at a viscosity range between approximately 1 and 100 mPas are desirable. Compared to other rheological methods used in protein formulation development, such as capillary viscosimeters (e.g., Micro-Ubbelohde-Viscometer/ViscoClock, Schott instruments [2 – 4 mL]; Texture Analyzer [few milliliters] (Allahham et al., 2004; Allmendinger et al., 2013; Rathore et al., 2011, 2012), falling ball viscosimeters (e.g., AMVn Microviscosimeter, Anton Paar [150 – 300 µL]), or standard plate/cone rheometer (e.g., MCR301, Anton Paar [80 µL]), the established CE method requires a small sample volume in the storage vial (100 µL) and a sample consumption of only a few microliters. The volume of 100 µL is a limitation of the instrument used and may be optimized by vial design or optimization of the inlet position. The CE instrumentation is a closed system which is temperature-controlled. The latter is a critical prerequisite for viscosity measurements. Most importantly, a unique feature of the CE instrumentation is that no time-consuming cleaning is needed due to automation of the method and cleaning process. This constitutes an advantage over other viscosimeters (including the micro-viscosimeter m-VrocTM, RheoSense Inc. (Pipe and McKinley, 2009; Pipe et al., 2008). As a result, the CE instrumentation allows for measurements in an automated manner with a throughput of approximately 30 samples per load defined by the capacity of the sample tray of the instrument used.

A method that provides a significantly higher throughput is based on DLS. The DLS-based method measures the diffusion coefficient of polystyrene beads added to the sample solution. The diffusion coefficient is related to the dynamic viscosity according to the Stokes-Einstein equation (He et al., 2010). The system involves a disposable 384-well

plate (e.g., DynaoPro Plate Reader, Wyatt, 45 µL) and requires no cleaning. A drawback of the DLS method is that it requires the addition of the polystyrene beads leading to dilution of the sample by 10% thus inducing a change of sample composition. This limits the method to the non-exponential viscosity range at low protein concentrations or to studies requiring relative rather than absolute determination of viscosity. Additionally, prior exclusion of the risk of interaction/aggregation of protein with the polystyrene beads is mandatory.

A limitation of the CE method may be the potential for clogging of the capillary with particles. However, since filtration of protein samples (using sterilizing-grade filters) is routinely performed during sample preparation, particles >0.2 µm are typically excluded. Furthermore, potential interaction of the sample with the capillary wall at high protein concentration might require coated capillaries. An alternative approach is the calibration of the capillary with the specific product itself or the performance of ranking experiments.

Our method reliably determined the viscosity of Newtonian solutions between 2 and 40 mPas. Variation in capillary length and capillary diameter led to different minimal and maximal viscosities. Moreover, using CE the shear rate applied to a sample can be varied by adjusting the pressure. Therefore, the method would also be applicable to non-Newtonian liquids showing shear-rate-dependent behavior, which is the subject of ongoing research. This is of considerably importance as we have recently reported that protein formulations can show shear-thinning behavior especially at high protein concentrations (Allmendinger et al., 2013; Rathore et al., 2012). A complete list of methods to determine viscosity in protein formulations, including the established CE method, is provided in the Supporting Information, Table S-2. The table details the measuring principle, application, required volume, advantages, and limitations from an experimental point of view, highlighting that each method has its advantages and limitations. Therefore, the viscosity method most suited to the formulation in question has to be carefully chosen.

CONCLUSION

In the present study, we developed a high-throughput method to determine the dynamic viscosity of Newtonian liquids using standard CE equipment. The method

generated precise and accurate results for different capillary lots and instruments, as well as for different capillary lengths and diameters. Viscosities in the range of 2 to 40 mPas were reliably measured. These values are in a typical range for protein formulations intended for therapeutic use. The CE method showed short measurement times (1 – 15 min), and modest sample consumption (few microliters) for a capillary with a diameter of 50 μm and a length of 20.5 cm. Moreover, the usefulness of our method was shown for protein formulations, and possible limitations were outlined. The clear advantage of this method over other rheological determinations is the automation/high-throughput application in combination with small sample volumes required.

Acknowledgements

The authors thank F. Hoffman-La Roche Ltd for the supply of protein samples.

Supporting Information Available:

This material is available free of charge via the Internet at http://pubs.acs.org.

REFERENCES

Allahham, A., Stewart, P., Marriott, J., and Mainwaring, D.E. (2004). Flow and injection characteristics of pharmaceutical parenteral formulations using a micro-capillary rheometer. Int J Pharm *270*, 139–148.

Allmendinger, A., Huwyler, J., Schwarb, E., and Mueller, R. (2013). Rheological characterization and injection forces of concentrated protein formulations: an alternative predictive model for non-Newtonian solutions. *submitted*

Bello, M.S., Rezzonico, R., and Righetti, P.G. (1994). Capillary electrophoresis instrumentation as a bench-top viscometer. Journal of Chromatography A *659*, 199–204.

Cannon, M.R., Manning, R.E., and Bell, J.D. (1960). Analytical Chemistry *32*, 355–358.

Chapman, A.., and Goodall, D.. (2008). A novel approach to measurement of hydrodynamic radius for a standard protein using UV area imaging detection. Chromatography Today *1*.

Cianciulli, C., Hahne, T., and Wätzig, H. (2012). Capillary gel electrophoresis for precise protein quantitation. Electrophoresis *33*, 3276–3280.

Grupi, A., and Minton, A.P. (2012). Capillary viscometer for fully automated measurement of the concentration and shear dependence of the viscosity of macromolecular solutions. Anal. Chem. *84*, 10732–10736.

Hagen, G. (1839). Über die Bewegung des Wassers in engen cylindrischen Röhren. Poggendorf's Annalen Der Physik Und Chemie *122*, 423–442.

Han, Z., Tang, X., and Zheng, B. (2007). A PDMS viscometer for microliter Newtonian fluid. J. Micromech. Microeng. *17*, 1828.

Harris, R.J., Shire, S.J., and Winter, C. (2004). Commercial manufacturing scale formulation and analytical characterization of therapeutic recombinant antibodies. Drug Development Research *61*, 137–154.

He, F., Becker, G.W., Litowski, J.R., Narhi, L.O., Brems, D.N., and Razinkov, V.I. (2010). High-throughput dynamic light scattering method for measuring viscosity of concentrated protein solutions. Anal. Biochem. *399*, 141–143.

Jezek, J., Rides, M., Derham, B., Moore, J., Cerasoli, E., Simler, R., and Perez-Ramirez, B. (2011). Viscosity of concentrated therapeutic protein compositions. Adv. Drug Deliv. Rev. *63*, 1107–1117.

Lehermayr, C., Mahler, H.-C., Mäder, K., and Fischer, S. (2011). Assessment of net charge and protein-protein interactions of different monoclonal antibodies. J Pharm Sci *100*, 2551–2562.

Lewandrowska, A., Majcher, A., Ochab-Marcinek, A., Tabaka, M., and Hołyst, R. (2013). Taylor dispersion analysis in coiled capillaries at high flow rates. Anal. Chem. *85*, 4051–4056.

Mach, H., and Arvinte, T. (2011). Addressing new analytical challenges in protein formulation development. Eur J Pharm Biopharm *78*, 196–207.

Macosko, C.W. (1994). Rheology : principles, measurements and applications (Wiley-VCH Verlag GmbH & Co. KGaA).

Mezger, T. (2010). Das Rheologie Handbuch: Für Anwender von Rotations- und Oszillations-Rheometern (Vincentz Network GmbH & C).

Ostwald, W. (1899). Grundriss der allgemeinen chemie (W. Engelmann).

Ostwald, W. (1911). Lehrbuch der allgemeinen Chemie: Bd. Stöchiometrie. (W. Engelmann).

Pipe, C.J., and McKinley, G.H. (2009). Microfluidic rheometry. Mechanics Research Communications *36*, 110–120.

Pipe, C.J., Majmudar, T.S., and McKinley, G.H. (2008). High shear rate viscometry. Rheol Acta *47*, 621–642.

Poiseuille, J.L.M. (1840). Recherches expérimentales sur le mouvement des liquides dans les tubes de trés petits diametres. C.R. Acad. Sci. *11*, 1041–1048.

Rathore, N., Pranay, P., Eu, B., Ji, W., and Walls, E. (2011). Variability in syringe components and its impact on functionality of delivery systems. PDA J Pharm Sci Technol *65*, 468–480.

Rathore, N., Pranay, P., Bernacki, J., Eu, B., Ji, W., and Walls, E. (2012). Characterization of protein rheology and delivery forces for combination products. J Pharm Sci *101*, 4472–4480.

Reynolds, O. (1883). An experimental investigation of the circumstances which determine whether the motion of water shall be direct or sinuous, and of the law of resistance in parallel channels. Philosophical Transactions of the Royal Society of London *174*, 935–982.

Reynolds, O. (1895). On the dynamical theory of incompressible viscous fluids and the determination of the criterion. Philosophical Transactions of the Royal Society of London *186*, 123–164.

Saluja, A., and Kalonia, D.S. (2008). Nature and consequences of protein-protein interactions in high protein concentration solutions. Int J Pharm *358*, 1–15.

Schiller, L. (1933). Drei Klassiker der Strömungslehre: Hagen, Poiseuille, Hagenbach. Akademische Verlagsgesellschaft Leipzig, 60–60.

Shire, S.J. (2009). Formulation and manufacturability of biologics. Current Opinion in Biotechnology *20*, 708–714.

Shire, S.J., Shahrokh, Z., and Liu, J. (2004). Challenges in the development of high protein concentration formulations. J Pharm Sci *93*, 1390–1402.

Srivastava, N., Davenport, R.D., and Burns, M.A. (2005). Nanoliter viscometer for analyzing blood plasma and other liquid samples. Anal. Chem. *77*, 383–392.

Stackhouse, N., Miller, A.K., and Gadgil, H.S. (2011). A high-throughput UPLC method for the characterization of chemical modifications in monoclonal antibody molecules. J Pharm Sci *100*, 5115–5125.

Ubbelohde, L. (1936). Das einfachste und genaueste Viskosimeter und andere Apparate mit hängendem Niveau. World Petroleum Congress *12*.

Ubbelohde, L., and Göttner, G.H. (1965). Zur Viskosimetrie mit Umwandlungs- und Rechentabellen: 7. völlig neubearb. Aufl (Hirzel).

Wacker, C., Berger, C.N., Girard, P., and Meier, R. (2011). Glycosylation profiles of therapeutic antibody pharmaceuticals. Eur J Pharm Biopharm *79*, 503–507.

White, F.M. (1991). Viscous fluid flow. McGraw-Hill Professional Publishing New York.

Yadav, S., Liu, J., Shire, S.J., and Kalonia, D.S. (2010a). Specific interactions in high concentration antibody solutions resulting in high viscosity. J Pharm Sci *99*, 1152–1168.

Yadav, S., Shire, S.J., and Kalonia, D.S. (2010b). Factors affecting the viscosity in high concentration solutions of different monoclonal antibodies. J Pharm Sci *99*, 4812–4829.

Yadav, S., Laue, T.M., Kalonia, D.S., Singh, S.N., and Shire, S.J. (2012a). The influence of charge distribution on self-association and viscosity behavior of monoclonal antibody solutions. Mol. Pharm. *9*, 791–802.

Yadav, S., Shire, S.J., and Kalonia, D.S. (2012b). Viscosity behavior of high-concentration monoclonal antibody solutions: correlation with interaction parameter and electroviscous effects. J Pharm Sci *101*, 998–1011.

Zhang, J., Burman, S., Gunturi, S., and Foley, J.P. (2010). Method development and validation of capillary sodium dodecyl sulfate gel electrophoresis for the characterization of a monoclonal antibody. J Pharm Biomed Anal *53*, 1236–1243.

4 Conclusion and Outlook

The BBB remains a major obstacle in the treatment of disorders affecting the CNS. Many drug candidates do not cross the BBB. Therefore, extensive research has been put on the development of strategies to deliver therapeutics to the brain. To quantify the permeability of compounds and to evaluate different targeting strategies, *in vitro* BBB cell culture models that represent the *in vivo* system as much as possible would be of great benefit. Furthermore, a sensitive analytical method is required in order to determine the transport of compounds across the BBB.

TY09 conditionally immortalized cell line: a useful BBB *in vitro* model

The existing high number of different BBB *in vitro* models to date reflects the challenge to obtain an ideal model retaining the BBB-specific key properties. Several immortalized BBB *in vitro* models have been established to overcome the limitations of primary cells (batch-to-batch variability, labor-intensive isolation). However, none of them reaches the paracellular tightness comparable to that of primary cells and downregulation of protein expression has been observed. Conditionally immortalized BBB cell lines have been suggested to better reflect the *in vivo* BBB properties than immortalized cell lines (Bickel, 2005; Pardridge, 2004; Sano et al., 2010; Terasaki et al., 2003). TY09, a conditionally immortalized cell line harboring a temperature-sensitive immortalization gene and the hTERT adopts its phenotype according to the culture temperature. At 33°C, the cells are immortalized and proliferate. When switching the temperature to 37°C, the immortalization gene degrades, which favors cell differentiation. TY09 cells express important BBB tight junction proteins and transporters up to a passage of 50. This is a clear benefit of TY09 cell line, since primary cells rapidly undergo

senescence upon a limited time of division and continuous cell lines may gradually lose some typical BBB-specific properties (Reichel et al., 2003). Characterization of TY09 cells with respect to transendothelial transport of reference compounds revealed slightly higher paracellular tightness as compared to the well-characterized hCMEC/D3 cell line. The enhanced tightness of the TY09 cell monolayers offers a slightly more sensitive discrimination of the transport rates of compounds. This characteristic allows bidirectional permeability studies of psychoactive compounds with similar physicochemical properties.

Therefore, the present study showed that the technique of conditionally immortalization of human primary brain endothelial cells offers the possibility to generate a BBB *in vitro* model retaining barrier-specific properties up to a high passage number. TY09 *in vitro* model is slightly tighter than the well-characterized hCMEC/D3 cell line and presents a useful tool for transendothelial transport screening of molecules with different physicochemical properties and for mechanistic investigations of transport processes.

Although TY09 is slightly tighter than hCMEC/D3 cells, it is by far less tight than the primary brain endothelial cells. Therefore, the paracellular tightness of TY09 cell line may be further optimized. The improvement of the paracellular tightness of immortalized cell lines remains a major challenge and is of ongoing research in different laboratories. It is known that co-culture systems with astrocytes or prericytes or both generally improve the tightness of endothelial cell monolayers and the expression of transporters (Abbott et al., 2012). Therefore, further investigations may focus on the improvement of culture conditions for TY09 cell line that better mimic the *in vivo* situation such as use of co-cultures with astrocytes and pericytes.

Static *in vitro* BBB models based on the Transwell system provide a simple and convenient experimental set-up for transport studies. However, static models do not include the factor of shear stress from fluid flow on endothelial cells that is critical in cell differentiation and tight junction formation. Recently, a microfluidic BBB *in vitro* model has been developed using the b.End3 cell line. This dynamic *in vitro* model showed significantly better paracellular tightness as compared to static models (Booth and Kim, 2012). Therefore, cultivating under flow conditions might be another option to improve the tightness of the TY09 *in vitro* cell culture model.

83-14 mAb conjugated polymersomes: a potential drug delivery approach

Polymersomes have considerable potential for the implementation of drug delivery systems. Therefore, a further focus of this thesis was to investigate the potential of 83-14 mAb conjugated polymersomes for drug delivery strategy to the brain. The high brain uptake of the 83-14 mAb compared to other well-known targeting vectors, such as anti-transferrin receptor OX26 mAb, favors its use for the implementation of specific drug delivery strategies to the brain (Pardridge and Boado, 2012). However, the acute and chronic considerations of toxicity using an antibody directed against such an important receptor to enable brain uptake have to be investigated in the future. Moreover, the widely expression of the insulin receptor in human body limits its use for brain drug targeting strategies. However to date, there is no specific targeting vector available that solely reacts with the BBB.

Polymersomes based on PDMS-*b*-PMOXA block copolymers were chosen for this study because they possess several advantages including mechanical stability and minimal toxicity *in vitro* (Broz et al., 2005; Kumar et al., 2007). *In vitro* experiments with hCMEC/D3 cells revealed specific binding and uptake of the 83-14 mAb conjugated polymersomes. Therefore, the 83-14 mAb polymersomes based on PDMS-*b*-PMOXA block copolymers can be potentially used to implement specific drug targeting strategies to the brain. Further studies of the transport process are needed in order to elucidate the exact molecular mechanism for the uptake and intracellular trafficking of the 83-14 mAb conjugated polymersomes. This information will help to understand the interaction of 83-14 mAb conjugated nanoparticles with brain endothelial cells and will therefore contribute to the optimization of this drug delivery strategy. Moreover, investigations of this drug delivery system in animals are required in order to confirm the *in vitro* data and to evaluate the *in vivo* biodistribution and potential toxicity. The PDMS-*b*-PMOXA block copolymers have been described to be biocompatible but not biodegradable (Lee and Feijen, 2012). Whereas the absence of biodegradability facilitates their experimental use, this characteristic also limits their clinical application in human. Therefore, further development in this field should focus on biodegradable drug delivery systems.

An approach may be the use of nanoparticles based on amphiphilic poly(ethylene oxide)-block-polycaprolactone (PEG-*b*-PCL) block copolymers. PEG and PCL polymers are

non-toxic, biodegradable, fully bioresorbable, and are FDA approved for drug delivery systems. Aggregates from block copolymers PEG-*b*-PCL have prolonged blood circulation times mediated by the hydrophilic PEG block and are biodegradable upon hydrolysis of the ester linkages of PCL in physiological condition. They maintain neutral pH environment upon degradation, and show slow erosion kinetics as compared to other biodegradable aliphatic polyester (Ghoroghchian et al., 2006). Hence, 83-14 mAb conjugated nanoparticles based on PEG-*b*-PCL block copolymer may be suitable to implement a drug targeting system to the brain in future.

The large variety of block copolymers allows the formation of nanocarriers with desirable and tunable properties. This offers a great potential to create nanocarriers that fulfill many requirements for an ideal (stealth property, biodegradable, non-toxic, stimuli-responsive, high targeting efficiency, optimal pharmacokinetic and pharmacodynamic profiles etc.) drug delivery system to the brain in the future.

BBB *in vitro* models: contribution to the development of drug delivery strategies

Research on targeting strategies would greatly benefit from a BBB *in vitro* system capable to predict the transport capacity of drug delivery systems or transport vectors, such as monoclonal antibodies. In contrast to *in vivo* data previously reported by Pardridge et al. (Pardridge et al., 1995), *in vitro* evaluation of 83-14 mAb transport across human BBB cell monolayers did not reveal transcytosis. The high-affinity interaction between the 83-14 mAb and the insulin receptor combined with the absence of acceptor cells in the *in vitro* system might contribute to the lack of transcytotic activity.

Mimicking the close cell association present *in vivo* with co-cultivation of the brain endothelial cells with astrocytes may facilitate the detachment of the antibody from the receptor. Moreover, using an antibody with lower binding affinity to the insulin receptor than the 83-14 mAb may further favor the release from the receptor to the acceptor side of the Transwell system. These experiments may help to elucidate the discrepancy between *in vitro* and *in vivo* data in future.

The constant high number of *in vivo* studies in this area reflects the technical difficulty accompanied with accurate quantification of transcytosis of macromolecules and drug delivery systems *in vitro*. Nevertheless, *in vitro* models enable mechanistic studies that

contribute to the understanding of the transport processes and are of substantial relevance in order to optimize drug delivery strategies.

Capillary electrophoresis: bioanalytical applications

Capillary electrophoresis (CE) equipped with laser-induced fluorescence detector provides a sensitive analytical method for the quantification of macromolecules. Detection limits in the picomolar to nanomolar range for fluorescently labeled macromolecules (83-14 mAb and albumin) were obtained in the present study. The high sensitivity and low sample volume requirement render this technique attractive for the use in the context of transport studies.

The application of CE was further extended for the determination of the viscosity of therapeutic antibody solutions. This technique allows fast and automated viscosity measurements, and requires only minimal volumes of the expensive antibody samples. These characteristics are of great benefit for the optimization of protein formulations in the drug development process. With the use of CE, the viscosity of the protein samples can be determined with a high experimental throughput that may help to speed up the optimization of the protein formulations.

The characteristics of CE, i.e. high throughput measurement, minimal sample volume requirement, and high sensitivity make this technique attractive for different bioanalytical applications. An analytical approach based on CE for the characterization of polymeric nanoparticles would be of great benefit in the development of polymeric drug delivery systems. Different studies indicate that CE may play a growing role in the characterization of liposomal drug delivery systems. In the recent years, CE has been used for the determination of the physicochemical properties (size and charge) of liposomal drug delivery systems, and for permeability and drug leakage studies (Franzen and Østergaard, 2012). The CE-based methods developed and applied for the characterization of liposomal drug delivery vehicles may be optimized and adapted for polymeric drug delivery systems in the future.

Bibliography

Abbott, N.J. (2004). Prediction of blood–brain barrier permeation in drug discovery from in vivo, in vitro and in silico models. Drug Discov. Today Technol. *1*, 407–416.

Abbott, N.J. (2013). Blood–brain barrier structure and function and the challenges for CNS drug delivery. J. Inherit. Metab. Dis. *36*, 437–449.

Abbott, N.J., Ronnback, L., and Hansson, E. (2006). Astrocyte-endothelial interactions at the blood-brain barrier. Nat Rev Neurosci *7*, 41–53.

Abbott, N.J., Patabendige, A.A.K., Dolman, D.E.M., Yusof, S.R., and Begley, D.J. (2010). Structure and function of the blood–brain barrier. Neurobiol. Dis. *37*, 13–25.

Abbott, N.J., Dolman, D.E.M., Drndarski, S., and Fredriksson, S.M. (2012). An improved in vitro blood-brain barrier model: rat brain endothelial cells co-cultured with astrocytes. Methods Mol. Biol. Clifton NJ *814*, 415–430.

Ahmed, F., and Discher, D.E. (2004). Self-porating polymersomes of PEG–PLA and PEG–PCL: hydrolysis-triggered controlled release vesicles. J. Controlled Release *96*, 37–53.

Audus, K.L., and Borchardt, R.T. (1986). Characteristics of the large neutral amino acid transport system of bovine brain microvessel endothelial cell monolayers. J. Neurochem. *47*, 484–488.

Begley, D.J. (2004). ABC transporters and the blood-brain barrier. Curr. Pharm. Des. *10*, 1295–1312.

Bickel, U. (2005). How to measure drug transport across the blood-brain barrier. NeuroRx *2*, 15–26.

Boado, R.J., and Pardridge, W.M. (2011). The Trojan Horse Liposome Technology for Nonviral Gene Transfer across the Blood-Brain Barrier. J. Drug Deliv. *2011*.

Boado, R.J., Zhang, Y., Zhang, Y., and Pardridge, W.M. (2007). Humanization of anti-human insulin receptor antibody for drug targeting across the human blood–brain barrier. Biotechnol. Bioeng. *96*, 381–391.

Booth, R., and Kim, H. (2012). Characterization of a microfluidic in vitro model of the blood-brain barrier (μBBB). Lab. Chip *12*, 1784–1792.

Bowman, P.D., Ennis, S.R., Rarey, K.E., Betz, A.L., and Goldstein, G.W. (1983). Brain microvessel endothelial cells in tissue culture: a model for study of blood-brain barrier permeability. Ann. Neurol. *14*, 396–402.

Brož, P., Benito, S.M., Saw, C., Burger, P., Heider, H., Pfisterer, M., Marsch, S., Meier, W., and Hunziker, P. (2005). Cell targeting by a generic receptor-targeted polymer nanocontainer platform. J. Controlled Release *102*, 475–488.

Cabane, E., Zhang, X., Langowska, K., Palivan, C.G., and Meier, W. (2012). Stimuli-responsive polymers and their applications in nanomedicine. Biointerphases *7*, 9.

Chappa, A.K., Cooper, J.D., Audus, K.L., and Lunte, S.M. (2007). Investigation of the metabolism of substance P at the blood-brain barrier using LC-MS/MS. J. Pharm. Biomed. Anal. *43*, 1409–1415.

Christian, D.A., Cai, S., Bowen, D.M., Kim, Y., Pajerowski, J.D., and Discher, D.E. (2009). Polymersome carriers: from self-assembly to siRNA and protein therapeutics. Eur. J. Pharm. Biopharm. Off. J. Arbeitsgemeinschaft Pharm. Verfahrenstechnik EV *71*, 463–474.

Clark, D.E. (2003). In silico prediction of blood–brain barrier permeation. Drug Discov. Today *8*, 927–933.

Coloma, M.J., Lee, H.J., Kurihara, A., Landaw, E.M., Boado, R.J., Morrison, S.L., and Pardridge, W.M. (2000). Transport across the primate blood-brain barrier of a genetically engineered chimeric monoclonal antibody to the human insulin receptor. Pharm. Res. *17*, 266–274.

Dallas, S., Miller, D.S., and Bendayan, R. (2006). Multidrug Resistance-Associated Proteins: Expression and Function in the Central Nervous System. Pharmacol. Rev. *58*, 140–161.

Dean, M. (2002). The Human ATP-Binding Cassette (ABC) Transporter Superfamily.

Dehouck, B., Fenart, L., Dehouck, M.-P., Pierce, A., Torpier, G., and Cecchelli, R. (1997). A New Function for the LDL Receptor: Transcytosis of LDL across the Blood–Brain Barrier. J. Cell Biol. *138*, 877–889.

Discher, D.E., and Ahmed, F. (2006). Polymersomes. Annu. Rev. Biomed. Eng. *8*, 323–341.

Discher, D.E., and Eisenberg, A. (2002). Polymer vesicles. Science *297*, 967–973.

Egli, S., Nussbaumer, M.G., Balasubramanian, V., Chami, M., Bruns, N., Palivan, C., and Meier, W. (2011). Biocompatible functionalization of polymersome surfaces: a new approach to surface immobilization and cell targeting using polymersomes. J. Am. Chem. Soc. *133*, 4476–4483.

Feng, M.R. (2002). Assessment of blood-brain barrier penetration: in silico, in vitro and in vivo. Curr. Drug Metab. *3*, 647–657.

Freed, A.L., Audus, K.L., and Lunte, S.M. (2001). Investigation of the metabolism of substance P at the blood-brain barrier using capillary electrophoresis with laser-induced fluorescence detection. ELECTROPHORESIS *22*, 3778–3784.

Freed, A.L., Audus, K.L., and Lunte, S.M. (2002). Investigation of substance P transport across the blood-brain barrier. Peptides *23*, 157–165.

Furuse, M., Hirase, T., Itoh, M., Nagafuchi, A., Yonemura, S., Tsukita, S., and Tsukita, S. (1993). Occludin: a novel integral membrane protein localizing at tight junctions. J. Cell Biol. *123*, 1777–1788.

Gabathuler, R. (2010). Approaches to transport therapeutic drugs across the blood-brain barrier to treat brain diseases. Neurobiol. Dis. *37*, 48–57.

Gaillard, P.J., Visser, C.C., and de Boer, A.G. (2005). Targeted delivery across the blood–brain barrier. Expert Opin. Drug Deliv. *2*, 299–309.

Gaitzsch, J., Canton, I., Appelhans, D., Battaglia, G., and Voit, B. (2012). Cellular interactions with photo-cross-linked and pH-sensitive polymersomes: biocompatibility and uptake studies. Biomacromolecules *13*, 4188–4195.

Ghoroghchian, P.P., Li, G., Levine, D.H., Davis, K.P., Bates, F.S., Hammer, D.A., and Therien, M.J. (2006). Bioresorbable Vesicles Formed through Spontaneous Self-Assembly of Amphiphilic Poly(ethylene oxide)-block-polycaprolactone. Macromolecules *39*, 1673–1675.

Gumbleton, M., and Audus, K.L. (2001). Progress and limitations in the use of in vitro cell cultures to serve as a permeability screen for the blood-brain barrier. J. Pharm. Sci. *90*, 1681–1698.

Ben-Haim, N., Broz, P., Marsch, S., Meier, W., and Hunziker, P. (2008). Cell-specific integration of artificial organelles based on functionalized polymer vesicles. Nano Lett. *8*, 1368–1373.

Hawkins, B.T., and Davis, T.P. (2005). The Blood-Brain Barrier/Neurovascular Unit in Health and Disease. Pharmacol. Rev. *57*, 173 –185.

Hirase, T., Staddon, J.M., Saitou, M., Ando-Akatsuka, Y., Itoh, M., Furuse, M., Fujimoto, K., Tsukita, S., and Rubin, L.L. (1997). Occludin as a possible determinant of tight junction permeability in endothelial cells. J. Cell Sci. *110 (Pt 14)*, 1603–1613.

Hosoya, K., Tetsuka, K., Nagase, K., Tomi, M., Saeki, S., Ohtsuki, S., Terasaki, T., Yanai, N., Obinata, M., Kikuchi, A., et al. (2000a). Conditionally immortalized brain capillary endothelial cell lines established from a transgenic mouse harboring temperature-sensitive simian virus 40 large T-antigen gene. AAPS PharmSci *2*, 69–79.

Hosoya, K.I., Takashima, T., Tetsuka, K., Nagura, T., Ohtsuki, S., Takanaga, H., Ueda, M., Yanai, N., Obinata, M., and Terasaki, T. (2000b). mRna expression and transport

characterization of conditionally immortalized rat brain capillary endothelial cell lines; a new in vitro BBB model for drug targeting. J. Drug Target. *8*, 357–370.

Huwyler, J., Wu, D., and Pardridge, W.M. (1996). Brain drug delivery of small molecules using immunoliposomes. Proc. Natl. Acad. Sci. *93*, 14164–14169.

Jeffrey, P., and Summerfield, S. (2010). Assessment of the blood-brain barrier in CNS drug discovery. Neurobiol. Dis. *37*, 33–37.

Joó, F. (1996). Endothelial cells of the brain and other organ systems: some similarities and differences. Prog. Neurobiol. *48*, 255–273.

Joó, F., and Karnushina, I. (1973). A procedure for the isolation of capillaries from rat brain. Cytobios *8*, 41–48.

Kamaly, N., Xiao, Z., Valencia, P.M., Radovic-Moreno, A.F., and Farokhzad, O.C. (2012). Targeted polymeric therapeutic nanoparticles: design, development and clinical translation. Chem. Soc. Rev. *41*, 2971–3010.

Kelder, J., Grootenhuis, P.D., Bayada, D.M., Delbressine, L.P., and Ploemen, J.P. (1999). Polar molecular surface as a dominating determinant for oral absorption and brain penetration of drugs. Pharm. Res. *16*, 1514–1519.

Konradi, R., Pidhatika, B., Mühlebach, A., and Textor, M. (2008). Poly-2-methyl-2-oxazoline: a peptide-like polymer for protein-repellent surfaces. Langmuir ACS J. Surf. Colloids *24*, 613–616.

Lee, J.S., and Feijen, J. (2012). Polymersomes for drug delivery: Design, formation and characterization. J. Controlled Release *161*, 473–483.

Lin, J.J., Ghoroghchian, P.P., Zhang, Y., and Hammer, D.A. (2006). Adhesion of antibody-functionalized polymersomes. Langmuir ACS J. Surf. Colloids *22*, 3975–3979.

Loscher, W., and Potschka, H. (2005). Blood-Brain Barrier Active Efflux Transporters: ATP-Binding Cassette Gene Family. NeuroRx *2*, 86–98.

Martin, I. (2004). Prediction of blood–brain barrier penetration: are we missing the point? Drug Discov. Today *9*, 161–162.

Le Meins, J.-F., Sandre, O., and Lecommandoux, S. (2011). Recent trends in the tuning of polymersomes' membrane properties. Eur. Phys. J. E Soft Matter *34*, 1–17.

Meng, F., Engbers, G.H.M., and Feijen, J. (2005). Biodegradable polymersomes as a basis for artificial cells: encapsulation, release and targeting. J. Controlled Release *101*, 187–198.

Najer, A., Wu, D., Vasquez, D., Palivan, C.G., and Meier, W. (2013). Polymer nanocompartments in broad-spectrum medical applications. Nanomed. *8*, 425–447.

Nardin, C., Hirt, T., Leukel, J., and Meier, W. (2000). Polymerized ABA Triblock Copolymer Vesicles. Langmuir *16*, 1035–1041.

Neuwelt, E.A., Frenkel, E.P., Gumerlock, M.K., Braziel, R., Dana, B., and Hill, S.A. (1986). Developments in the diagnosis and treatment of primary CNS lymphoma. A prospective series. Cancer *58*, 1609–1620.

Nicolazzo, J.A., Charman, S.A., and Charman, W.N. (2006). Methods to assess drug permeability across the blood-brain barrier. J. Pharm. Pharmacol. *58*, 281–293.

Nitta, T., Hata, M., Gotoh, S., Seo, Y., Sasaki, H., Hashimoto, N., Furuse, M., and Tsukita, S. (2003). Size-selective loosening of the blood-brain barrier in claudin-5-deficient mice. J. Cell Biol. *161*, 653–660.

Ohtsuki, S., Sato, S., Yamaguchi, H., Kamoi, M., Asashima, T., and Terasaki, T. (2007). Exogenous expression of claudin-5 induces barrier properties in cultured rat brain capillary endothelial cells. J. Cell. Physiol. *210*, 81–86.

De Oliveira, H., Thevenot, J., and Lecommandoux, S. (2012). Smart polymersomes for therapy and diagnosis: fast progress toward multifunctional biomimetic nanomedicines. Wiley Interdiscip. Rev. Nanomed. Nanobiotechnol. *4*, 525–546.

Omidi, Y., Campbell, L., Barar, J., Connell, D., Akhtar, S., and Gumbleton, M. (2003). Evaluation of the immortalised mouse brain capillary endothelial cell line, b.End3, as an in vitro blood-brain barrier model for drug uptake and transport studies. Brain Res. *990*, 95–112.

Pang, Z., Lu, W., Gao, H., Hu, K., Chen, J., Zhang, C., Gao, X., Jiang, X., and Zhu, C. (2008). Preparation and brain delivery property of biodegradable polymersomes conjugated with OX26. J. Controlled Release *128*, 120–127.

Pardridge, W.M. (1997). Drug delivery to the brain. J. Cereb. Blood Flow Metab. Off. J. Int. Soc. Cereb. Blood Flow Metab. *17*, 713–731.

Pardridge, W.M. (1999). Blood-brain barrier biology and methodology. J. Neurovirol. *5*, 556–569.

Pardridge, W.M. (2002). Drug and gene targeting to the brain with molecular trojan horses. Nat. Rev. Drug Discov. *1*, 131–139.

Pardridge, W.M. (2003). Blood-brain barrier drug targeting: the future of brain drug development. Mol. Interv. *3*, 90–105, 51.

Pardridge, W.M. (2004a). Log(BB), PS products and in silico models of drug brain penetration. Drug Discov. Today *9*, 392–393.

Pardridge, W.M. (2004b). Holy grails and in vitro blood–brain barrier models. Drug Discov. Today *9*, 258.

Pardridge, W.M. (2005a). The blood-brain barrier: bottleneck in brain drug development. NeuroRx J. Am. Soc. Exp. Neurother. *2*, 3–14.

Pardridge, W.M. (2005b). The Blood-Brain Barrier and Neurotherapeutics. NeuroRx *2*, 1–2.

Pardridge, W.M. (2012). Drug transport across the blood–brain barrier. J. Cereb. Blood Flow Metab.

Pardridge, W.M., and Boado, R.J. (2012). Chapter eleven - Reengineering Biopharmaceuticals for Targeted Delivery Across the Blood–Brain Barrier. In Methods in Enzymology, K. Dane Wittrup and Gregory L. Verdine, ed. (Academic Press), pp. 269–292.

Pardridge, W.M., Kang, Y.S., Buciak, J.L., and Yang, J. (1995). Human insulin receptor monoclonal antibody undergoes high affinity binding to human brain capillaries in vitro and rapid transcytosis through the blood-brain barrier in vivo in the primate. Pharm. Res. *12*, 807–816.

Pidhatika, B., Rodenstein, M., Chen, Y., Rakhmatullina, E., Mühlebach, A., Acikgöz, C., Textor, M., and Konradi, R. (2012). Comparative stability studies of poly(2-methyl-2-oxazoline) and poly(ethylene glycol) brush coatings. Biointerphases *7*, 1.

Poller, B., Gutmann, H., Krähenbühl, S., Weksler, B., Romero, I., Couraud, P.-O., Tuffin, G., Drewe, J., and Huwyler, J. (2008). The human brain endothelial cell line hCMEC/D3 as a human blood-brain barrier model for drug transport studies. J. Neurochem. *107*, 1358–1368.

Prudhomme, J.G., Sherman, I.W., Land, K.M., Moses, A.V., Stenglein, S., and Nelson, J.A. (1996). Studies of Plasmodium falciparum cytoadherence using immortalized human brain capillary endothelial cells. Int. J. Parasitol. *26*, 647–655.

Régina, A., Romero, I.A., Greenwood, J., Adamson, P., Bourre, J.M., Couraud, P.O., and Roux, F. (1999). Dexamethasone regulation of P-glycoprotein activity in an immortalized rat brain endothelial cell line, GPNT. J. Neurochem. *73*, 1954–1963.

Reichel, A., Begley, D.J., and Abbott, N.J. (2003). An overview of in vitro techniques for blood-brain barrier studies. Methods Mol. Med. *89*, 307–324.

Ribatti, D., Nico, B., Crivellato, E., and Artico, M. (2006). Development of the blood-brain barrier: A historical point of view. Anat. Rec. B. New Anat. *289B*, 3–8.

Roux, F., Durieu-Trautmann, O., Chaverot, N., Claire, M., Mailly, P., Bourre, J.-M., Strosberg, A.D., and Couraud, P.-O. (1994). Regulation of gamma-glutamyl transpeptidase and alkaline phosphatase activities in immortalized rat brain microvessel endothelial cells. J. Cell. Physiol. *159*, 101–113.

Sano, Y., Shimizu, F., Abe, M., Maeda, T., Kashiwamura, Y., Ohtsuki, S., Terasaki, T., Obinata, M., Kajiwara, K., Fujii, M., et al. (2010). Establishment of a new conditionally

immortalized human brain microvascular endothelial cell line retaining an in vivo blood-brain barrier function. J. Cell. Physiol. *225*, 519–528.

Schnyder, A., and Huwyler, J. (2005). Drug Transport to Brain with Targeted Liposomes. NeuroRx *2*, 99–107.

Shah, M.V., Audus, K.L., and Borchardt, R.T. (1989). The Application of Bovine Brain Microvessel Endothelial-Cell Monolayers Grown onto Polycarbonate Membranes in Vitro to Estimate the Potential Permeability of Solutes Through the Blood–Brain Barrier. Pharm. Res. *6*, 624–627.

Siakotos, A.N., and Rouser, G. (1969). Isolation of highly purified human and bovine brain endothelial cells and nuclei and their phospholipid composition. Lipids *4*, 234–239.

Simmler, L., Buser, T., Donzelli, M., Schramm, Y., Dieu, L.-H., Huwyler, J., Chaboz, S., Hoener, M., and Liechti, M. (2013). Pharmacological characterization of designer cathinones in vitro. Br. J. Pharmacol. *168*, 458–470.

Sloan, C.D.K., Nandi, P., Linz, T.H., Aldrich, J.V., Audus, K.L., and Lunte, S.M. (2012). Analytical and Biological Methods for Probing the Blood-Brain Barrier. Annu. Rev. Anal. Chem. Palo Alto Calif *5*, 505–531.

Tanner, P., Balasubramanian, V., and Palivan, C.G. (2013). aiding nature's organelles: artificial peroxisomes play their role. Nano Lett.

Terasaki, T., Ohtsuki, S., Hori, S., Takanaga, H., Nakashima, E., and Hosoya, K. (2003). New approaches to in vitro models of blood-brain barrier drug transport. Drug Discov. Today *8*, 944–954.

Torchilin, V.P. (2005). Recent advances with liposomes as pharmaceutical carriers. Nat. Rev. Drug Discov. *4*, 145–160.

Török, M., Huwyler, J., Gutmann, H., Fricker, G., and Drewe, J. (2003). Modulation of transendothelial permeability and expression of ATP-binding cassette transporters in cultured brain capillary endothelial cells by astrocytic factors and cell-culture conditions. Exp. Brain Res. *153*, 356–365.

Tuma, P.L., and Hubbard, A.L. (2003). Transcytosis: Crossing Cellular Barriers. Physiol. Rev. *83*, 871–932.

Van de Waterbeemd, H., Camenisch, G., Folkers, G., Chretien, J.R., and Raevsky, O.A. (1998). Estimation of Blood-Brain Barrier Crossing of Drugs Using Molecular Size and Shape, and H-Bonding Descriptors. J. Drug Target. *6*, 151–165.

Waterhouse, R.N. (2003). Determination of lipophilicity and its use as a predictor of blood-brain barrier penetration of molecular imaging agents. Mol. Imaging Biol. MIB Off. Publ. Acad. Mol. Imaging *5*, 376–389.

Weksler, B.B., Subileau, E.A., Perrière, N., Charneau, P., Holloway, K., Leveque, M., Tricoire-Leignel, H., Nicotra, A., Bourdoulous, S., Turowski, P., et al. (2005). Blood-brain barrier-specific properties of a human adult brain endothelial cell line. FASEB J. Off. Publ. Fed. Am. Soc. Exp. Biol. *19*, 1872–1874.

Wilhelm, I., Fazakas, C., and Krizbai, I.A. (2011). In vitro models of the blood-brain barrier. Acta Neurobiol. Exp. (Warsz.) *71*, 113–128.

Wolburg, H., and Lippoldt, A. (2002). Tight junctions of the blood–brain barrier: development, composition and regulation. Vascul. Pharmacol. *38*, 323–337.

Wolburg, H., Wolburg-Buchholz, K., Kraus, J., Rascher-Eggstein, G., Liebner, S., Hamm, S., Duffner, F., Grote, E.-H., Risau, W., and Engelhardt, B. (2003). Localization of claudin-3 in tight junctions of the blood-brain barrier is selectively lost during experimental autoimmune encephalomyelitis and human glioblastoma multiforme. Acta Neuropathol. (Berl.) *105*, 586–592.

Zhang, Y., and Pardridge, W.M. (2005). Delivery of beta-galactosidase to mouse brain via the blood-brain barrier transferrin receptor. J. Pharmacol. Exp. Ther. *313*, 1075–1081.

Zhang, Y., and Pardridge, W.M. (2006). Blood-brain barrier targeting of BDNF improves motor function in rats with middle cerebral artery occlusion. Brain Res. *1111*, 227–229.

Zhang, Y., Schlachetzki, F., and Pardridge, W.M. (2003a). Global non-viral gene transfer to the primate brain following intravenous administration. Mol. Ther. J. Am. Soc. Gene Ther. *7*, 11–18.

Zhang, Y., Boado, R.J., and Pardridge, W.M. (2003b). Marked enhancement in gene expression by targeting the human insulin receptor. J. Gene Med. *5*, 157–163.